Final Report

GUIDELINES FOR USE OF MODIFIERS IN SUPERPAVE MIXTURES

VOLUME 2 OF 3 VOLUMES:

USE OF BINDER RHEOLOGY TO PREDICT THE CRACKING PERFORMANCE OF SBS MODIFIED MIXTURES

UF Project No.:	4910-4504-718-12
State Job No.:	99052793
Contract No.:	BC-354 (RPWO#1)

Submitted to:

Florida Department of Transportation
605 Suwannee Street
Tallahassee, FL 32399

by

Principal Investigator: Reynaldo Roque, Professor
Co-Principal Investigators: Bjorn Birgisson, Assistant Professor; Mang Tia, Professor
Researcher: Booil Kim; Zhanwu Cui

Department of Civil and Coastal Engineering
College of Engineering
University of Florida
365 Weil Hall
P.O. Box 116580
Gainesville, FL 32611-6580
Tel: (352) 392-9537, extension 1458
Fax: (352) 392-3394

UNIVERSITY OF FLORIDA

January 2004

Technical Report Documentation Page

1. Report No.	2. Government Accession No.	3. Recipient's Catalog No.
Final Report, 3 volumes		

Comment: Print all, especially Metric Conversion page on Scanner Printer . . .

4. Title and Subtitle	5. Report Date
Guidelines for Use of Modifiers in Superpave Mixtures: Use of Binder Rheology to Predict the Cracking Performance of SBS Modified Mixtures	January 2004
	6. Performing Organization Code
7. Author(s)	8. Performing Organization Report No.
Reynaldo Roque, Bjorn Birgisson, Mang Tia, Booil Kim and Zhanwu Cui	4910-4504-718-12
9. Performing Organization Name and Address	10. Work Unit No. (TRAIS)
University of Florida Department of Civil and Coastal Engineering 365 Weil Hall / P.O. Box 116580 Gainesville, FL 32611-6580	11. Contract or Grant No. BC354, RPWO #1
12. Sponsoring Agency Name and Address	13. Type of Report and Period Covered
Florida Department of Transportation Research Management Center 605 Suwannee Street, MS 30 Tallahassee, FL 32301-8064	Final Report, Vol. 2 of 3 Sept. 15, 1999 – Sept. 15, 2003
	14. Sponsoring Agency Code

15. Supplementary Notes

Prepared in cooperation with the Federal Highway Administration

16. Abstract

A laboratory investigation was conducted to identify and evaluate the relationships between binder stiffness and mixture stiffness that could be used to predict the effects of polymer-modified binder on mixture cracking performance once mixture properties are determined with unmodified binder. This work was part of a larger study that was evaluating the effects and cost-benefits of using polymer-modified mixtures.

The laboratory investigation was conducted with both unmodified binders and SBS modified binders. Both types of binders included extracted binders from short-term oven aged (STOA) mixtures and the virgin binders after rolling thin film oven test (RTFOT). The binders were tested with bending beam rheometer (BBR) and dynamic shear rheometer (DSR) to obtain properties over a range of temperatures.

Properties of the binders that were tested and evaluated include creep at low temperatures and complex modulus and phase angle at intermediate and high temperatures. These properties were used to construct the creep compliance master curve of the binders. Mixture creep compliance was measured at multiple temperatures using the Superpave IDT. Test results were used to develop and evaluate the potential use of binder-to-mixture stiffness relationships.

Test results indicate that there is no single binder-to-mixture stiffness relationship that is suitable for multiple temperatures. At each temperature in this study, there was one binder-to-mixture stiffness relationship. It appears that microdamage develops in mixtures upon cooling to temperatures below 20°, which affects mixture response in a way that is not captured by binder test results. For any given temperature, it appears the modified binder behaves more stiffly in the mix than would be predicted by the unmodified binder-to-mixture stiffness relationship. Although this yields conservative estimates of cracking performance, it may not give enough credit to the modification.

17. Key Words	18. Distribution Statement
SBS Modifier, Asphalt Mixture, Master Curve, Polymer, Asphalt Binder, Rheology	No restrictions. This document is available to the public through the National Technical Information Service, Springfield, VA, 22161

19. Security Classif. (of this report)	20. Security Classif. (of this page)	21. No. of Pages	22. Price
Unclassified	Unclassified	139	

Form DOT F 1700.7 (8-72)

DISCLAIMER

"The opinions, findings and conclusions expressed in this publication are those of the authors and not necessarily those of the Florida Department of Transportation or the U.S. Department of Transportation.

Prepared in cooperation with the State of Florida Department of Transportation and the U.S. Department of Transportation."

SI* (MODERN METRIC) CONVERSION FACTORS

APPROXIMATE CONVERSIONS TO SI UNITS

Symbol	When You Know	Multiply By	To Find	Symbol
		LENGTH		
in	inches	25.4	millimeters	mm
ft	feet	0.305	meters	m
yd	yards	0.914	meters	m
mi	miles	1.61	kilometers	km
		AREA		
in^2	square inches	645.2	square millimeters	mm^2
ft^2	square feet	0.093	square meters	m^2
yd^2	square yards	0.836	square meters	m^2
ac	acres	0.405	hectares	ha
mi^2	square miles	2.59	square kilometers	km^2
		VOLUME		
fl oz	fluid ounces	29.57	milliliters	ml
gal	gallons	3.785	liters	l
ft^3	cubic feet	0.028	cubic meters	m^3
yd^3	cubic yards	0.765	cubic meters	m^3
NOTE: Volumes greater than 1000 l shall be shown in m^3.				
		MASS		
oz	ounces	28.35	grams	g
lb	pounds	0.454	kilograms	kg
T	short tons (2000 lb)	0.907	megagrams	Mg
		TEMPERATURE (exact)		
°F	Fahrenheit temperature	5(F-32)/9 or (F-32)/1.8	Celcius temperature	°C
		ILLUMINATION		
fc	foot-candles	10.76	lux	l
fl	foot-Lamberts	3.426	candela/m^2	cd/m^2
		FORCE and PRESSURE or STRESS		
lbf	poundforce	4.45	newtons	N
psi	poundforce per square inch	6.89	kilopascals	kPa

APPROXIMATE CONVERSIONS FROM SI UNITS

Symbol	When You Know	Multiply By	To Find	Symbol
		LENGTH		
mm	millimeters	0.039	inches	in
m	meters	3.28	feet	ft
m	meters	1.09	yards	yd
km	kilometers	0.621	miles	mi
		AREA		
mm^2	square millimeters	0.0016	square inches	in^2
m^2	square meters	10.764	square feet	ft^2
m^2	square meters	1.195	square yards	yd^2
ha	hectares	2.47	acres	ac
km^2	square kilometers	0.386	square miles	mi^2
		VOLUME		
ml	milliliters	0.034	fluid ounces	fl oz
l	liters	0.264	gallons	gal
m^3	cubic meters	35.71	cubic feet	ft^3
m^3	cubic meters	1.307	cubic yards	yd^3
		MASS		
g	grams	0.035	ounces	oz
kg	kilograms	2.202	pounds	lb
Mg	megagrams	1.103	short tons (2000 lb)	T
		TEMPERATURE (exact)		
°C	Celcius temperature	1.8C + 32	Fahrenheit temperature	°F
		ILLUMINATION		
lx	lux	0.0929	foot-candles	fc
cd/m^2	candela/m^2	0.2919	foot-Lamberts	fl
		FORCE and PRESSURE or STRESS		
N	newtons	0.225	poundforce	lbf
kPa	kilopascals	0.145	poundforce per square inch	psi

* SI is the symbol for the International System of Units. Appropriate rounding should be made to comply with Section 4 of ASTM E380.

(Revised August 1992)

ACKNOWLEDGMENTS

The authors would like to acknowledge and thank the Florida Department of Transportation (FDOT) for providing technical and financial support and materials for this project. Special thanks go to engineers and technicians of the Bituminous Section of the State Materials Office for their contributions in terms of their expert knowledge, experience, and construction advice throughout the course of this work. Their efforts are sincerely appreciated and clearly made a decisive impact on the quality of the research.

TABLE OF CONTENTS

LIST OF TABLES

LIST OF FIGURES

CHAPTER 1
INTRODUCTION

1.1 Background

The Strategic Highway Research Program (SHRP) was established in 1988 to improve the performance and durability of roads in the United States (Roberts et al. 1996). The Superpave (Superior Performing Asphalt Pavements) mix design method was one of the SHRP research program outcomes.

The Superpave mix design method has become very popular in most of the states in America, including Florida. Compared with the traditional Marshall and Hveem mix design methods, Superpave has the following advantages:

- Criteria were introduced to minimize the potential use of substandard or unacceptable aggregates
- A broader range of in-service temperatures is incorporated in the binder selection specifications, including low temperatures
- The Gyratory compactor which simulates more closely the field compaction and traffic conditions was introduced (Twumasi 2001).

The creep compliance of the asphalt mixture is a function of time and temperature and can be used to predict the stresses and cracking in asphalt pavement. The master creep compliance curve can be determined using a testing and analysis system developed in the SHRP program that incorporates the Superpave Indirect Tensile Test (IDT). Since it is very costly and time consuming to run mixture tests, especially over a wide range of temperature and time, identification of the reliable binder-to-mixture stiffness relationships would be extremely useful.

Binder-to-mixture stiffness relationships have been used to study the cracking behavior of asphalt mixtures at low temperature (Buttlar 1996). However, previous study showed that due to the temperature-dependent damage at low temperatures, the binder-to-mixture stiffness relationship at a single temperature cannot be used to accurately predict the stiffness at other temperatures. Therefore, the study showed that the use of a single-function binder-to-mixture stiffness relationship will result in the poor estimates of mixture stiffness (Buttlar 1996).

The above observation was made at low temperatures (below 0°). Therefore, it would be important to determine whether a single-function binder-to-mixture stiffness relationship could be used at intermediate temperatures (0 to 20°). It would also be important to determine whether binder-to-mixture stiffness relationships apply to modified binders. This would preclude the need to perform physical test on asphalt mixture, specifically modified asphalt mixture, once the mixture properties are determined with a binder of known properties.

1.2 Study Objectives

The primary objectives of this research follow.

- To determine whether creep properties, namely m-value and D_1 of the polymer-modified mixtures can be determined once the creep properties of the unmodified mixture and the properties of the modified binder are known. If so, there is no need to test polymer modified mixtures.
- To determine whether mixture properties, particularly D_1 and *m*-value, can be determined for multiple temperatures using the mixture properties at one temperature along with the binder master curve.
- To determine whether the energy ratio (ER) at multiple temperatures can be determined using the binder-to-mixture stiffness relationship at one temperature and whether the ER of polymer modified mixtures can be determined using unmodified binder-to-mixture stiffness relationship and the modified binder properties.

1.3 Scope of Study

This laboratory investigation was conducted with both unmodified and polymer (SBS) modified binders, PG 67-22 and PG 76-22, respectively, and asphalt mixtures produced with these two binders. Tests were performed on two sets of binders: 1) binder extracted from asphalt mixture; and 2) virgin binder subjected to rolling thin film oven tests (RTFOT). The bending beam rheometer (BBR) and dynamic shear rheometer (DSR) were used. The four mixtures in this study were coarse-graded (gradation below the restricted zone) Superpave mixtures produced by using South Florida Limestone. The design asphalt contents were 6.1% and 7.2% which corresponded to two different traffic levels using the Superpave mixture design procedure. The SBS modified mixtures were prepared to have the same effective asphalt content as the unmodified asphalt mixtures. All the mixtures were short-term oven aged for two hours and then compacted to 7% (±0.5%) air voids. The creep compliance, m-value, tensile strength, failure strain, fracture energy and dissipated creep strain energy to failure were obtained from IDT test.

CHAPTER 2
LITERATURE REVIEW

2.1 Introduction

The purpose of this chapter is to review various binder-to-mixture stiffness relationships. The use and effects of the asphalt modifiers are also reviewed. Available data and information regarding binder creep compliance master curve and shift factors are also studied. Some miscellaneous issues regarding binder-to-mixture stiffness relationships are also covered.

2.2 Binder-to-mixture Stiffness Relationship

The practical goal of developing binder-to-mixture stiffness relationships is to predict mixture performance with little or no mixture testing. There are two ways to achieve this goal: theoretical and empirical binder-to-mixture stiffness relationships.

2.2.1 Theoretical Binder-to-mixture Stiffness Relationship

Theoretical binder-to-mixture stiffness relationships use micromechanical analysis to develop the relationship. In this method, the properties of the composite materials can be obtained from the properties of the constituents. Several micromechanical models have been proposed. The following were reviewed:

1. Paul's equation (1960), rule of mixtures;
2. Hashin and Shtrikman's arbitrary phase geometry model (1963);
3. Hashin's composite spheres model (1965);
4. Christensen and Lo's generalized self-consistent scheme model (1979, 1986).

2.2.1.1 Paul's equations and the rule of mixtures

Paul's equations (Equations 2.1 and 2.2) calculate the effective elastic moduli of two-phase, irregular geometry composite materials.

$$\frac{1}{\frac{c_1}{K_1}+\frac{c_2}{K_2}} \le K^* \le K_1 c_1 + K_2 c_2 \tag{2.1}$$

$$\frac{1}{\frac{c_1}{G_1}+\frac{c_2}{G_2}} \le G^* \le G_1 c_1 + G_2 c_2 \tag{2.2}$$

where K^*, G^* = effective bulk and shear moduli of the composite

K_1, K_2 = bulk moduli of phase 1 and 2

G_1, G_2 = shear moduli of phase 1 and 2

c_1, c_2 = volume fractions of phase 1 and 2.

The shear and bulk moduli can be related to Young's modulus (E), and Poisson's ratio by the following equations:

$$E = \frac{1}{\frac{1}{3G}+\frac{1}{9K}} \tag{2.3}$$

$$G = \frac{E}{3(1+\upsilon)} \tag{2.4}$$

The right-hand side of the Equations 2.1 and 2.2 are referred to as the "Law of Mixtures."

2.2.1.2 Hashin and Shtrikman's arbitrary phase geometry model

Hashin and Shtrikman (1963) derived the equations for an n-phase composite of arbitrary phase geometry. The following equations are based on a two-phase composite.

$$K_L^* = K_1 + \frac{c_2}{\frac{1}{K_2 - K_1} + \frac{3c_1}{2K_1 + 4G_1}} \tag{2.5}$$

$$K_U^* = K_2 + \frac{c_1}{\frac{1}{K_1 - K_2} + \frac{3c_2}{2K_2 + 4G_2}} \tag{2.6}$$

where

$$K_L^* \le K^* \le K_U^* \tag{2.7}$$

$$G_L^* = G_1 + \frac{c_2}{\frac{1}{G_2 - G_1} + \frac{6(K_1 + 2G_1)c_1}{5G_1(3K_1 + 4G_1)}} \tag{2.8}$$

$$G_U^* = G_1 + \frac{c_1}{\frac{1}{G_1 - G_2} + \frac{6(K_2 + 2G_2)c_2}{5G_2(3K_2 + 4G_2)}} \tag{2.9}$$

$$G_L^* \le G^* \le G_U^* \tag{2.10}$$

and the following conditions must be met:

$$K_2 \ge K_1 \quad \text{and} \quad G_2 \ge G_1 \tag{2.11}$$

where K_L^* = effective bulk modulus of the composite, lower bound

G_L^* = effective shear modulus of the composite, lower bound

K_U^* = effective bulk modulus of the composite, upper bound

G_U^* = effective bulk modulus of the composite, upper bound.

2.2.1.3 Hashin's composite spheres model

The composite spheres model consists of a gradation of infinitely-packed spherical particles in a continuous matrix phase (Buttlar 1996). The model assumes that the ratio of particle diameter to the diameter of the surrounding concentric matrix (*a*/*b*) is constant for all particles. Under these assumptions, the bulk properties of a single composite are identical to the bulk properties of the complete composite spheres. Figure 2.1 is the classical micromechanics composite sphere model.

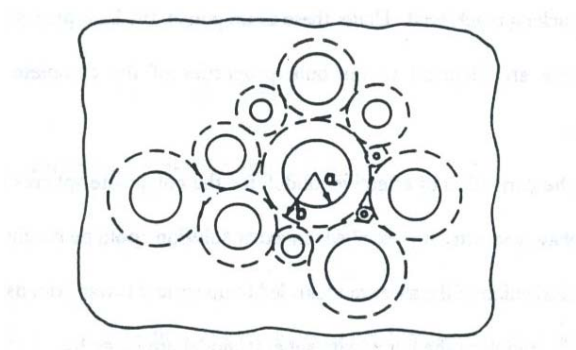

Figure 2.1 The composite spheres model (Buttlar 1996).

The equations for the composite spheres model are given as:

$$K^* = K_m + \frac{(K_p + K_m)(4G_m + 3K_m)c}{4G_m + 3K_p + 3(K_m - K_p)c} \tag{2.12}$$

$$G_L^* = \frac{G_m}{1 + c(1-\eta)y_1^{(\sigma)}} \tag{2.13}$$

$$G_U^* = G_m \left(1 + c(\eta - 1)y_1^{(\varepsilon)}\right) \tag{2.14}$$

where

$$\eta = \frac{G_p}{G_m} \tag{2.15}$$

K_m, G_m = bulk and shear moduli of the matrix

K_p, G_p = bulk modulus of the particles (or inclusions)

c = volume concentration of inclusions = $(a/b)^3$

a, b = radii of particle and concentric matrix

$y_1^{(\varepsilon)}$, $y_1^{(\sigma)}$ = complicated functions of the elastic constants.

2.2.1.4 Christensen and Lo's generalized self-consistent scheme

The generalized self-consistent scheme is illustrated in Figure 2.2.

Figure 2.2 The generalized self-consistent scheme model.

The shear modulus is given by the following equation:

$$A\left(\frac{G^*}{G_m}\right)^2 + 2B\left(\frac{G^*}{G_m}\right) + C = 0 \tag{2.16}$$

where A, B, C = lengthy functions of the elastic constants.

Up to this point, four micromechanical models have been reviewed. Figure 2.3 (Roque et al. 1997) gives a comparison of mixture stiffness calculated from using these four micro-mechanical models to measured creep stiffness. The figure shows that the bounds of Paul are the widest, followed by the arbitrary geometry bounds and the composite spheres bounds. Paul's model and the arbitrary geometry model cover some measured values, but they are too wide

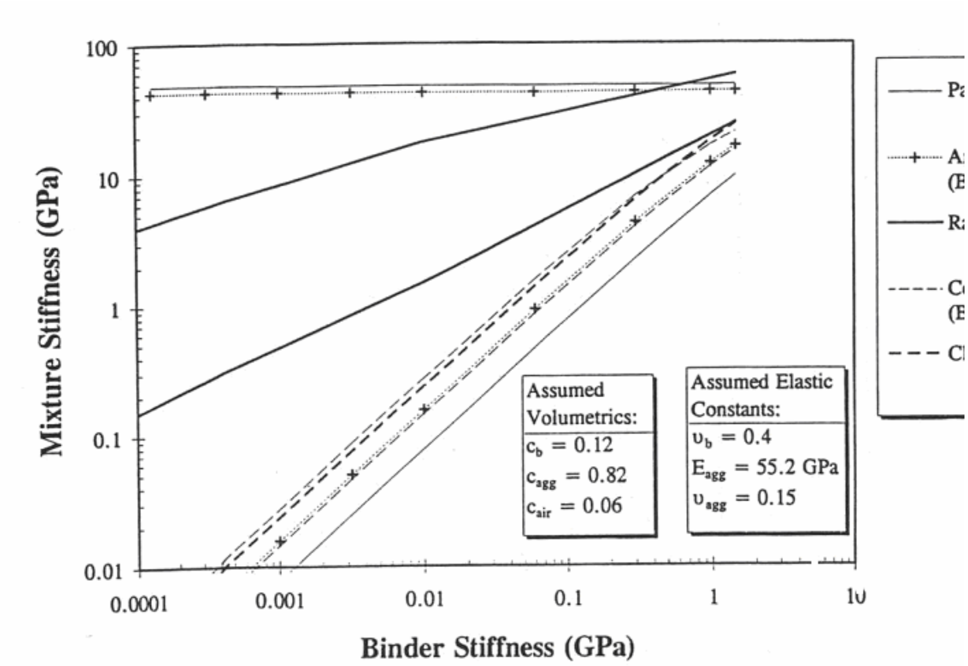

Figure 2.3 Comparison of mixture stiffness: Micromechanical models versus IDT range established using me

to provide useful information. Only when the binder stiffness is very high, the micromechanical models tend to converge with the measured values. Predicted values from Christensen and Lo's scheme are much lower than the measured ones. Figure 2.3 shows that the micromechanical models give poor estimation on the binder-to-mixture stiffness relationships. Research by Reynaldo Roque et al. (1997) shows that aggregate stiffness, Poisson's ratio of the aggregate, combinations of various constants and the sensitivity to air voids were not found to explain the large differences observed in Figure 2.3.

Due to the large discrepancies between the predicted stiffness by the micromechanical models and the IDT measurements, it is believed that the use of these models to predict the mixture stiffness is not warranted.

2.2.2 Empirical Binder-to-mixture Stiffness Relationship

The following empirical binder-to-mixture stiffness models will be discussed:

1. Heukelom and Klomp (1964)
2. Bonnaure et al. (1977)

2.2.2.1 Heukelom and Klomp

The following equations (Equations 2.17 through 2.19) were given to calculate the mixture stiffness from the binder stiffness and the volumetric parameters of the aggregate:

$$S_m = S_b\left[1+\left(\frac{2.5}{n}\right)\left(\frac{C_v}{1-C_v}\right)\right]^n \quad (2.17)$$

$$n = 0.83\log\left[\frac{4\times10^5}{S_b}\right] \quad (2.18)$$

$$C_v = \frac{volume\ \ of\ \ aggregate}{volume\ of\,(aggregate + binder)} \quad (2.19)$$

where S_m = stiffness of mixture (GPa or Psi)

S_b = stiffness of binder (GPa or Psi).

But these equations are for mixtures with C_v between 0.7 and 0.9 and air voids less than or equal to 3%. If the air voids is greater than 3%, C_v' is recommended by Van Draat et al. (1965).

$$C_v' = \frac{C_v}{1+H} \tag{2.20}$$

where $H = (P_{av}/100) - 0.03$

P_{av} = percent air voids in the mixture.

The equations above are only valid for mixtures satisfying the following equations

$$C_B = \frac{2}{3}\,(1-C_v') \tag{2.21}$$

where

$$C_B = \frac{volume\ \ of\ \ binder}{volume\ \ of\,(aggregate+binder)} \tag{2.22}$$

The use of Hekelom and Klomp's binder-to-mixture stiffness relationship is restricted to the binder stiffness to be above 0.02 GPa.

2.2.2.2 Bonnaure's relationship

Bonnaure presented another series of equations to predict mixture stiffness from binder stiffness:

For $5 \times 10^5\ Pa < S_b < 10^5\ Pa$,

$$\log S_m = \frac{\beta_4+\beta_3}{2}\left(\log S_b - 8\right) + \frac{\beta_4-\beta_3}{2}\left|\log S_b - 8\right| + \beta_2 \tag{2.23}$$

For 10^9 *Pa* < S_b < 3 × 10^9 *Pa*,

$$\log S_m = \beta_2 + \beta_4 + 2.0959(\beta_1 - \beta_2 - \beta_4)(\log S_b - 9) \tag{2.24}$$

where

$$\beta_1 = 10.82 - \frac{1.342\,(100 - V_g)}{V_g - V_b} \tag{2.25}$$

$$\beta_2 = 8.0 + 0.00568 V_g + 0.0002135 {V_g}^2 \tag{2.26}$$

$$\beta_3 = 0.6\,\log\left(\frac{1.37 {V_b}^2 - 1}{1.33 V_b} - 1\right) \tag{2.27}$$

$$\beta_4 = 0.7582(\beta_1 - \beta_2) \tag{2.28}$$

S_b = binder stiffness, *Pa*

V_g = percent volume of aggregate

V_b = percent volume of binder.

2.3 Binder Master Curve and Shift Factor

The creep compliance master curve and shift factors are very useful tools to characterize the viscoelastic properties of asphalt materials at different temperatures. These are used to extrapolate the creep compliance of a material over a broader range of temperatures and loading times from a limited set of experiments. The time-temperature superposition principle is used to construct the creep compliance master curve. Figure 2.4 (Roque et al. 1994a and 1994b) illustrates this principle. For linear viscoelastic materials, there is a relationship between the loading time and temperature. To construct a creep compliance master curve, the creep compliance at different temperatures should be obtained and plotted on a log compliance-log time scale. Then a single temperature is selected to which the creep compliance at other temperatures is shifted horizontally to form a continuous smooth curve at this temperature. This smooth curve is called the master creep compliance curve. The selected temperature is called the reference temperature.

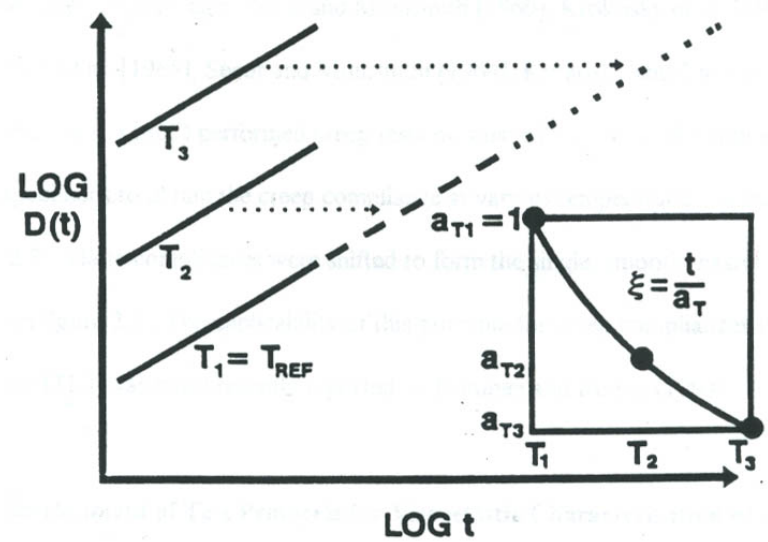

Figure 2.4 Construction of the master compliance curve (Roque et al. 1994a, 1994b).

The method of reduced time is used to obtain the creep compliance at temperatures other than the reference temperature:

$$\xi = \frac{t}{a_T} \tag{2.29}$$

where ξ = reduced time

t = real time

a_T = temperature shift factor.

The shift factor is another very important parameter obtained from constructing the master creep compliance curve. On a log creep compliance – log time scale, log (1/ a_t) corresponds to the horizontal distance of the shifting. Two equations are commonly used to obtain shift factors for asphalt binders:

For $T > T_d$, the Williams-Landel-Ferry (WLF) (Christensen and Anderson 1992) Equation (2.30) is used:

$$Log\left(\frac{a_T}{a_{T_d}}\right) = \frac{-19(T - T_d)}{92 + (T - T_d)} \tag{2.30}$$

For $T < T_d$, the Ahrennius function (2.31) is used:

$$Log\left(\frac{a_T}{a_{T_d}}\right) = \frac{E_a}{2.303R_g}\left(\frac{1}{T} - \frac{1}{T_d}\right) \tag{2.31}$$

where a_T/a_{Td} = the shift factor relative to the defining temperature

T = temperature at which properties are desired, (°K)

T_d = defining temperature, (°K)

E_a = activation energy for flow below T_d , 261,000 J/mol

R_g = ideal gal constant, 8.34 J/mol-°K

°K = °C + 273.

2.4 Power Model

The power model is often used to fit to describe the master curve:

$$D(\xi) = D_0 + D_1\xi^m \tag{2.32}$$

where $D(\xi)$ = creep compliance at reduced time, ξ

ξ = reduced time

D_0, D_1, m = power model parameters.

The m-value describes the linear part of the master curve on the log creep compliance-log time scale. Figure 2.5 shows the power model and the parameters in the master curve. D_0 represents the elastic portion of the creep compliance. Christensen and Anderson (1992) found that the maximum stiffness for all asphalts is 3 GPa. Therefore, the minimum D_0 is:

$$D_0 = 1/3\,GPa = 3.33\times10^{-10}\,Pa \qquad (2.33)$$

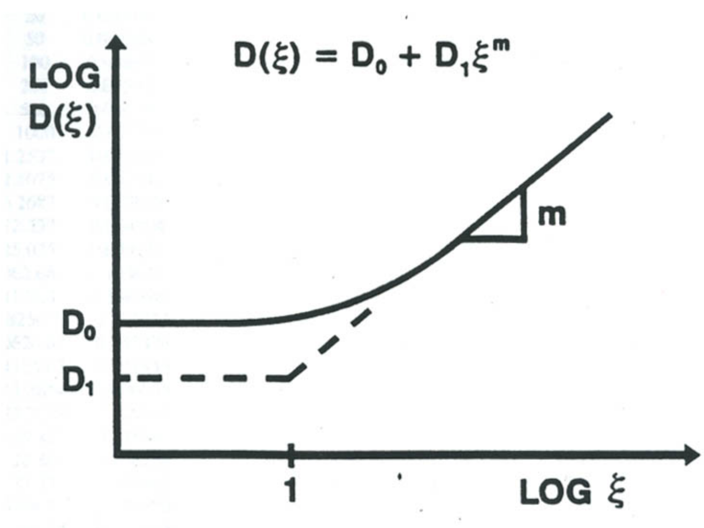

Figure 2.5 Power model.

2.5 Modifiers in Asphalt Pavement Materials

Asphalt modifiers and additives have been used in asphalt pavement materials for about 100 years (Usmani 1997). With the increase of the traffic volume, higher performance asphalt binder for road construction is required. Modified asphalt binders are expected to have higher performance than pure asphalt. Among modifiers, polymer is one of the most important types used to improve the performance of the asphalt binder (Hunter 2000). Research showed that the polymer modifiers can improve the resistance to high temperature rutting and low temperature cracking (Nicholls 1998). Studies by Kim (2003) also showed that the SBS modified mixture generally has a lower m-value than unmodified mixture. However, the modifier's function in the asphalt mixture is still not clearly understood. A general description on the modifiers used in asphalt mixtures is provided below.

Polymer is the name given to a kind of materials with high molecular weight, normally 104~106. The word polymer is derived from the classical Greek "poly" meaning "many" and Mers meaning "parts". So, polymer is a substance manufactured by linking many parts of a repeating unit together through chemical reaction.

Polymer modifiers are the most advanced asphalt modifiers currently used today (Nicholls 1998). There are three main kinds of polymer modifiers: the thermoplastic, crystalline polymers, the thermoplastic rubbers and the thermosetting polymers.

Thermoplastics, when reacted with appropriate ingredients, can usually withstand several heating and cooling cycles without suffering structural breakdown. Crystalline polymers, also known as "plastomers" includes polyethylene, polypropylene, polyvinyl chloride (PVC), polystyrene, ethylene vinyl acetate (EVA) and ethylene methyl acrylate (EMA). Thermoplastic rubber, also known as "elastomers", includes natural rubber, styrene-butadiene rubber (SBR), styrene-butadiene-styrene (SBS), styrene-isoprene-styrene (SIS), polybutadiene (PBD) and polyisoprene. Both the plastomers and the elastomers have an important effect on the temperature susceptibility of the stiffness of the asphalt. Because the polymers are generally far less susceptible to changes in temperature due to their chemical structure (Nicholls 1998), it will greatly reduce the temperature susceptibility of asphalt binders. A recent study showed that a highly entangled fibril network structure has been seen from both unmodified and modified asphalt binders, but the fibrils in the SBS modified asphalt concrete is long and thin, while those found in the unmodified asphalt concrete is thick and short (Shin 1996). It also showed that the fibrils exhibited some recovery behavior which may be good for "healing" (Shin 1996).

A thermoset is a polymer that, when heated, undergoes a chemical change to produce a crosslinked solid polymer, but is incapable of undergoing repeated cycles of softening and hardening (Ferry 1961). Epoxy falls into this category. It has been showed that the benefit of the epoxy for asphalt mixture is that it could increase the stiffness and reduce the rutting characteristics of the asphalt concrete (Hunter 2000).

2.6 HMA Fracture Mechanics Model

Research at the University of Florida has shown that the dissipated creep strain energy limit can be used to identify the crack initiation and propagation (Zhang 2000). Furthermore, this property can be obtained from Superpave IDT. For cyclic loading, the numbers of cycles to failure is defined as:

$$N = \frac{dissipated\ creep\ strain\ energy\ limit\ \ from\ strength\ test}{DCSE / cycle} \tag{2.34}$$

$$DCSE / cycle = \frac{1}{20}(\sigma_{AVE})^2 D_1 m 100^{m-1} \tag{2.35}$$

Another parameter to compare the cracking resistance of different pavement structures is the energy ratio (ER) developed by Jajliardo (2003). Energy ratio represents the fracture toughness of the asphalt mixtures. The equation for energy ratio is given below:

$$ER = \frac{a \times DCSE_f}{m^{2.98} \times D_1} \tag{2.36}$$

where $a = 0.0299\sigma^{-3.1}(6.36 - S_t) + 2.46 \times 10^{-8}$

σ = tensile stress of asphalt layer, psi

S_t = tensile strength, MPa

$DCSE_f$ = dissipated creep strain energy, KJ/m^3

D_1 = creep parameter, 1/psi

m = creep parameter.

CHAPTER 3
RESEARCH PROGRAM AND INSTRUMENTATION

3.1 Introduction

This chapter provides information on the materials and procedures for the production of binder and mixture specimens in the laboratory, and a summary of the testing procedures and instrumentation. Also presented is the information on the mixtures used in this study.

3.2 Materials

This section provides information on the asphalt binders and the corresponding mixtures used in this study.

3.2.1 Binders

Two kinds of asphalt binders were used in this study, PG 67-22 and PG 76-22. Both of these binders were produced by CITGO Asphalt Refining Company. PG 67-22 is unmodified binder and its properties are similar to AC-30. PG 76-22 is SBS (Styrene Butadiene Styrene) modified binder. There is approximately 3% SBS in the modified asphalt, and the base asphalt used for modification was the unmodified PG 67-22. The SBS was blended with the base asphalt by the manufacturer using high shear milling. PG 67-22 was used as the control binder in this study. Some binder test results provided by the supplier are presented as in Tables 3.1, 3.2 and 3.3.

The two binders tested in this study were the binders extracted from asphalt mixtures after short-term oven aging (STOA) and the virgin binders after rolling thin film oven test (RTFOT). The results of these tests are presented later.

Table 3.1 Penetration at 25°C (77°F)

Binder Type	Replicate	Penetration	Average	Standard Deviation
AC-30	1	61	60	1
	2	60		
	3	60		
SBS	1	50	50	1
	2	51		
	3	50		

Table 3.2 Dynamic Shear Rheometer at 25°C (77°F)

Binder Type	Replicate	G* (KPa)	δ	G* × sin (δ)	Average
AC-30	1	1110	66.7	1020	946
	2	1070	67.4	985	
	3	902	67.4	833	
SBS	1	748	58.7	639	640
	2	737	61.0	644	
	3	733	60.5	638	

Table 3.3 Dynamic Shear Rheometer at 64°C (147°F)

Binder Type	Replicate	G* (KPa)	δ	G* / sin (δ)	Average
AC-30	1	1.93	86.2	1.93	1.99
	2	2.01	86.1	2.02	
	3	2.01	86.2	2.02	
SBS	1	6.16	63.9	6.86	6.86
	2	6.24	64.5	6.91	
	3	6.12	64.5	6.80	

3.2.2 Mixtures

Four types of asphalt mixture were used in this study. All these mixtures were coarse-graded Superpave mixtures produced with South Florida limestone. The design asphalt contents were 6.1% and 7.2% which corresponded to two traffic levels in the Superpave mixture design procedure. The modified mixtures had the same effective asphalt content as the unmodified mixtures to assure that the SBS modifier was the only factor affecting the test results. All mixtures were laboratory-prepared samples and were short-term oven aged (STOA) for two hours (AASHTO PP2-94) and then compacted to 7% (±0.5%) air voids using the Superpave Gyratory Compactor. The mixing temperature for the SBS modified mixture is recommended by the manufacturer. Details about the mixtures are presented in Table 3.4 (Kim 2003).

Table 3.4 Mixture Test Samples

Samples	Binder content*	Binder type**	Aggregate type/gradation	Designation
6.1	6.1%	Straight	Limestone/C1***	Control sample
7.2	7.2%	Straight	Limestone/C1	Unmodified higher binder content
6.1SBS	6.1%	Modified	Limestone/C1	Modified Same binder content
7.2SBS	7.2%	Modified	Limestone/C1	Modified higher binder content

* 6.1% and 7.2 % binder content are corresponding to traffic level 5 and 3 based on Superpave level 1 mix design, respectively.
** Straight binder and modified binder are corresponding to PG 67-22 and PG 76-22, respectively.
*** C1 is most commonly used in Florida Department of Transportation for coarse gradation with 12.5 mm nominal maximum aggregate size.

Details on gradation and pavement mixture design are in Appendix A.

3.3 Binder Preparation

3.3.1 Extraction and Recovery of the Binder

Binder extraction for both the PG 67-22 and PG 76-22 were performed in accordance with FM 5-524 and ASTM 3-D5404.

3.3.2 Rolling Thin Film Oven Test (RTFOT)

Both PG 67-22 and PG 76-22 virgin binders were aged using the rolling thin film oven test (RTFOT) in accordance with D 2872-97, to simulate the aging process during the conventional hot-mixing which is comparable with the short-term oven aging (STOA) in mixtures.

3.4 Testing of Binders

To develop binder master curve and binder-to-mixture stiffness relationships, the binder was tested by performing bending beam rheometer (BBR) and dynamic shear rheometer (DSR) tests.

3.4.1 Bending Beam Rheometer (BBR) Test

The bending beam rheometer (BBR) measures the stiffness of binders at low service temperatures. The device was developed as part of the SHRP binder research program. The BBR consists of three parts: the loading system, the temperature control bath and the data acquisition system as illustrated in the following schematic in Figure 3.1 (Roberts et al. 1996).

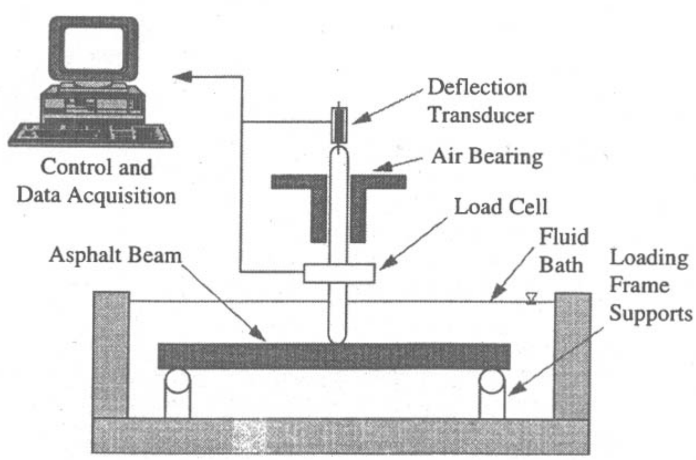

Figure 3.1 Schematic of bending beam rheometer.

The bending beam rheometer is shown in Figure 3.2 (Tia 2001):

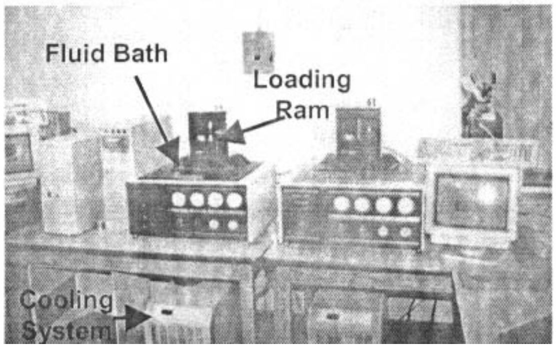

Figure 3.2 Bending beam rheometer.

The BBR applies a transient creep load in bending mode to load the specimen, which is held at a constant temperature. The data acquisition system records the load and deflection results and calculate the creep stiffness, $S(t)$, and m-value, which is the slope of the stiffness-time relationship at t = 60 s.

The creep stiffness of the asphalt binder is a measurement of how the asphalt binder resists creep loading. It is calculated using the following equation (Roberts et al. 1996):

$$S(t) = \frac{PL^3}{4bh^3\delta(t)} \tag{3.1}$$

where $S(t)$ = creep stiffness at time, t = 60 seconds

P = applied constant load, 100 g (980 mN)

L = distance between beam supports, 102 mm

B = beam width, 12.5 mm

h = beam thickness, 6.25 mm

$\delta(t)$ = deflection at time, t = 60 seconds.

The m-value is defined as the slope of the log creep stiffness versus log time curve at a loading time of 60s. It indicates the rate of change in stiffness with time, $S(t)$. Below in Figure 3.3 is a plot of m-value (Roberts et al. 1996).

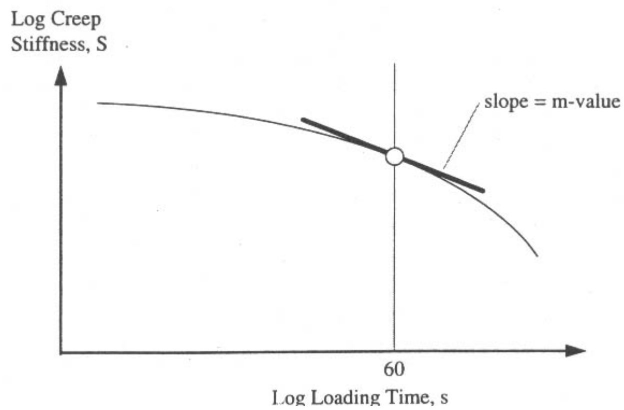

Figure 3.3 m-value from the bending beam rheometer.

In this study, the BBR test is conducted at -10° C. Three specimens of each kind of binder were prepared and tested and the stiffness results were used to develop Power Law parameters and the creep compliance master curve of the binder.

3.4.2 Dynamic Shear Rheometer (DSR) Test

The dynamic shear rheometer (DSR) characterizes the viscous and elastic properties of asphalt binders at intermediate to high temperatures. It measures the complex modulus, G^*, and phase angle, δ of the binder. Figure 3.4 shows a schematic of the dynamic shear rheometer (Roberts et al. 1996).

The complex modulus, G^*, is the total resistance of the binder to deformation and it has two components: the storage modulus, G', which reflects the elastic response and the loss modulus, G'', which reflects the viscous response. The relationship between G^*, G', and G'' is shown in Figure 3.5 (Roberts et al. 1996).

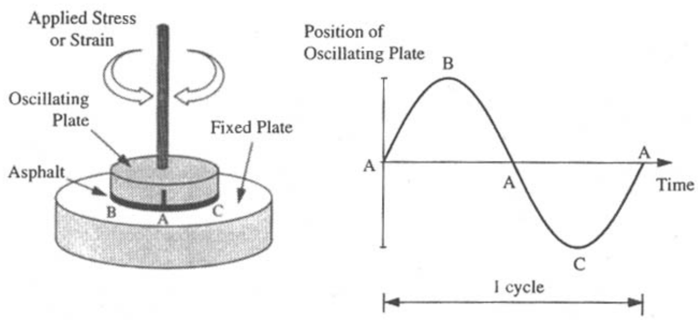

Figure 3.4 Schematic of dynamic shear rheometer.

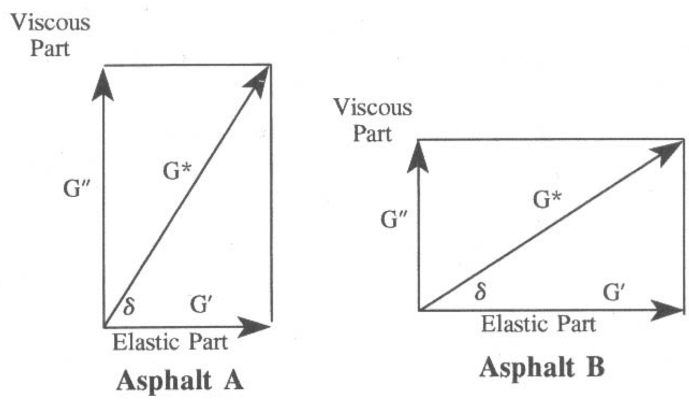

Figure 3.5 Components of complex modulus *G**.

Figure 3.5 also shows that the two asphalt binders with the same complex modulus may have different phase angle and so the storage modulus and the loss modulus are different.

The following equations are used to calculate the complex modulus, *G**.

$$G^* = \frac{\tau_{\max}}{\gamma_{\max}} \tag{3.2}$$

$$\tau_{maz} = \frac{2T}{\pi r^3} \tag{3.3}$$

$$\gamma_{max} = \frac{\theta r}{h} \qquad (3.4)$$

where T = maximum applied torque

r = radius of binder specimen/plate (12.5 mm or 4 mm)

θ = deflection angle

h = specimen height (1 mm or 2 mm).

In Superpave binder testing, the test is conducted at a single frequency of 10 rad /sec. A constant stress is applied as the loading mode. The G^* and δ are reported at the end of the test. But in this study, the dynamic shear rheometer research software was used to run the DSR test so that the binder can be tested at multiple frequencies. G', G'', viscosity, stress and strain were also obtained in addition to G^* and δ. From the DSR test at multiple frequencies, the data can then be converted into creep compliance power law parameters. The DSR test was conducted at 10° and 20°. Frequencies of 0.5 Hz, 1Hz, 2 Hz, 4 Hz, 8 Hz and 15 Hz were used at each temperature. The constant strain mode is chosen and the 8-mm sample with 2-mm gap was used in this study.

The following views in Figure 3.6 illustrate the DSR equipment (Tia 2001).

3.5 Testing of Mixtures

Mixture test were obtained using Superpave Indirect Tensile Test (IDT). Resilient modulus, creep compliance, m-value, tensile strength, failure strain, fracture energy and dissipated creep strain energy to failure were obtained from the tests.

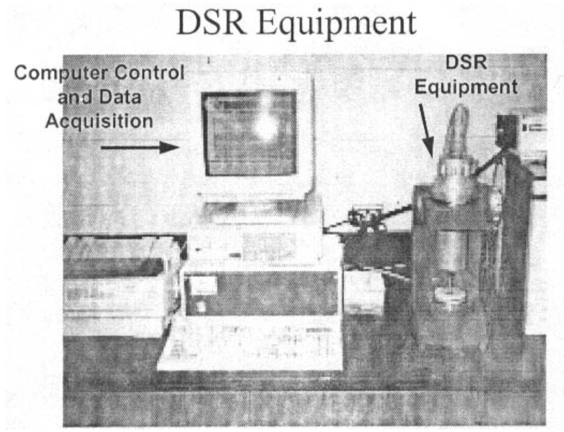

(a) overview

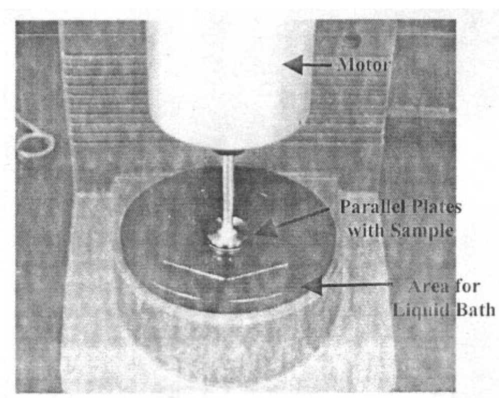

(b) close-up view

Figure 3.6 DSR equipment: a) overview; b) close-up view.

CHAPTER 4
SUMMARY AND ANALYSIS OF LABORATORY TEST RESULTS

4.1 Introduction

This chapter presents a discussion of the binder and mixture test results. The test results of the binder include creep stiffness, $S(t)$, m-value, complex modulus, G^*, and phase angle, δ. The mixture test result includes creep compliance, tensile strength, dissipated creep strain energy, m-value.

4.2 Summary of Binder Test

4.2.1 Bending Beam Rheometer (BBR) Test

A summary of the bending beam rheometer results at 60 sec. is presented in Table 4.1. The bending beam rheometer tests were conducted at -10° for both the extracted binders and the virgin binders after the rolling thin film oven test. Comparisons of the results at 60 seconds indicate that the stiffness of the SBS modified binders are lower than those of the unmodified binders (see Figures 4.1 and 4.2). However the m-value at 60 seconds was similar for all binders. The variation in m-value change observed was probably a result of the effects of the extraction process which may break the molecular structure of the modified binder and affect the results.

A summary of the bending beam rheometer test results for each kind of binders are also presented in Appendix A.

4.2.2 Dynamic Shear Rheometer (DSR) Test

The dynamic shear rheometer test was conducted to obtain G^* and δ at both 10° and 20°. This test was conducted at multiple frequencies to convert the dynamic test results to power model creep compliance parameters.

Table 4.1 Bending Beam Rheometer Test Result at -10°, 60 sec

Binder Type	Replicate	Measured Stiffness (MPa)	Average	m-value	Average
PG 67-22 6.1% asphalt content	1	49	51.07	0.484	0.475
	2	52.8		0.472	
	3	51.4		0.469	
PG 76-22 6.1% asphalt content	1	45.9	46.57	0.450	0.460
	2	46.7		0.470	
	3	47.1		0.461	
PG 67-22 7.2% asphalt content	1	46.6	46.83	0.483	0.479
	2	46.4		0.479	
	3	47.5		0.475	
PG 76-22 7.2% asphalt content	1	39	39.80	0.483	0.477
	2	39.6		0.478	
	3	40.8		0.469	
PG 67-22 RTFOT aged	1	48.3	51.40	0.485	0.479
	2	51.7		0.476	
	3	54.2		0.476	
PG 76-22 RTFOT aged	1	37.7	37.40	0.496	0.492
	2	37.8		0.491	
	3	36.7		0.488	

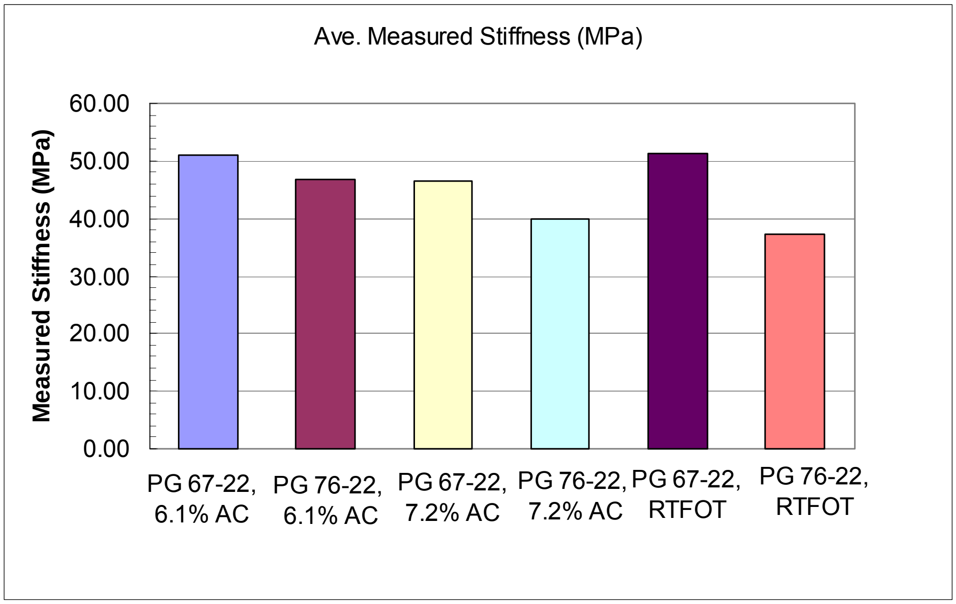

Figure 4.1 Comparison of the measured stiffness.

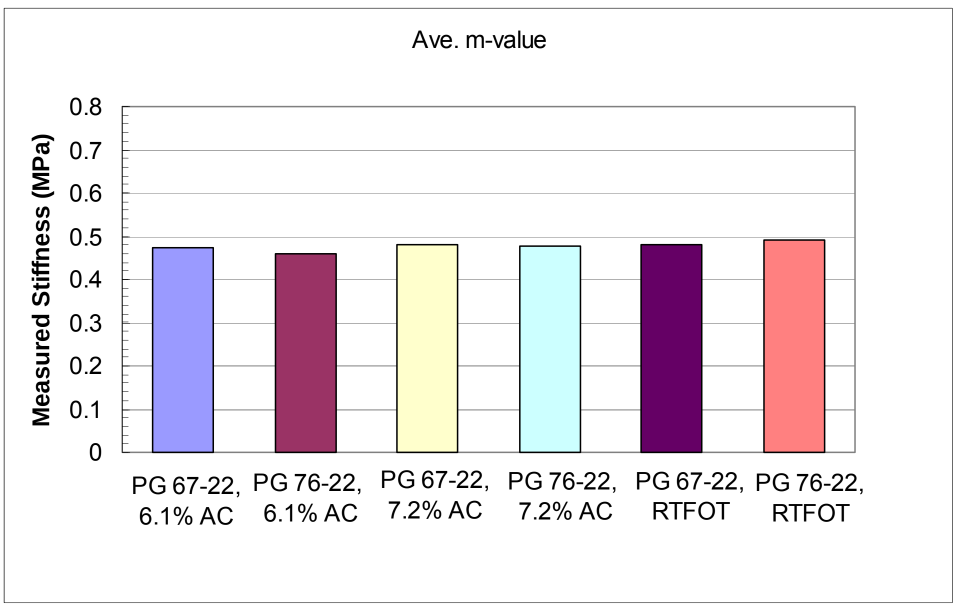

Figure 4.2 Comparison of the m-value.

4.2.2.1 Dynamic shear rheometer at low frequencies

The frequencies used in the low frequency test were: 0.001, 0.002, 0.004, 0.008, 0.015, 0.03 Hz. The typical test result is shown in Table 4.2.

Table 4.2 Dynamic Shear Rheometer Test Results at Low Frequencies at 10°

Frequency (Hz)	Phase Angle (δ)	Viscosity (Pa·s)	Shear Stress (Pa)
0.001	10.72	2.78×10^6	3.68×10^2
0.002	78.80	2.42×10^7	8.60×10^1
0.004	58.93	2.16×10^7	1.02×10^3
0.008	55.97	1.66×10^7	1.67×10^3
0.015	56.48	1.26×10^7	2.38×10^3
0.03	53.86	9.70×10^6	3.77×10^3

The results indicated that, reasonable results could not be obtained at very low frequencies. Therefore, the conversion to power model parameters was more difficult and unreliable. Figure 4.3 shows another problem with very low frequency tests. The results indicate that the binder response is not in the linear range at low frequencies, consequently. Low frequency tests were not used in this study.

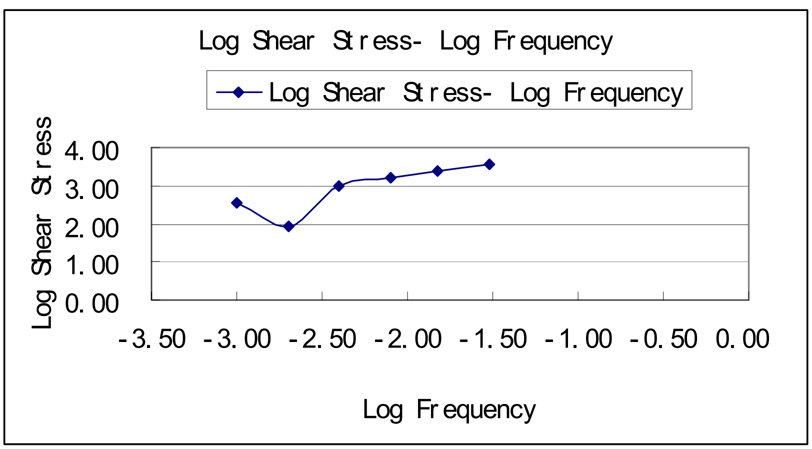

Figure 4.3 The log shear stress - log frequency relationship.

4.2.2.2 The dynamic shear rheometer test at high frequencies

The higher frequency sweeps used in the study included: 0.5, 1.0, 2.0, 4.0, 8.0, and 15.0 Hz. Test results were presented in Appendix B. The test results indicate that there is no big difference between the unmodified binder and the SBS modified binder.

4.3 Binder Creep Compliance Master Curve

The binder creep compliance master curve and associated shift factors are two critical elements in developing binder-to-mixture stiffness relationships. These two topics will be discussed in this section.

4.3.1 Shift Factors

The equations for the shift factor were presented in Chapter 2 as follows.

For $T > T_d$, the Williams-Landel-Ferry (WLF) Equation (2.30) is used:

$$log\left(\frac{a_T}{a_{T_d}}\right) = \frac{-19(T - T_d)}{92 + (T - T_d)} \tag{2.30}$$

For $T < T_d$, the Ahrennius function (2.31) is used:

$$log\left(\frac{a_T}{a_{T_d}}\right) = \frac{E_a}{2.303R_g}\left(\frac{1}{T} - \frac{1}{T_d}\right) \tag{2.31}$$

where a_T/a_{Td} = the shift factor relative to the defining temperature

T = temperature at which properties are desired, (°K)

T_d = defining temperature, (°K)

E_a = activation energy for flow below T_d , 261,000 J/mol

R_g = ideal gal constant, 8.34 J/mol-°K

°K = °C + 273.

To make the computation easy and simple, T_d was made to coincide with T_{ref}, so the equation above resulted in the following equations:

For $T > T_{ref}$, the Williams-Landel-Ferry (WLF) Equation (2.30) is used:

$$log\left(\frac{a_T}{a_{Tref}}\right) = \frac{-19(T - T_{ref})}{92 + (T - T_{ref})} \tag{4.1}$$

For $T < T_{ref}$, the Ahrennius function (2.31) is used:

$$log\left(\frac{a_T}{a_{Tref}}\right) = \frac{E_a}{2.303R_g}\left(\frac{1}{T} - \frac{1}{T_{ref}}\right) \tag{4.2}$$

A review of literature indicated that the relationship between log a_T and $T - T_d$ is linear when $T - T_d$ is between -15 and 35° and T_d is between -15 and 5° (Christensen and Anderson 1992). In this study, the temperature of interest was between -10 and 20°, and $T - T_d$ falls between -15 and 35°. Linear regression was performed for Equation 4.1 within this temperature range, which resulted in the following equation for the shift factor:

$$\log a_T = -0.175(T - T_{ref}) \tag{4.3}$$

This equation can be used regardless of whether $T > T_d$ or $T < T_d$ because this relationship was obtained when $T - T_d$ is between -15 and 35°. It only depends on how to choose the reference temperature chosen.

4.3.2 The Master Creep Compliance Curve

Using the shift factor developed above, the binder master creep compliance curve can be generated from bending beam rheometer test date at -10°, and dynamic shear rheometer test at 10° and 20°. However, the dynamic shear rheometer test results must be converted to obtain the creep compliance. A power model was used for this purpose.

4.3.2.1 Creep compliance from dynamic shear rheometer test results

Dynamic shear rheometer test results can be converted into a power model of the following form,

$$D(t) = D_0 + D_1 t^m \tag{4.4}$$

from a computer software developed by Jaesung Kim at the University of Florida. Tables 4.3 and 4.4 show the results after conversion for DSR data at 10 and 20°, respectively. The creep compliance can be obtained by inputting *t*. In this case, the inverse of the frequencies at which the dynamic shear rheometer tests were conducted were chosen to determine the creep compliance. On the log creep compliance – log *t* plot, the number of log cycles covered by log *t* was the same for the dynamic shear rheometer test as for the bending beam rheometer test.

Table 4.3 Power Model Parameters from DSR Test Results at 10°

Binder Type	D_0	D_1	m
PG 67-22, 6.1% asphalt content	4.834×10^{-9}	2.101×10^{-7}	0.476
PG 67-22, 7.2% asphalt content	5.550×10^{-9}	2.211×10^{-7}	0.490
PG 76-22, 6.1% asphalt content	5.899×10^{-9}	1.744×10^{-7}	0.494
PG 76-22, 7.2% asphalt content	6.575×10^{-9}	2.275×10^{-7}	0.498
PG 67-22, RTFOT aged	7.419×10^{-9}	1.879×10^{-7}	0.538
PG 76-22, RTFOT aged	5.491×10^{-9}	2.202×10^{-9}	0.478

Table 4.4 Power Model Parameters from DSR Test Results at 20°

Binder Type	D_0	D_1	m
PG 67-22, 6.1% asphalt content	1.650×10^{-8}	1.384×10^{-6}	0.595
PG 67-22, 7.2% asphalt content	1.854×10^{-8}	1.552×10^{-6}	0.606
PG 76-22, 6.1% asphalt content	1.513×10^{-8}	1.134×10^{-6}	0.581
PG 76-22, 7.2% asphalt content	1.702×10^{-8}	1.316×10^{-6}	0.587
PG 67-22, RTFOT aged	1.532×10^{-8}	1.198×10^{-6}	0.589
PG 76-22, RTFOT aged	1.808×10^{-8}	1.469×10^{-6}	0.595

4.3.2.2 Construction of binder creep compliance master curve

To construct the master curve, the log creep compliance-log t relationship must first be plotted. Creep compliance from the BBR test was simply taken as the inverse of the stiffness. The creep compliance from DSR test was obtained by inputting t into the power model (Equation 2.32) and the reduced time, ξ, (Equation 2.29), was used to calculate the real time at the appropriate temperature. In this study, 20° was chosen as the reference temperature.

Figures 4.4 through Figure 4.9 illustrate the log creep compliance- log ξ relationship before and after shifting. These results indicate that the creep compliance data at 10° did not match well with the master curve at 20°. It appears that it may not be possible to obtain accurate measurements from the dynamic shear rheometer at 10° when the stiffness of the binder is too high relative to the instruments stiffness. Therefore, it was decided that the data at 10° cannot be used to develop the master curve. The creep compliance master curve was developed using the BBR test results at -10° and the DSR test results at 20°. The resulting master curves are shown in Figure 4.10 through Figure 4.15. The master curve developed by using only the DSR test

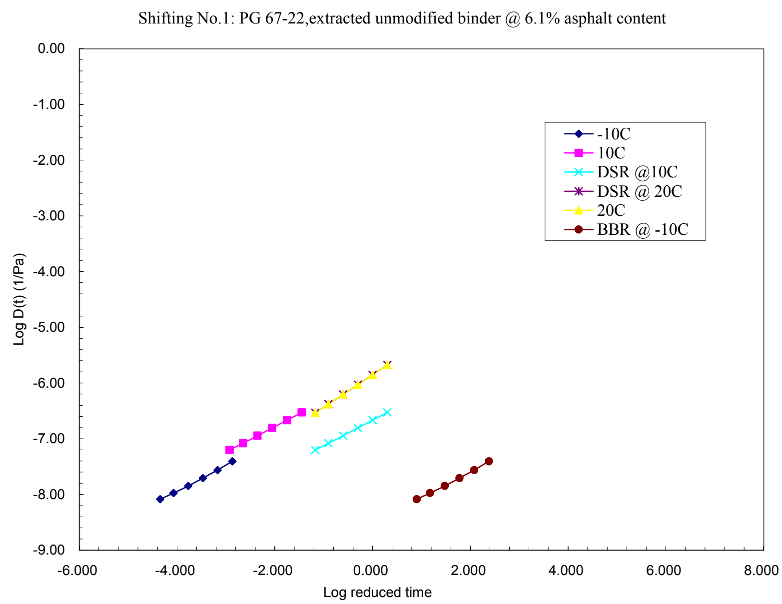

Figure 4.4 Master curve relationship: PG 67-22, extracted binder @ 6.1% AC.

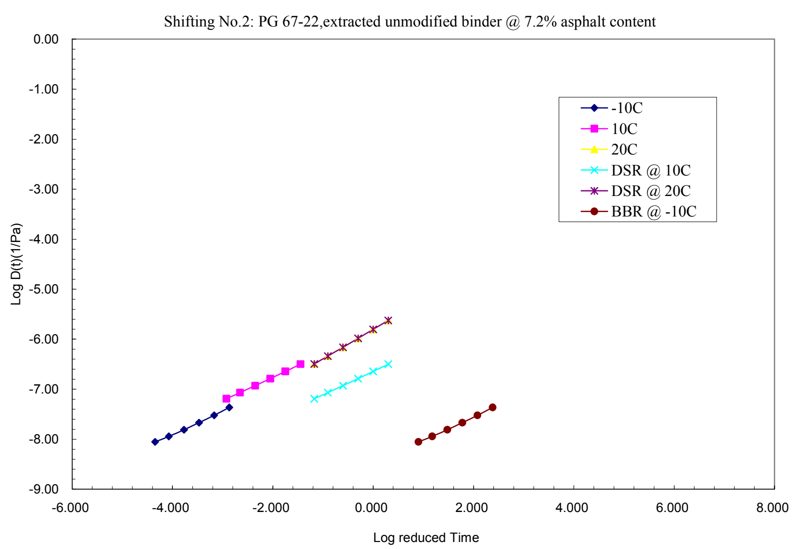

Figure 4.5 Master curve relationship: PG 67-22, extracted binder @ 7.2% AC.

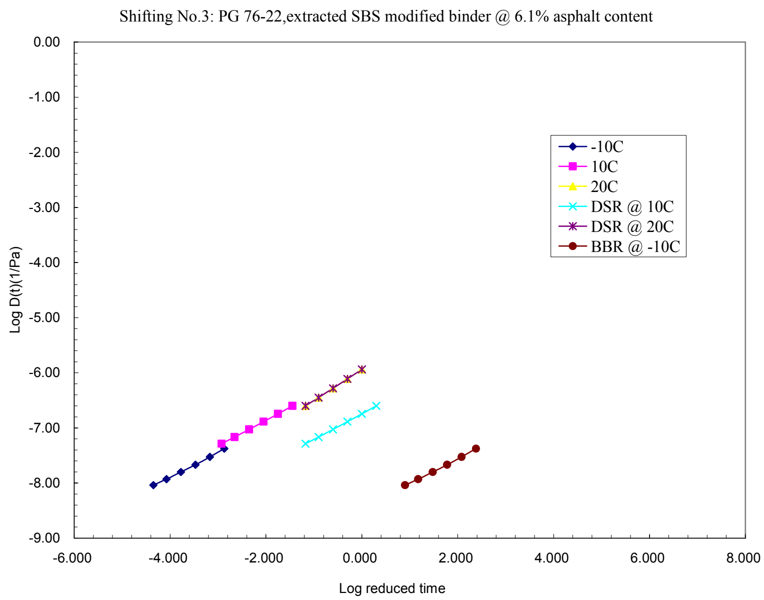

Figure 4.6 Master curve relationship: PG 76-22, extracted binder @ 6.1% AC.

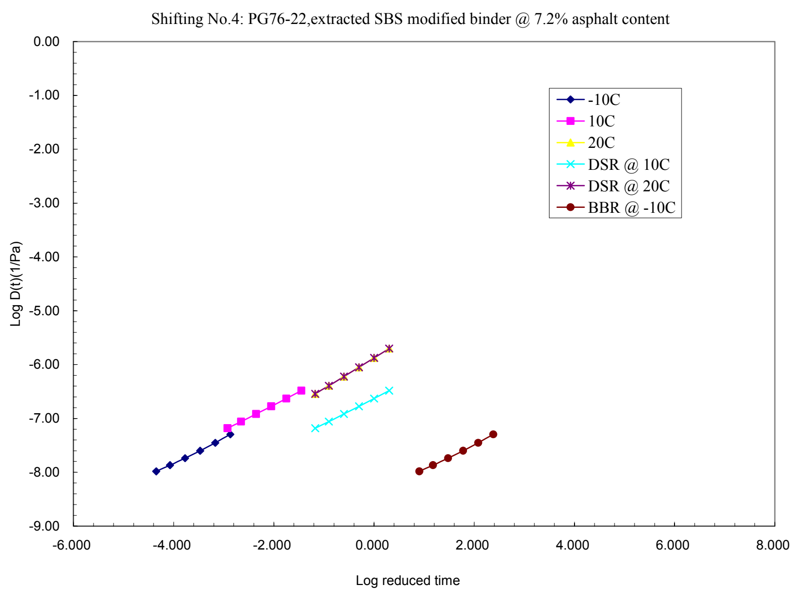

Figure 4.7 Master curve relationship: PG 76-22, extracted binder @ 7.2% AC.

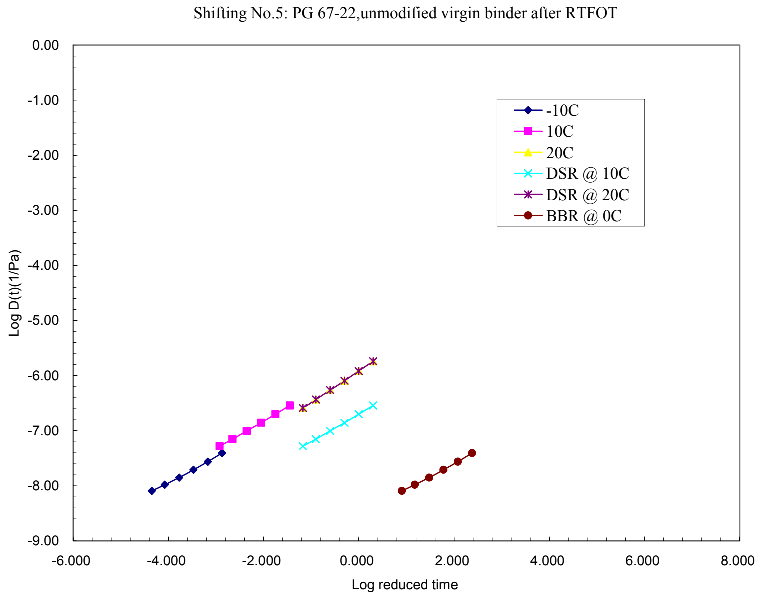

Figure 4.8 Master curve relationship: PG 67-22, RTFOT aged.

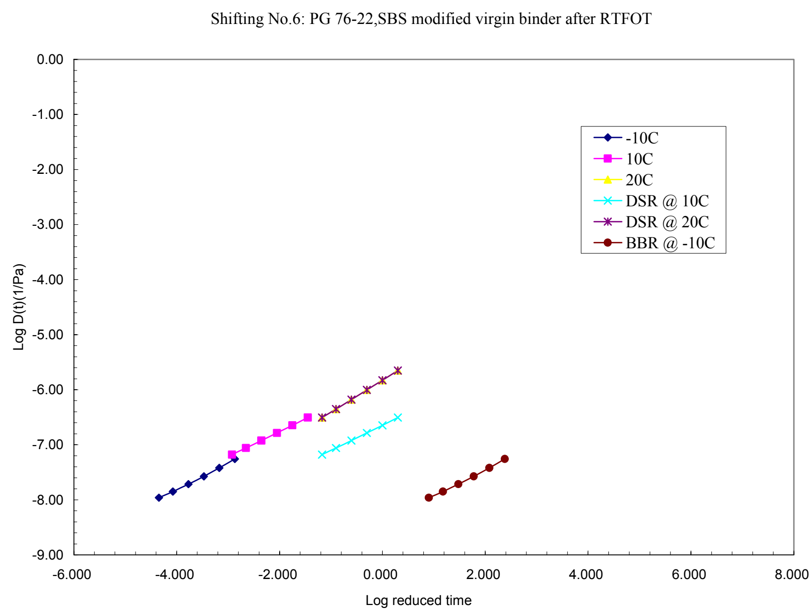

Figure 4.9 Master curve relationship: PG 76-22, RTFOT aged.

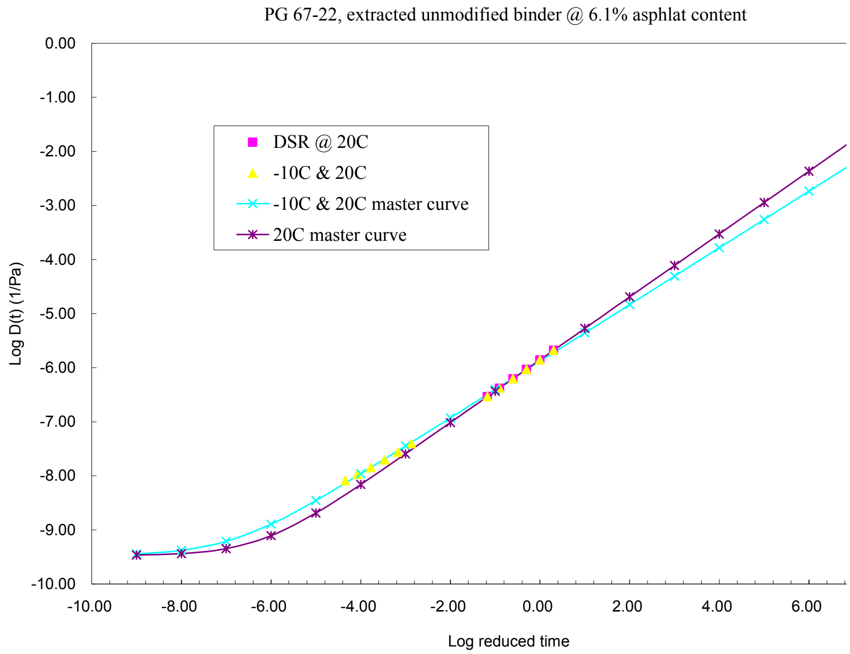

Figure 4.10 Master curve: PG 67-22, extracted binder @ 6.1% AC.

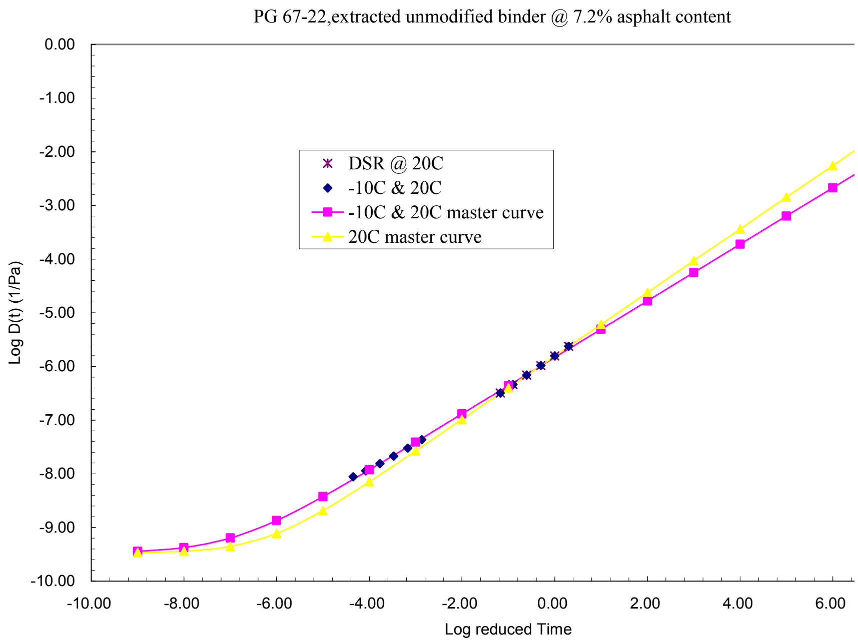

Figure 4.11 Master curve: PG 67-22, extracted binder @ 7.2% AC.

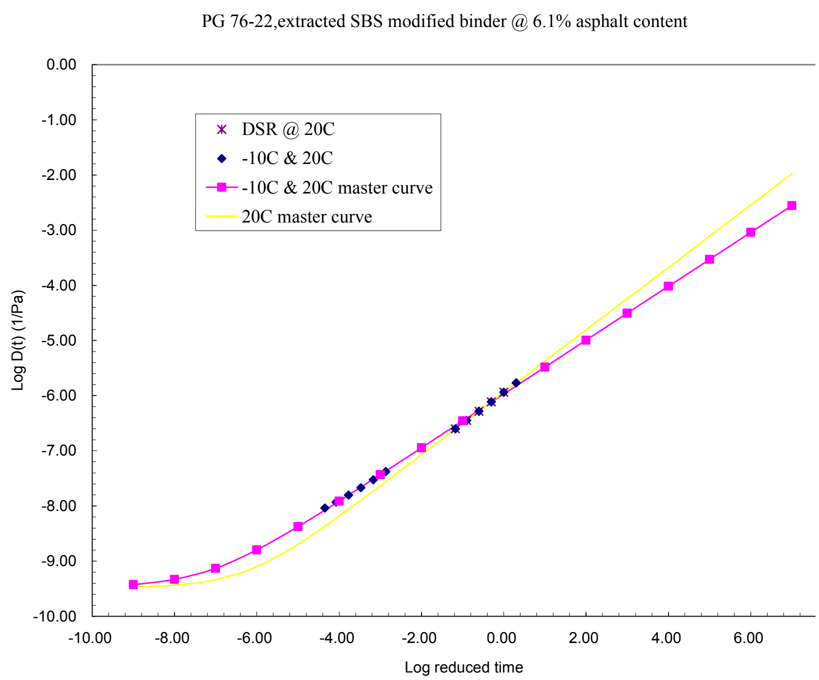

Figure 4.12 Master curve: PG 76-22, extracted binder @ 6.1% AC.

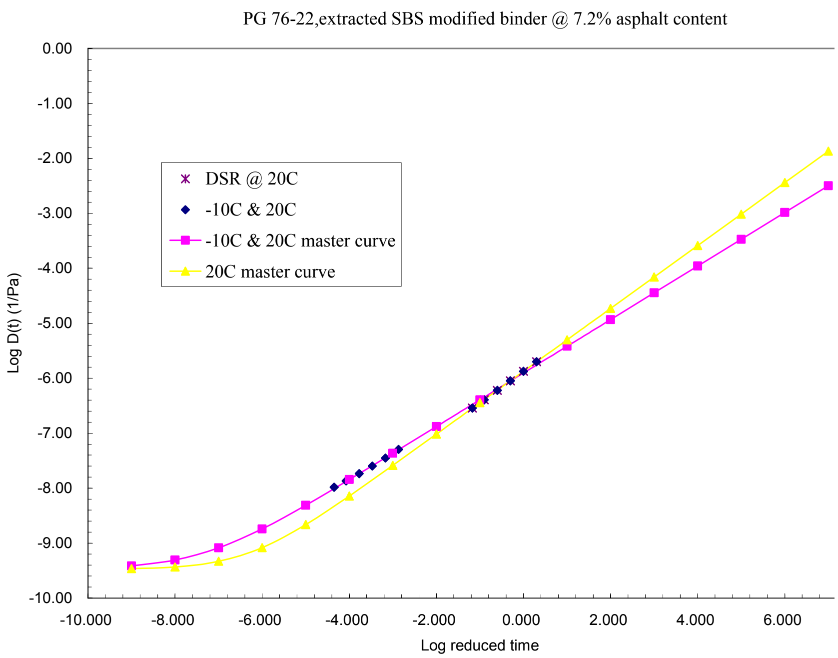

Figure 4.13 Master curve: PG 76-22, extracted binder, 7.2% AC.

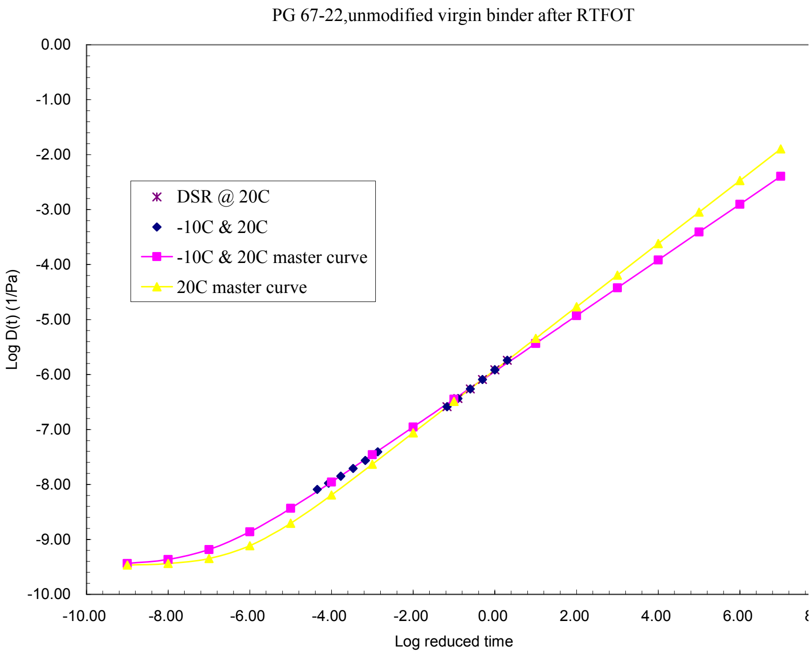

Figure 4.14 Master curve: PG 67-22, RTFOT aged.

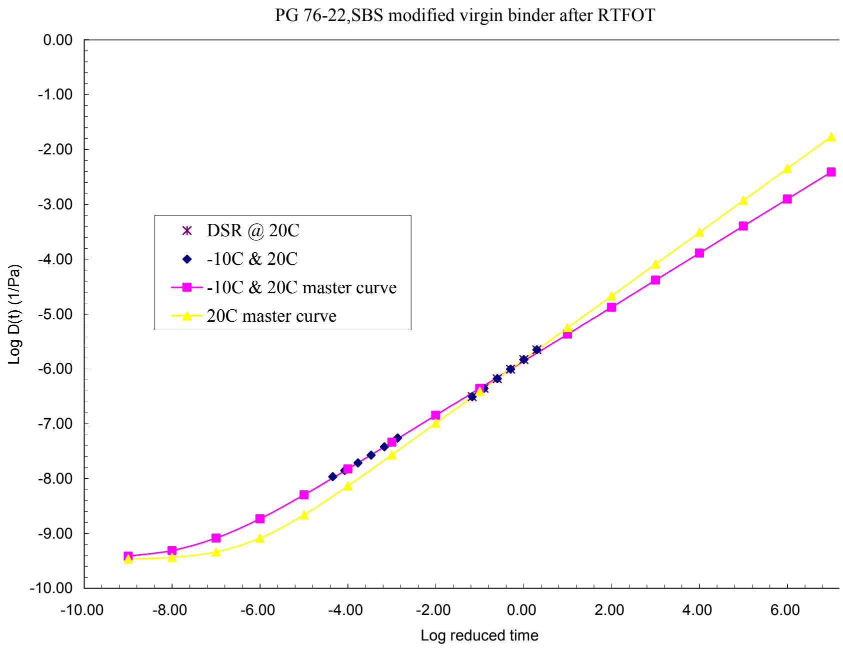

Figure 4.15 Master curve; PG 76-22, RTFOT aged.

results at 20° was also plotted for comparison. The figures clearly show that the characteristics of the master curve are highly dependent on how it was developed. In this case, there is no big difference between the two master curves from two methods.

The master curve was fitted using *a* of the following equation:

$$D(\xi) = D_0 + D_1\xi^m \tag{2.32}$$

The parameter D_0 was taken as constant, as it has been determined that this leads to greater consistency in fitting master curve parameters. As mentioned in Chapter 2, D_0 for all binders, which is defined as the minimum compliance (or the inverse of the elastic stiffness) is:

$$D_0 = 1/3\,GPa = 3.33\times10^{-10}\,Pa$$

The parameters D_1 and m were then fit by performing linear regression on binder data shifted to a reference temperature of 20°. Table 4.5 gives the resulting power model parameters for the master curves.

Table 4.5 Power Model Parameters for Master Curve

Binder Type	D_0	D_1	m
PG 67-22, 6.1% asphalt content	3.33×10^{-10}	1.321×10^{-6}	0.524
PG 67-22, 7.2% asphalt content	3.33×10^{-10}	1.474×10^{-6}	0.527
PG 76-22, 6.1% asphalt content	3.33×10^{-10}	1.070×10^{-6}	0.488
PG 76-22, 7.2% asphalt content	3.33×10^{-10}	1.238×10^{-6}	0.487
PG 67-22, RTFOT aged	3.33×10^{-10}	1.140×10^{-6}	0.507
PG 76-22, RTFOT aged	3.33×10^{-10}	1.380×10^{-6}	0.493

The creep compliance at any other temperatures was obtained by using shift factors in the method of reduced time (Equation 2.29).

4.4 Binder-to-mixture Stiffness Relationship

This section describes how the binder-to-mixture stiffness relationships were developed and used.

4.4.1 Empirical Binder-to-mixture Stiffness Relationship

In Chapter 2, both micromechanical and empirical binder-to-mixture stiffness relationships were reviewed. In this study, Heukelom and Klomp's equation (2.17 through 2.19) were used to develop relationships between binder and mixture properties. These relationships are presented again for the sake of convenience:

$$S_m = S_b' \left[1 + \left(\frac{2.5}{n} \right) \left(\frac{C_v}{1 - C_v} \right) \right]^n \qquad (2.17)$$

$$n = 0.83 \log \left[\frac{4 \times 10^5}{S_b} \right] \qquad (2.18)$$

$$C_v = \frac{volume\ of\ \ aggregate}{volume\ of\,(aggregate + binder)} \qquad (2.19)$$

where S_m = stiffness of mixture (GPa or Psi)

S_b = stiffness of binder (GPa or Psi).

Research by Mori-Tanaka showed the binder stiffness in the Equation 2.17 needs to be calibrated using the following equation (Roberts et al. 1996)

$$S_b' = a\,(S_b(t,T))^b \qquad (4.5)$$

where S_b' = calibrated binder stiffness

S_b = binder stiffness obtained at loading time, t, and temperature, T

a, b = coefficients determined through regression

In this study, the binder stiffness was calibrated using Equation 4.3 to develop the binder-to-mixture stiffness relationship.

4.4.2 Volumetrics of the aggregate

The binder-to-mixture stiffness relationship is related to the volumetrics as seen in Equation 2.19. The gradation and volumetrics of the mixture in this study are presented in Appendix C. The following relationships were used to calculate necessary parameters from the measured values.

Volume of aggregate = Total Volume – Voids in Mineral Aggregate

= (1- VMA) × 100%

Volume of (Aggregate + Binder) = Total Volume - % Air Voids

= 100 - % Air Voids

In this study, all mixtures had the same gradation but two different asphalt content levels corresponding to two traffic level, 6.1% and 7.2%. Therefore, mixtures with the same asphalt content had the same volumetrics.

For mixtures with 6.1% asphalt content:

$$\frac{C_v}{1-C_v} = 8.163$$

For mixtures with 7.2% asphalt content:

$$\frac{C_v}{1-C_v} = 6.440$$

4.4.3 Calibration of the binder stiffness

The data used to calibrate binder stiffness is illustrated in Table 4.6.

Table 4.6 Data Used to Calibrate Binder Stiffness

Temp.(°)	Time (sec.)	S_m	S_b	S'_b
0	1	S_{m1}	$S_{b(1/at)}$	S'_{b1}
	10	S_{m10}	$S_{b(10/at)}$	S'_{b10}
	...	…	…	…
	1000	S_{m1000}	$S_{b(1000/at)}$	S'_{b1000}
10	1	S_{m1}	$S_{b(1/at)}$	S'_{b1}
	10	S_{m10}	$S_{b(10/at)}$	S'_{b10}
	…	…	…	…
	1000	S_{m1000}	$S_{b(1000/at)}$	S'_{b1000}
20	1	S_{m1}	S_{b1}	S'_{b1}
	10	S_{m10}	S_{b10}	S'_{b10}
	…	…	…	…
	1000	S_{m1000}	S_{b1000}	S'_{b1000}

Mixture stiffness, S_m, for loading times of 1, 2, 5, 10, 20, 50, 100, 200, 500, 1000 sec. was measured at each test temperatures. Binder creep compliance at 20° was obtained from the master curve (power model Equation 2.32) by inputting the loading times as in column 2, Table 4.6. At 0° and 10°, the reduced time was used to obtain the binder creep compliance. The binder stiffness, S_b, was taken as the inversion of the creep compliance. The calibrated binder stiffness, S'_b, was obtained by iteration such that S_m from Equation 2.17 match the measured S_m. Linear regression was then conducted between log S_b and log S'_b to obtain a and b in Equation 4.3. The log S_b - log S'_b and log S_b - log S_m relationships were plotted for each mixture and presented in Figures 4.16 through 4.31.

The figures indicated that for each kind of mixture, there is a separate relationship between log S_b - log S'_b for each of the three temperatures. This implied that one cannot obtain a single (unique) set of a and b for all mixture temperatures. The log S_b - log S_m indicated that the

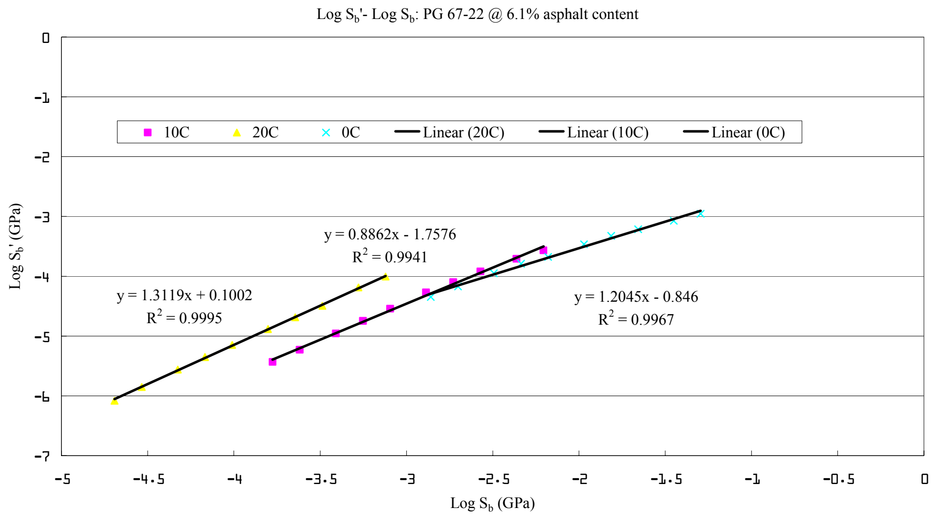

Figure 4.16 Log S_b' – log S_b relationship: PG 67-22, extracted binder 6.1% AC.

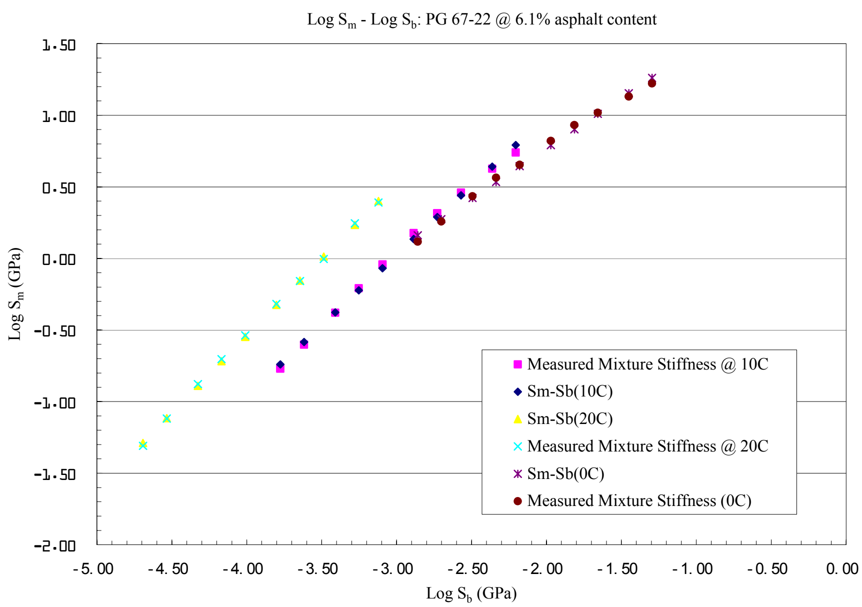

Figure 4.17 Log S_m – log S_b relationship: PG 67-22, extracted binder @ 6.1% AC.

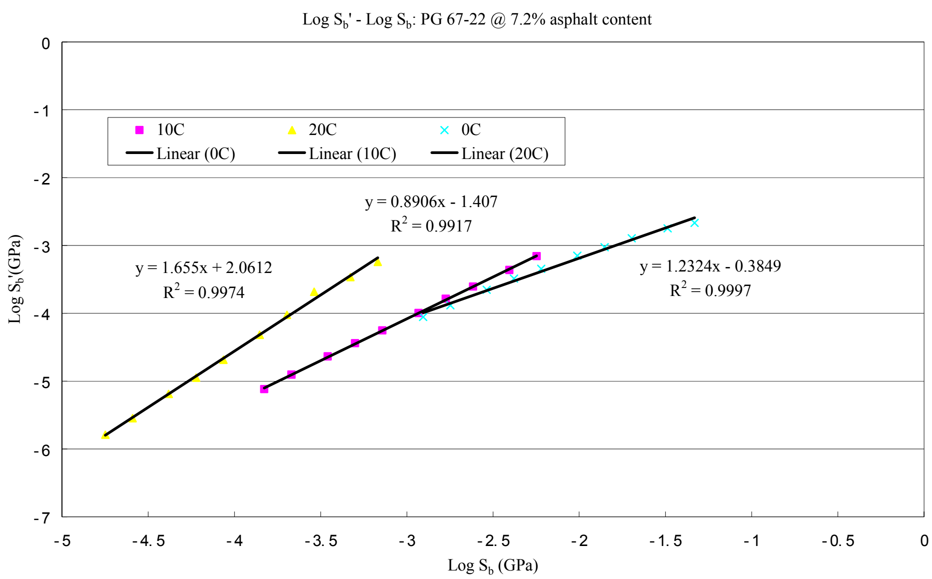

Figure 4.18 Log S_b' – log S_b relationship: PG 67-22, extracted binder @ 7.2% AC.

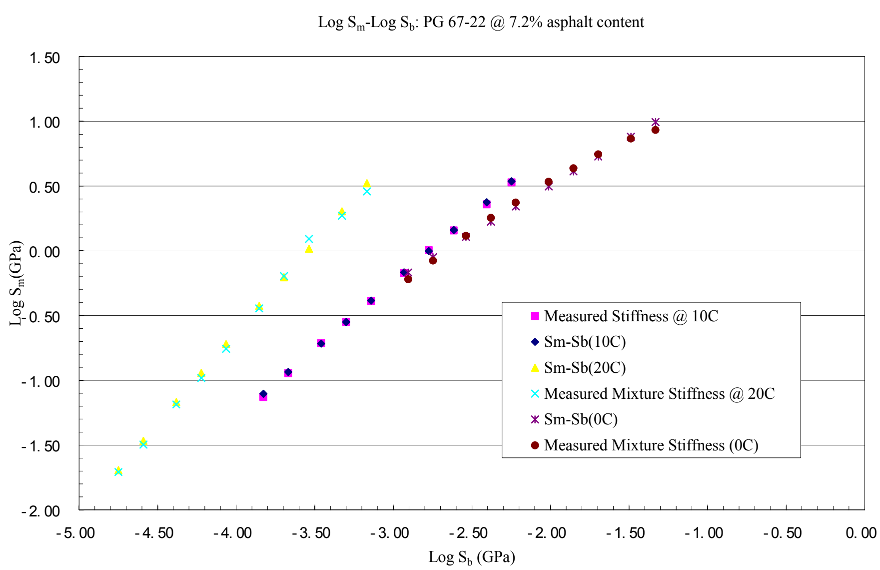

Figure 4.19 Log S_m – log S_b relationship: PG 67-22, extracted binder @ 7.2% AC.

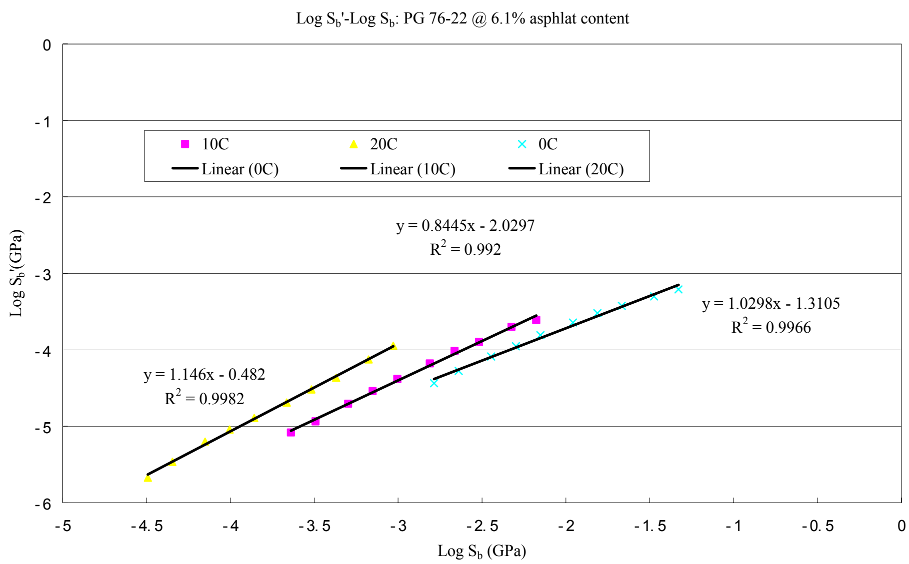

Figure 4.20 Log S_b' – log S_b relationship: PG 76-22, extracted binder @ 6.1% AC.

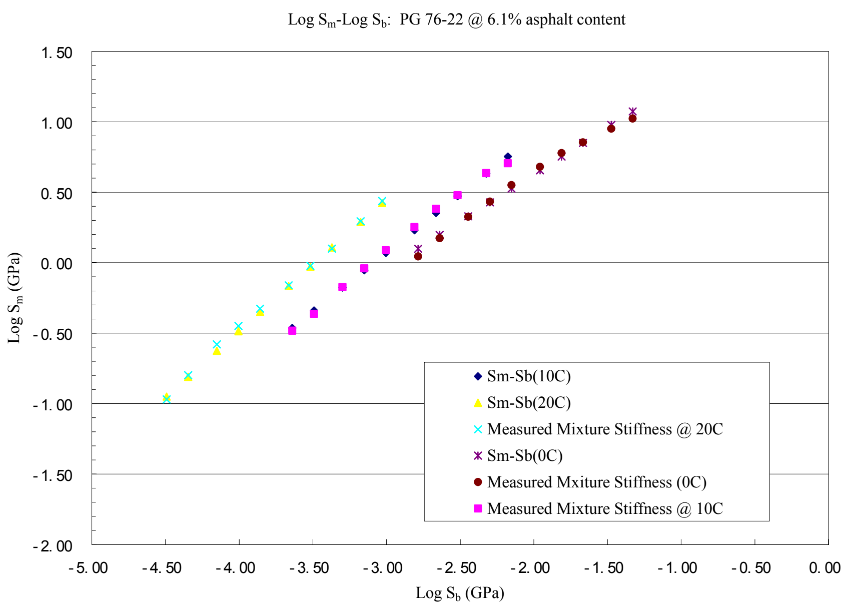

Figure 4.21 Log S_m – log S_b relationship: PG 76-22, extracted binder @ 6.1% AC.

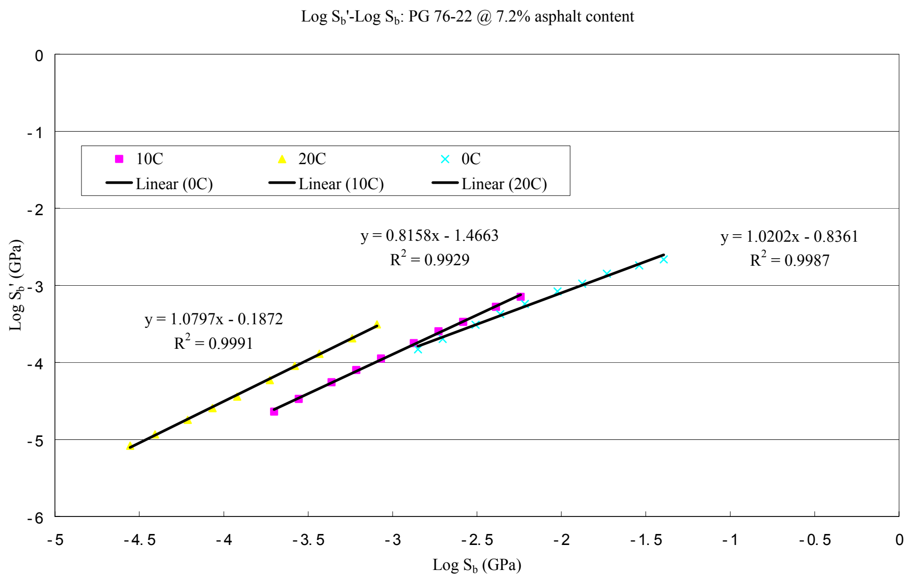

Figure 4.22 Log S_b' – log S_b relationship: PG 76-22, extracted binder @ 7.2% AC.

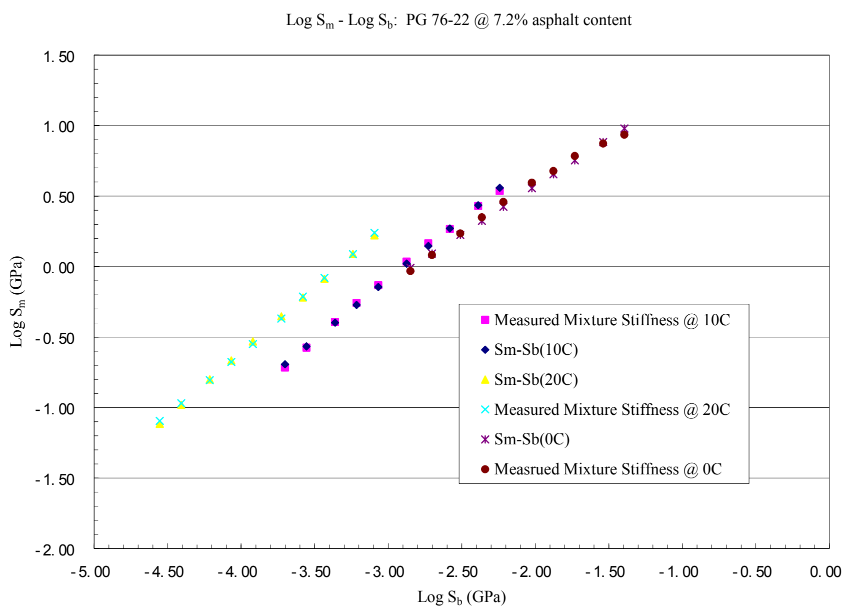

Figure 4.23 Log S_m – log S_b relationship: PG 76-22, extracted binder @ 7.2% AC.

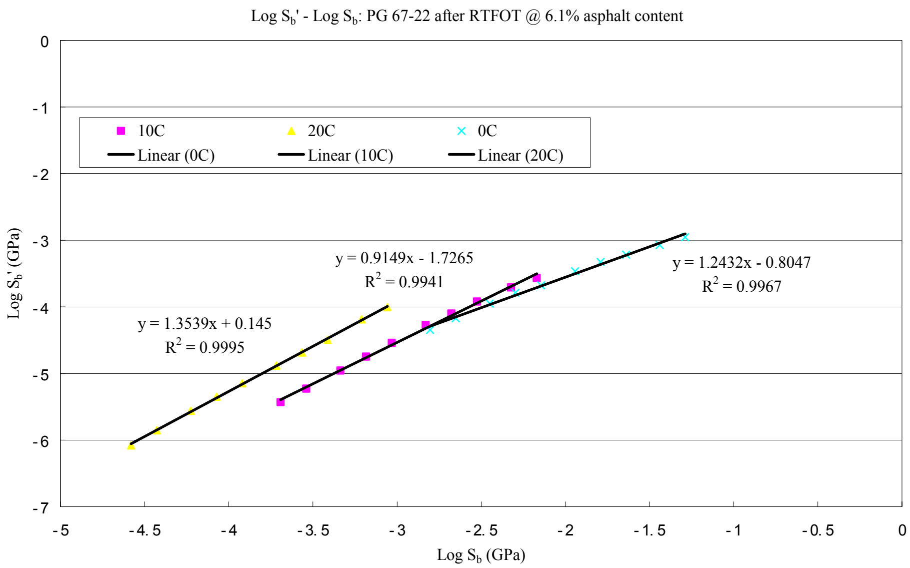

Figure 4.24 Log S_b' – log S_b relationship: PG 67-22, RTFOT aged @ 6.1% AC.

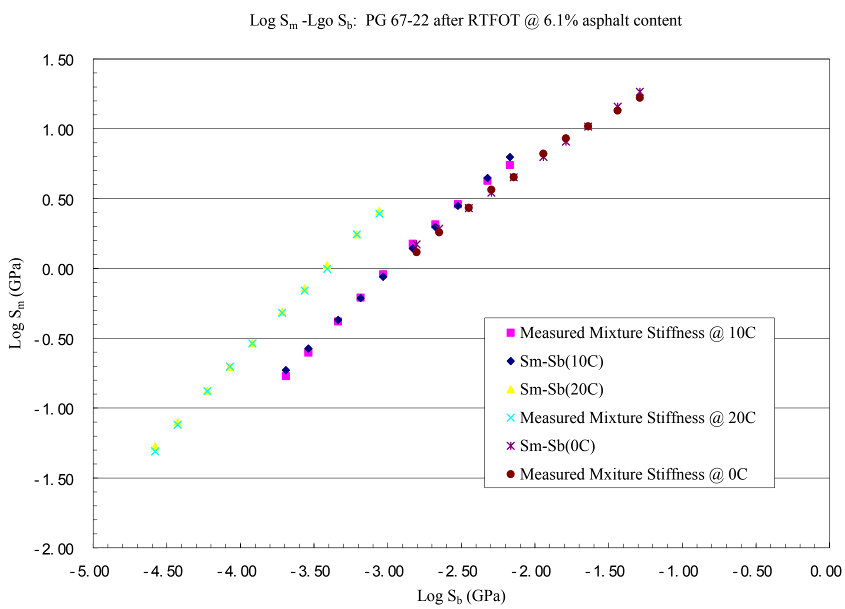

Figure 4.25 Log S_m – log S_b relationship: PG 67-22, RTFOT aged @ 6.1% AC.

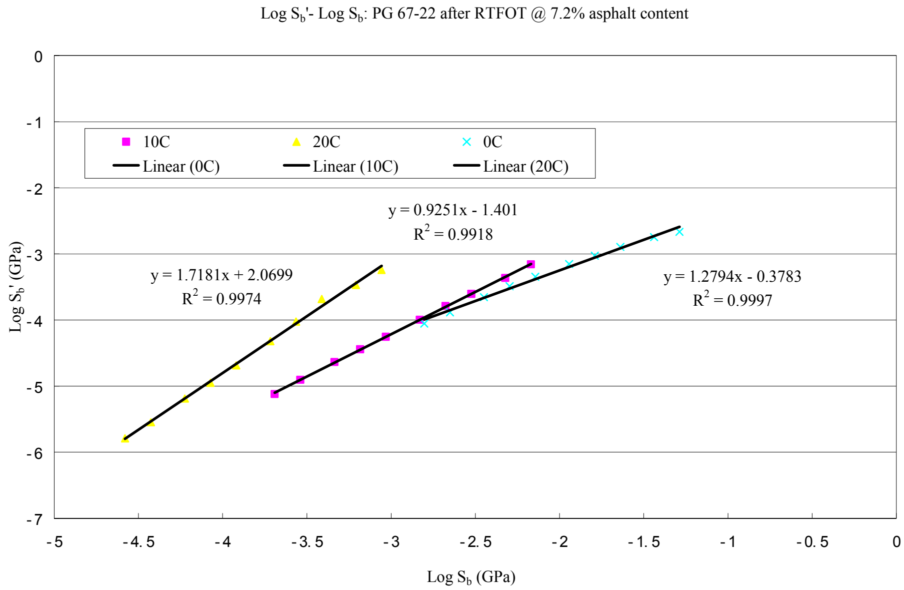

Figure 4.26 Log S_b' – log S_b relationship: PG 67-22, RTFOT aged @ 7.2% AC.

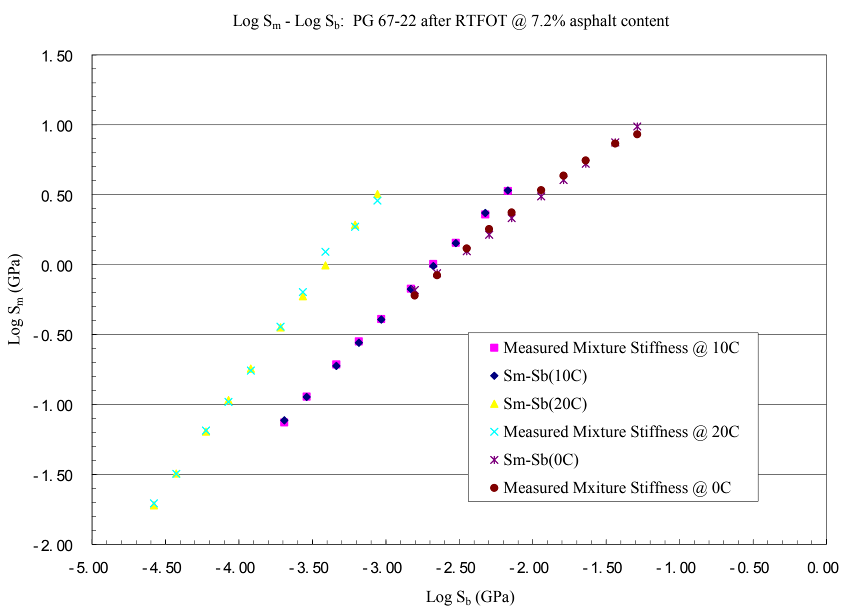

Figure 4.27 Log S_m – log S_b relationship: PG 67-22, RTFOT aged @ 7.2% AC.

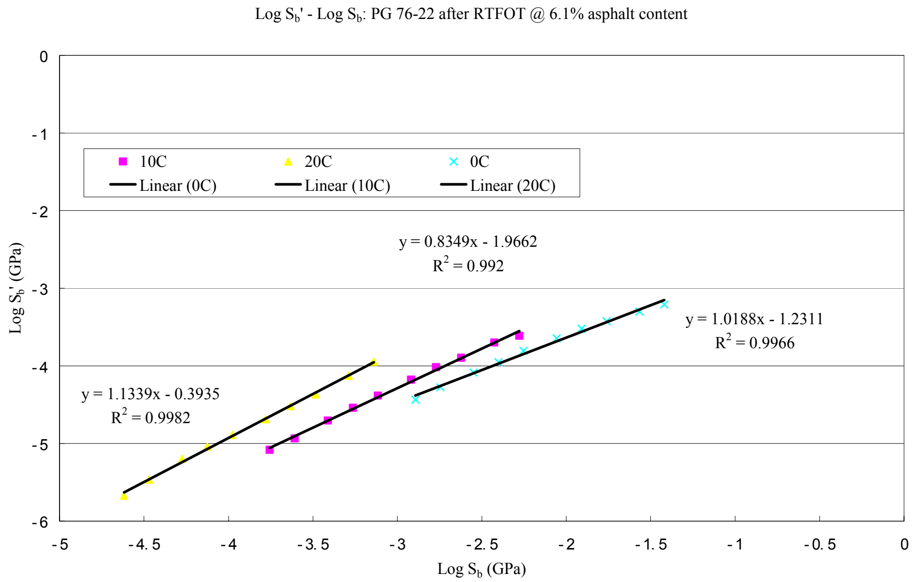

Figure 4.28 Log S_b' – log S_b relationship: PG 76-22, RTFOT aged @ 6.1% AC.

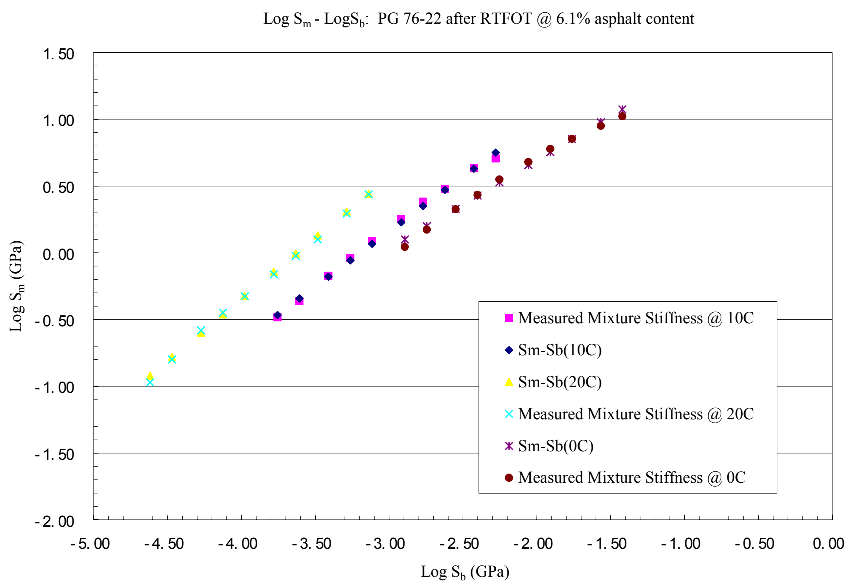

Figure 4.29 Log S_m – log S_b relationship: PG 76-22, RTFOT aged @ 6.1% AC.

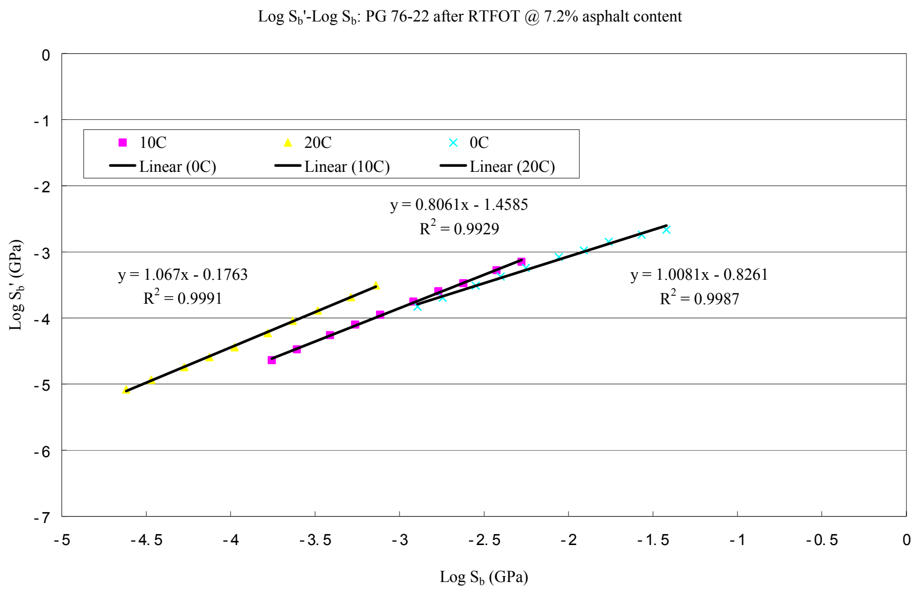

Figure 4.30 Log S_b' – log S_b relationship: PG 76-22, RTFOT aged @ 7.2% AC.

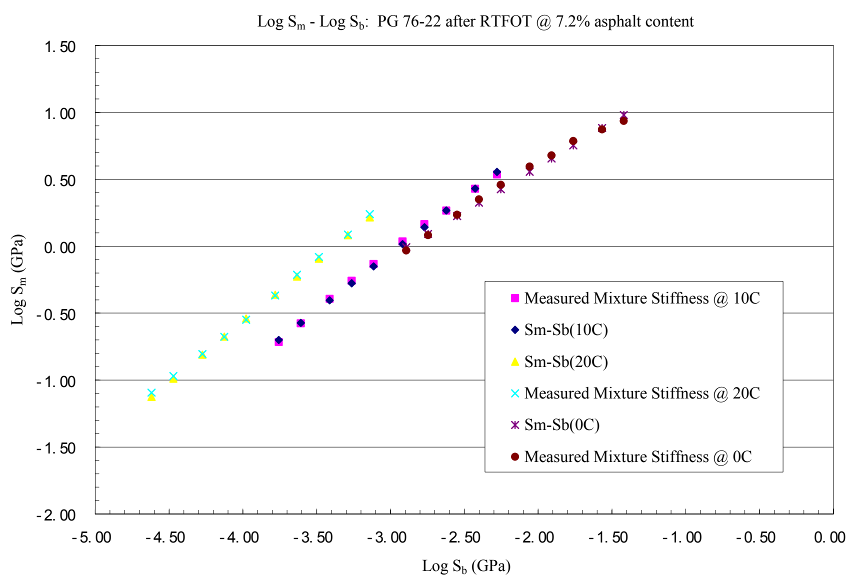

Figure 4.31 Log S_m – log S_b relationship: PG 76-22, RTFOT aged @ 7.2% AC.

predicted mixture stiffness using Equations 2.17 through 2.19, and Equation 4.3 matched well with the measured mixture stiffness.

4.5 Use of Binder-to-mixture Stiffness Relationship

This section discuss the use of the binder-to-mixture stiffness relationship to predict the mixture properties.

4.5.1 Prediction of the Mixture Stiffness for the Same Mixture

The above discussion showed that there is a separate binder-to-mixture stiffness relationship at each of the three temperatures for the same mixture. One of the objectives of this study is to investigate if the binder and mixture test results at one temperature could be used to predict the mixture properties at other temperatures. Predictions were made by taking the binder-to-mixture stiffness relationship at one temperature (Equations 4.5 and 2.17) and applying this relationship at other temperatures. The resulting predictions were plotted in Figures 4.32 through Figure 4.55.

These figures showed that the stiffness prediction using the binder-to-mixture stiffness relationship at 0° mostly underestimated the mixture stiffness at 10° and 20°, but matched well with the measured stiffness at 0°. The stiffness prediction using the binder-to-mixture stiffness relationship at 10° overestimated the mixture stiffness at 0° and underestimated the mixture stiffness at 20°, but matched well with the measured stiffness at 10°. The stiffness prediction using the binder-to-mixture stiffness relationship at 20° over estimated the mixture stiffness at 0° and 10°, but matched well with the measured stiffness at 20°.

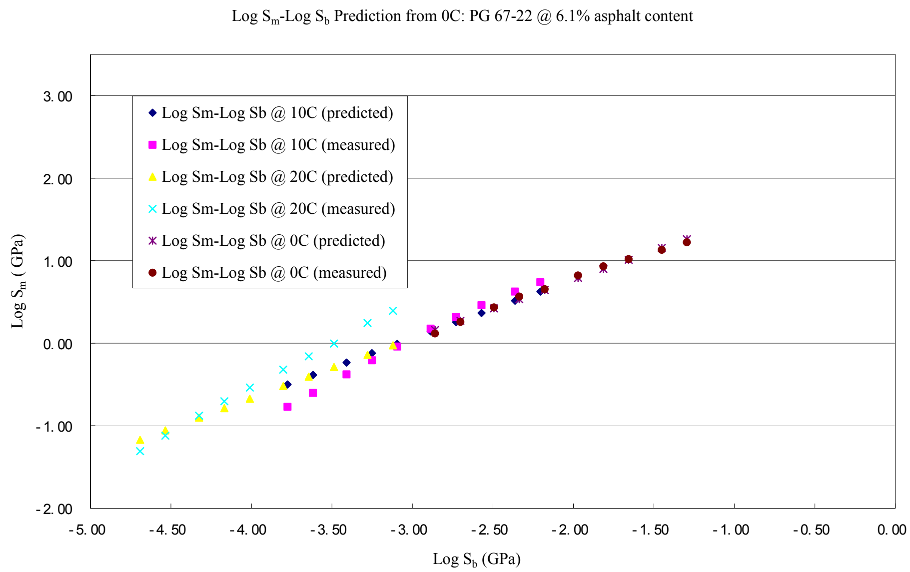

Figure 4.32 Stiffness prediction from PG 67-22,extracted binder @ 6.1% AC @ 0°.

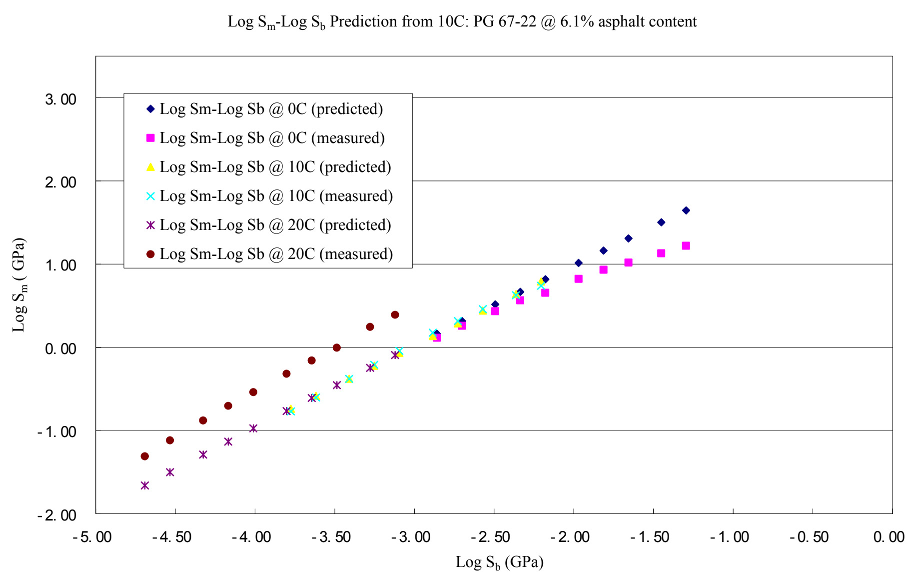

Figure 4.33 Stiffness prediction from PG 67-22,extracted binder @ 6.1% AC @ 10°.

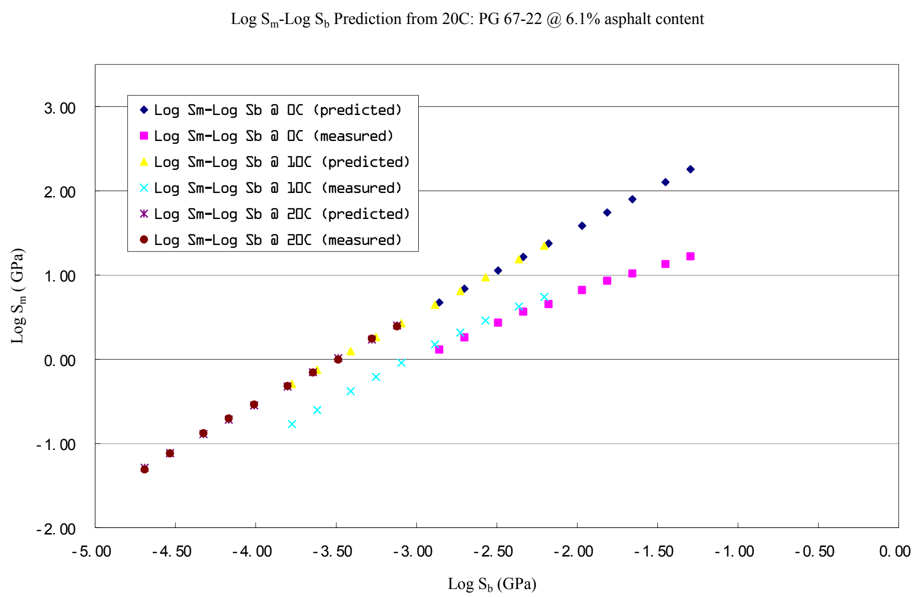

Figure 4.34 Stiffness prediction from PG 67-22,extracted binder @ 6.1% AC @ 20°.

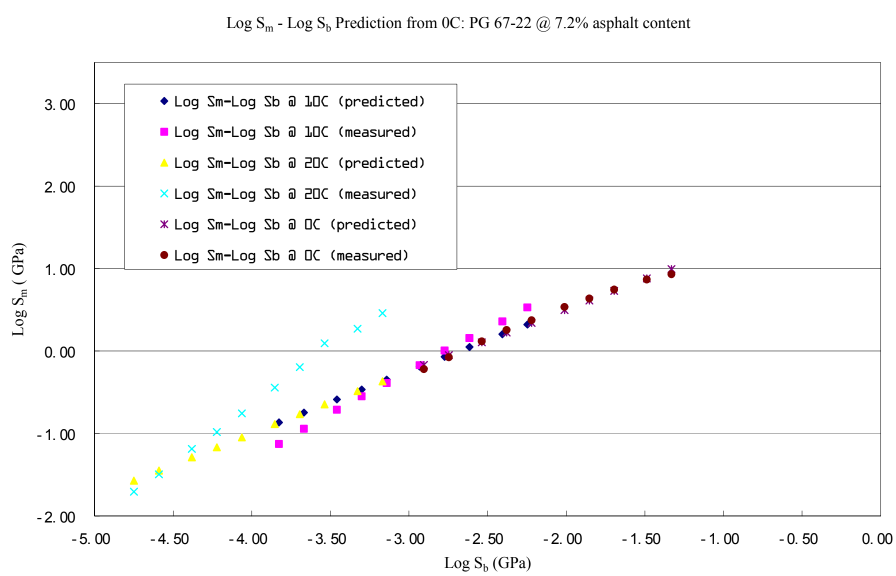

Figure 4.35 Stiffness prediction from PG 67-22, extracted binder @ 7.2% AC @ 0°.

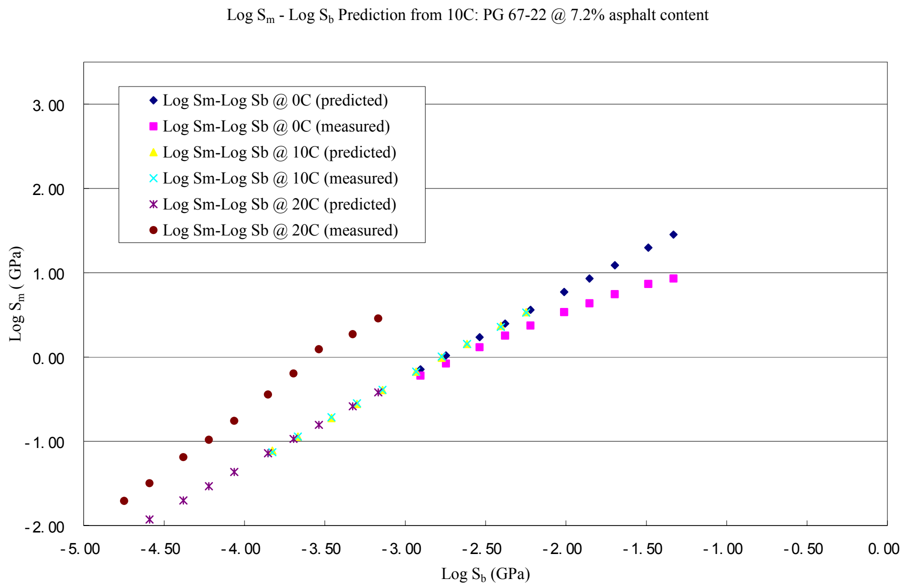

Figure 4.36 Stiffness prediction from PG 67-22,extracted binder @ 7.2% AC @ 10°.

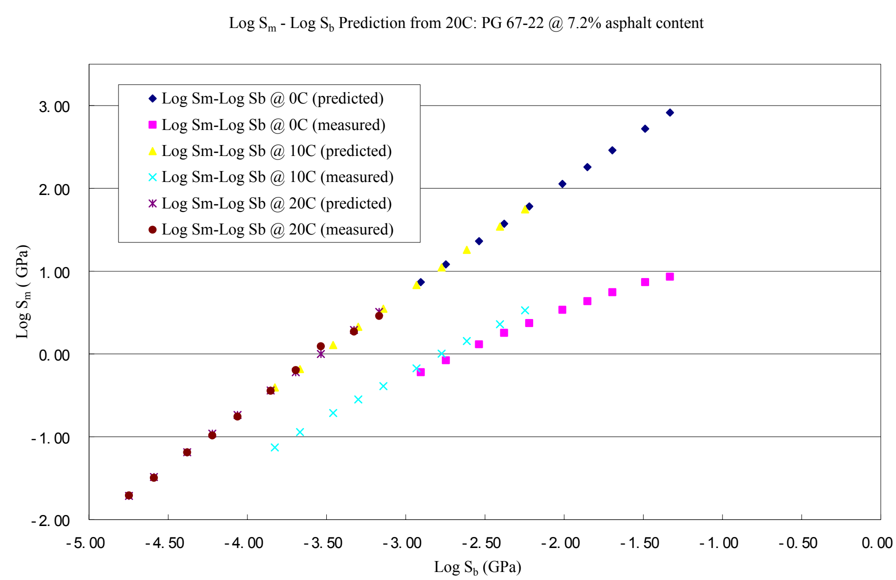

Figure 4.37 Stiffness prediction from PG 67-22, extracted binder @ 7.2% AC @ 20°.

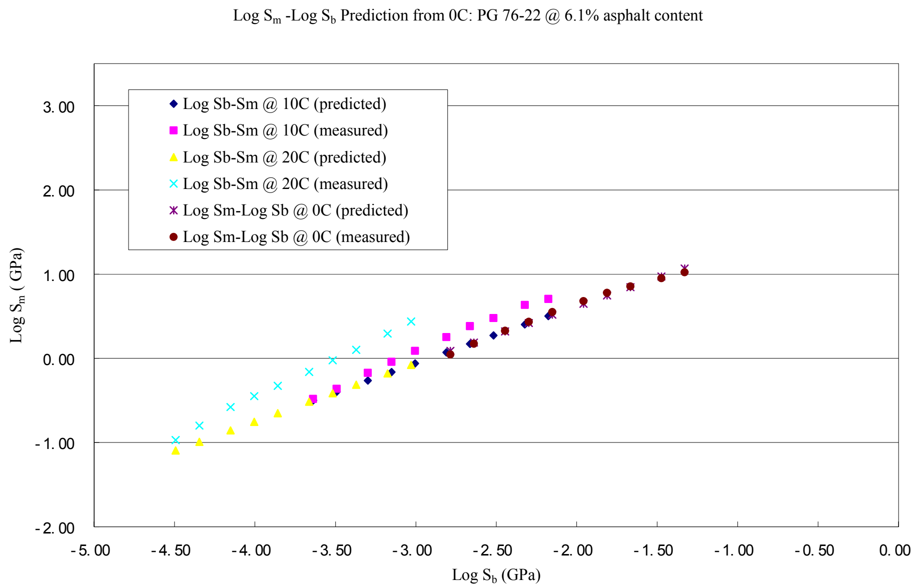

Figure 4.38 Stiffness prediction from PG 76-22, extracted binder @ 6.1% AC @ 0°.

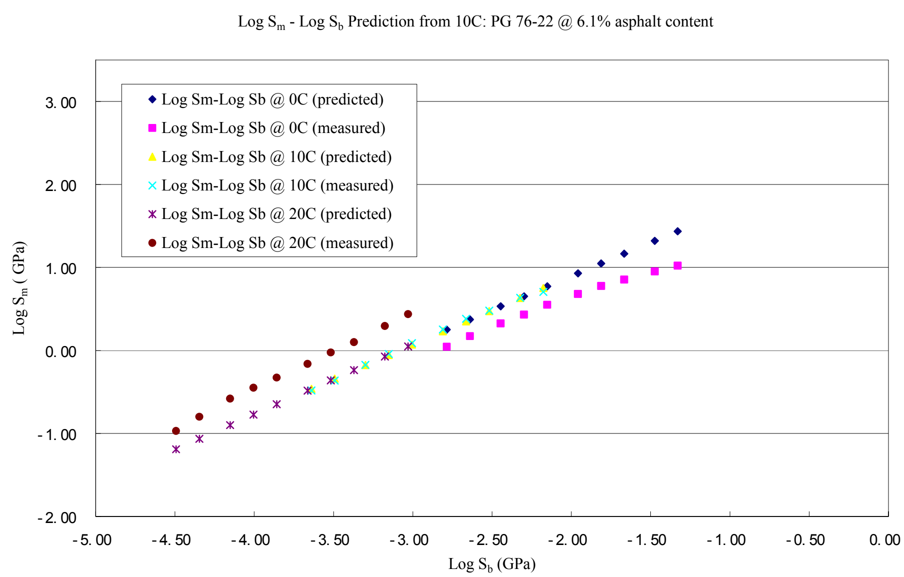

Figure 4.39 Stiffness prediction from PG 76-22, extracted binder @ 6.1% AC @ 10°.

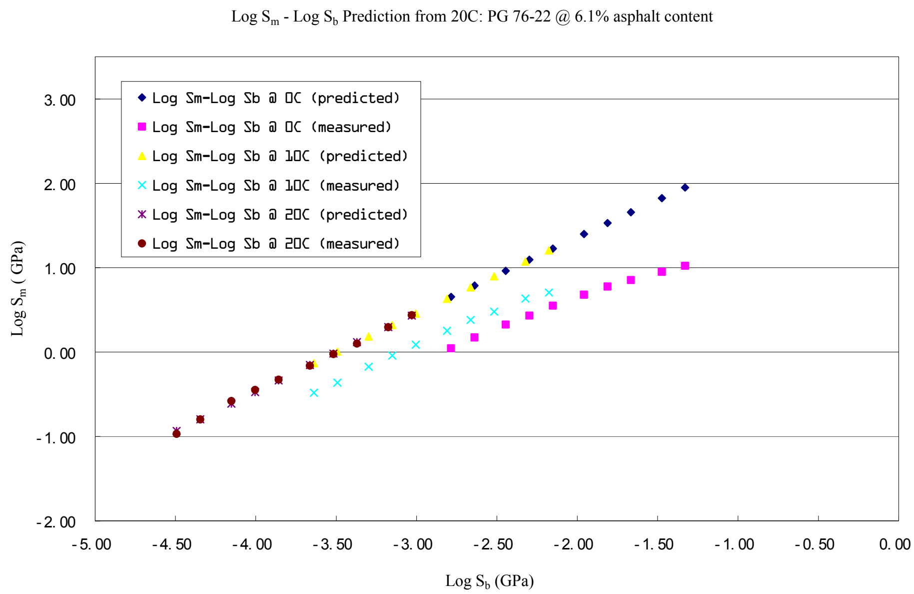

Figure 4.40 Stiffness prediction from PG 76-22, extracted binder @ 6.1% AC @ 20°.

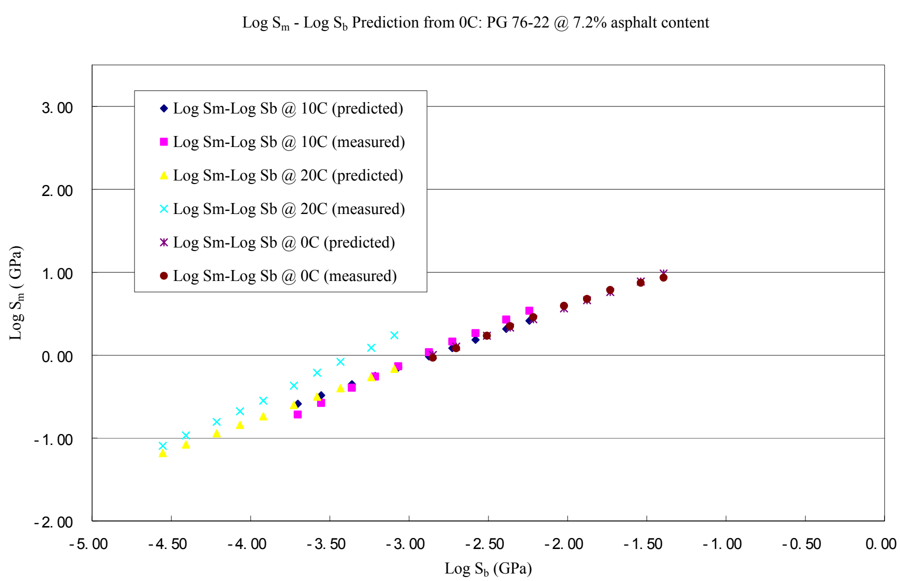

Figure 4.41 Stiffness prediction from PG 76-22, extracted binder @ 7.2% AC @ 0°.

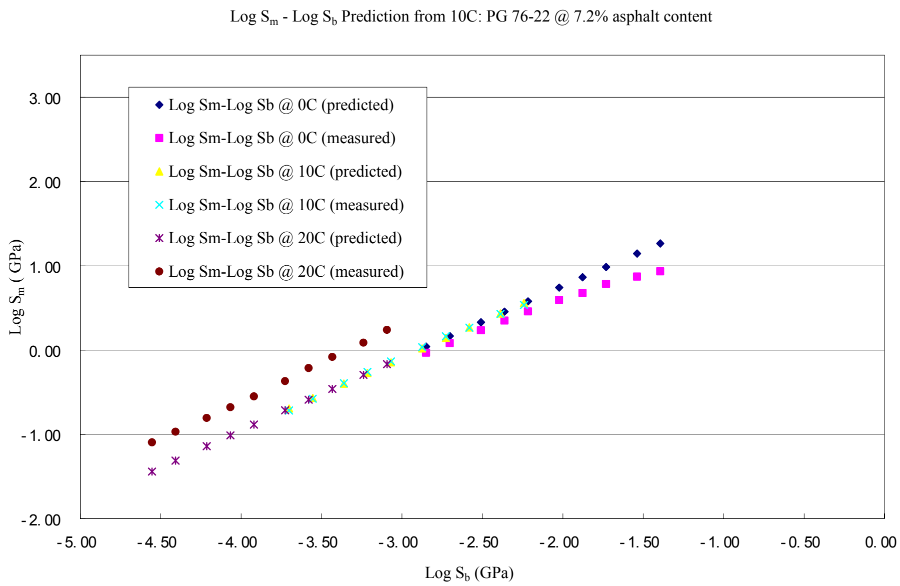

Figure 4.42 Stiffness prediction from PG 76-22,extracted binder @ 7.2% AC @ 10°.

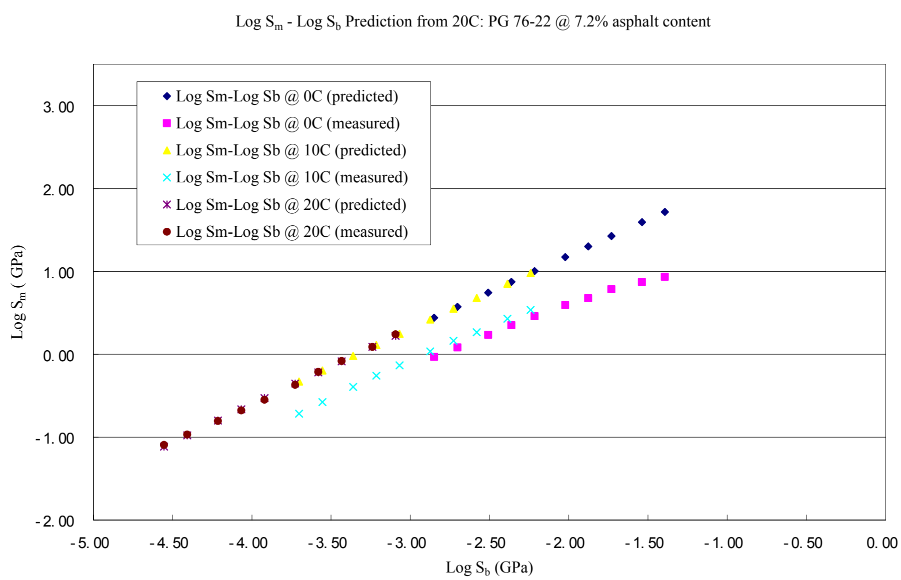

Figure 4.43 Stiffness prediction from PG 76-22, extracted binder @ 7.2% AC @ 20°.

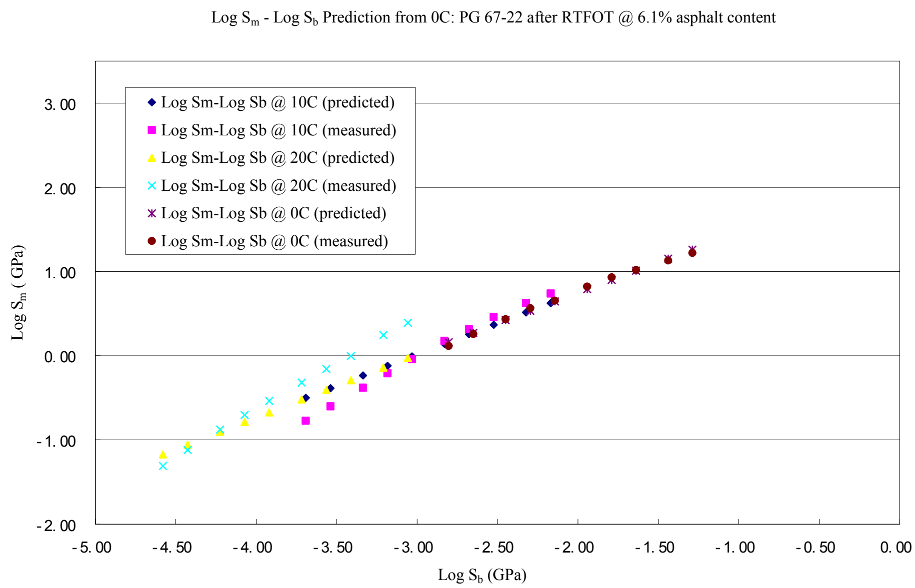

Figure 4.44 Stiffness prediction from PG 67-22, RTFOT aged @ 6.1% AC @ 0°.

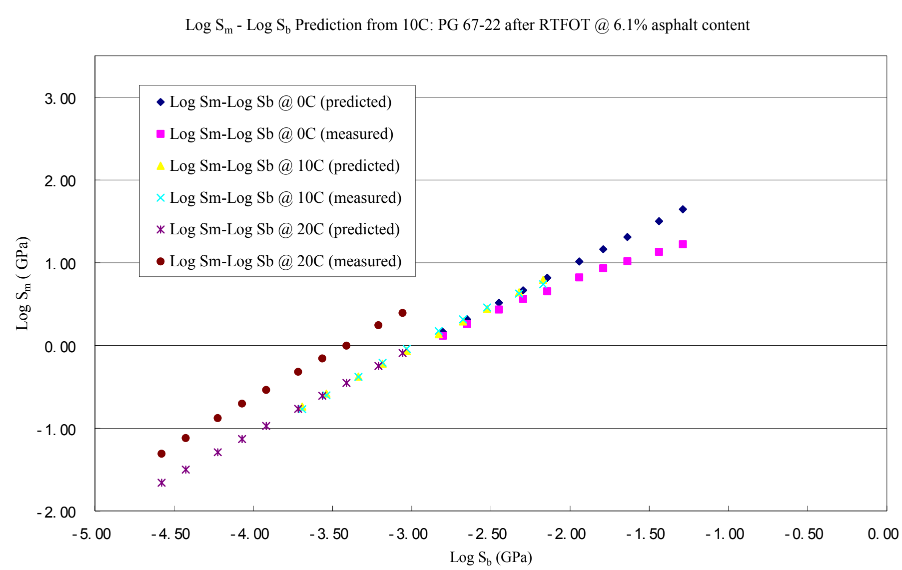

Figure 4.45 Stiffness prediction from PG 67-22, RTFOT aged @ 6.1% AC @ 10°.

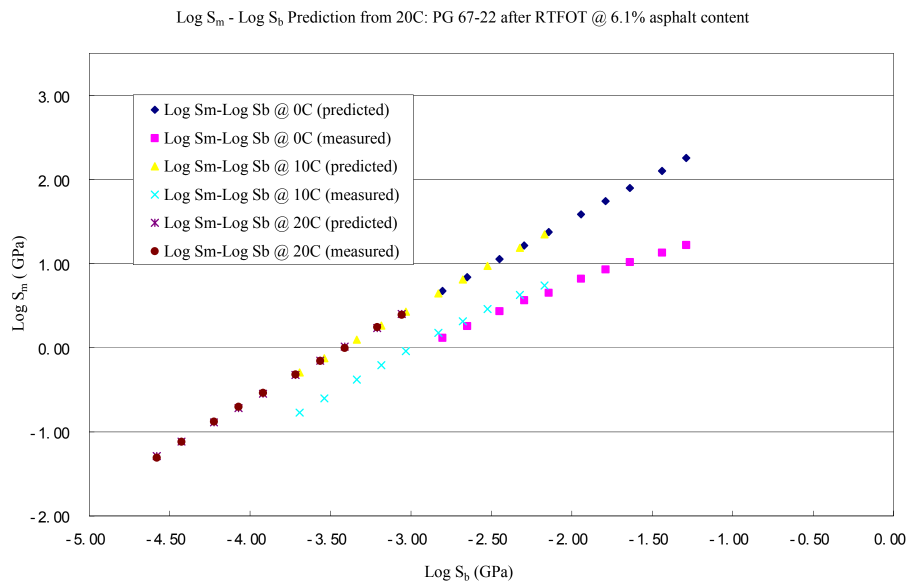

Figure 4.46 Stiffness prediction from PG 67-22, RTFOT aged @ 6.1% AC @ 20°.

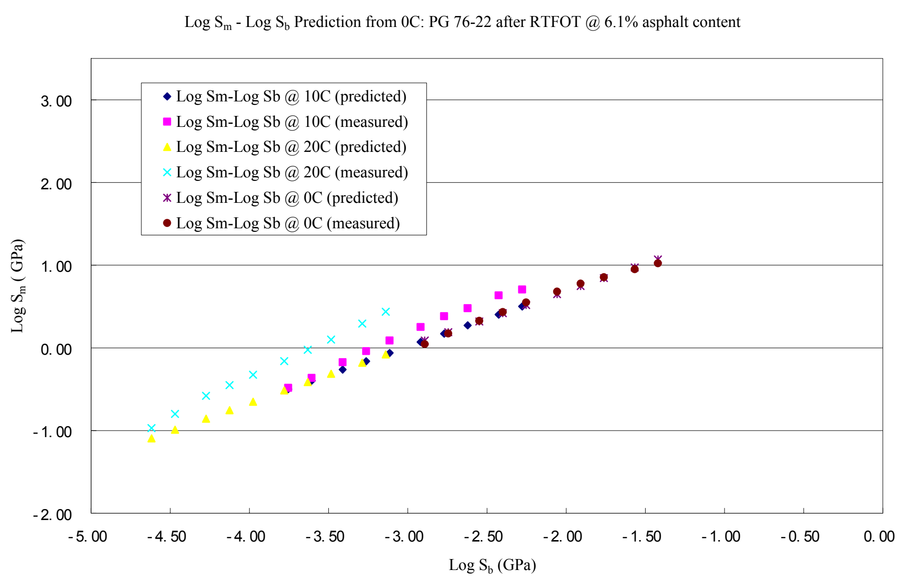

Figure 4.47 Stiffness prediction from PG 76-22, RTFOT aged @ 6.1% AC @ 0°.

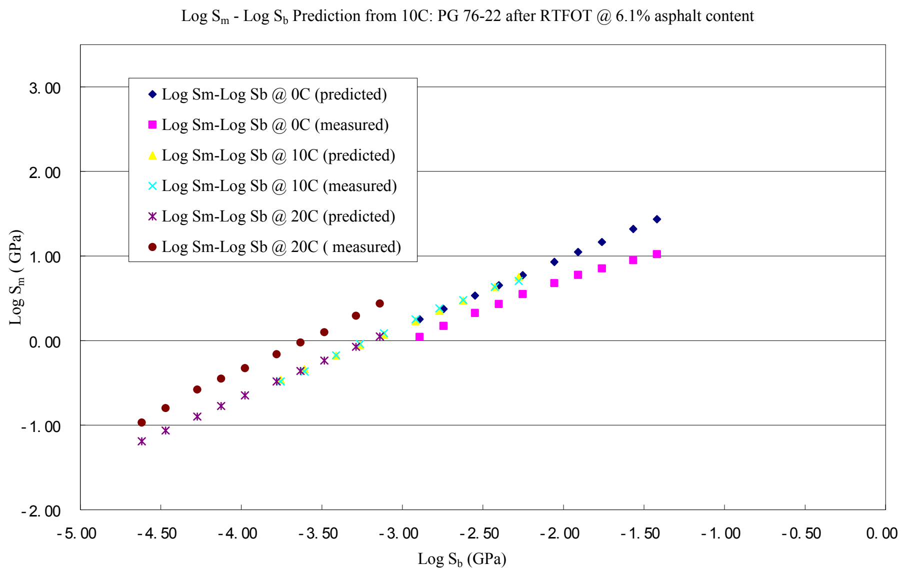

Figure 4.48 Stiffness prediction from PG 76-22, RTFOT aged @ 6.1% AC @ 10°.

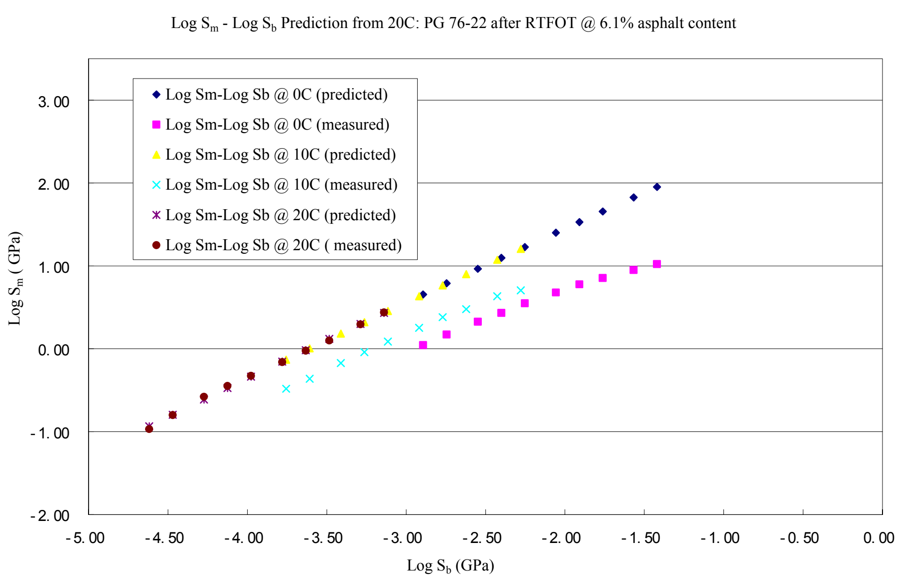

Figure 4.49 Stiffness prediction from PG 76-22, RTFOT aged @ 6.1% AC @ 20°.

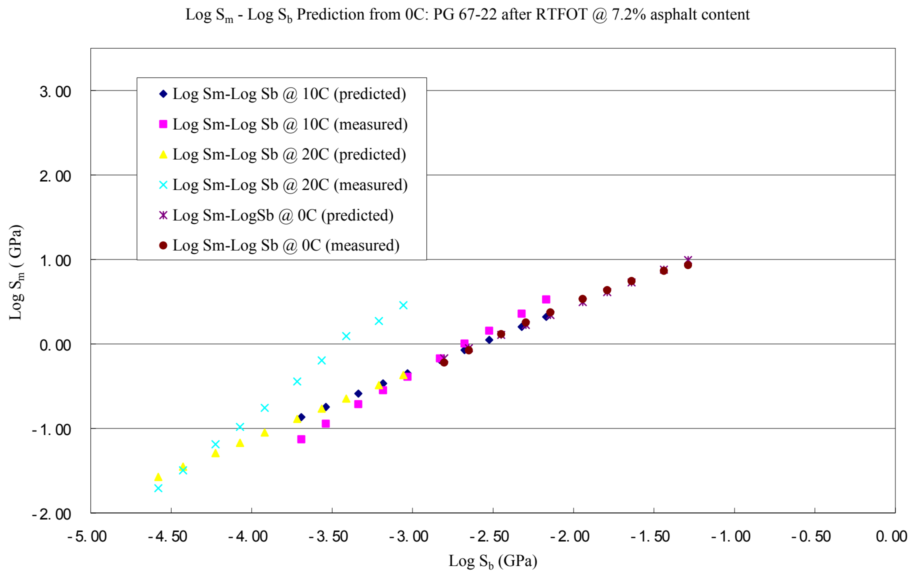

Figure 4.50 Stiffness prediction from PG 67-22, RTFOT aged @ 7.2% AC @ 0°.

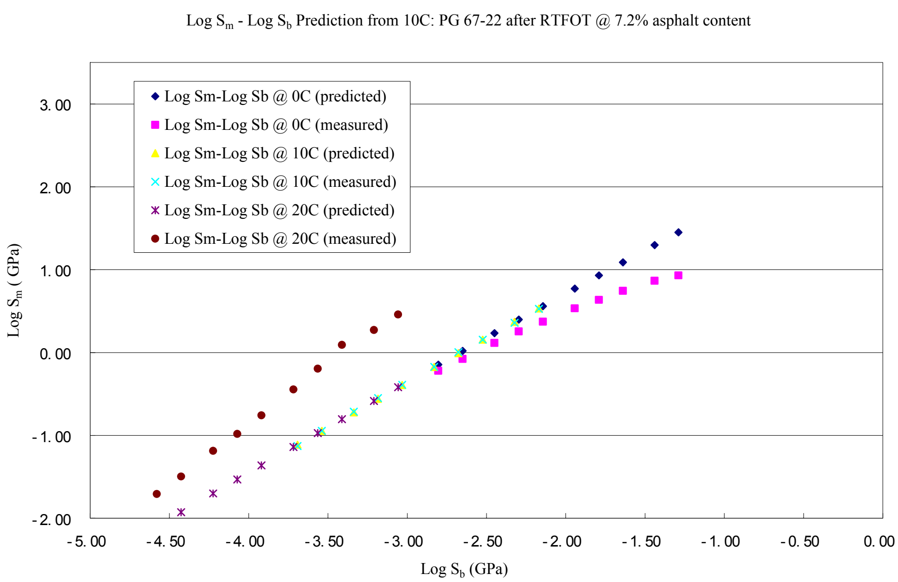

Figure 4.51 Stiffness prediction from PG 67-22, RTFOT aged @ 7.2% AC @ 10°.

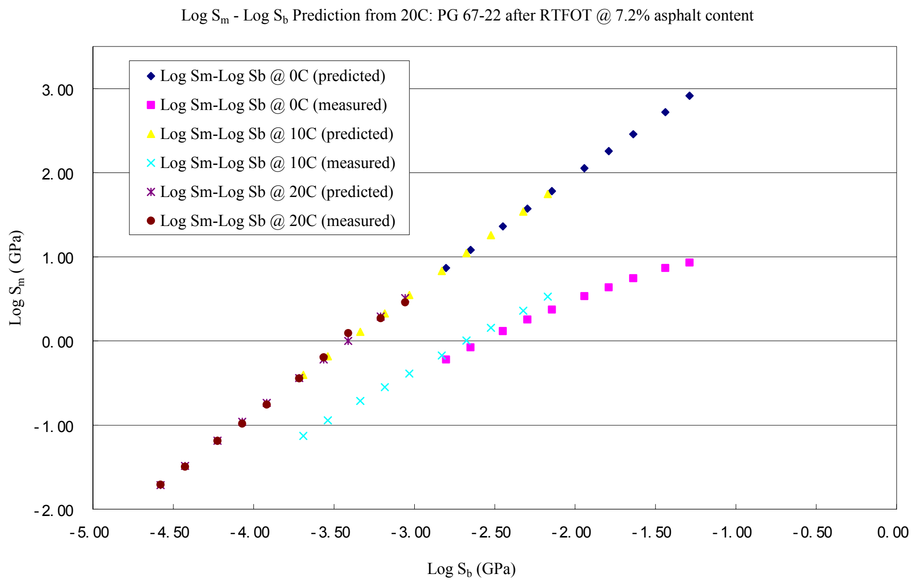

Figure 4.52 Stiffness prediction from PG 67-22, RTFOT aged @ 7.2% AC @ 20°.

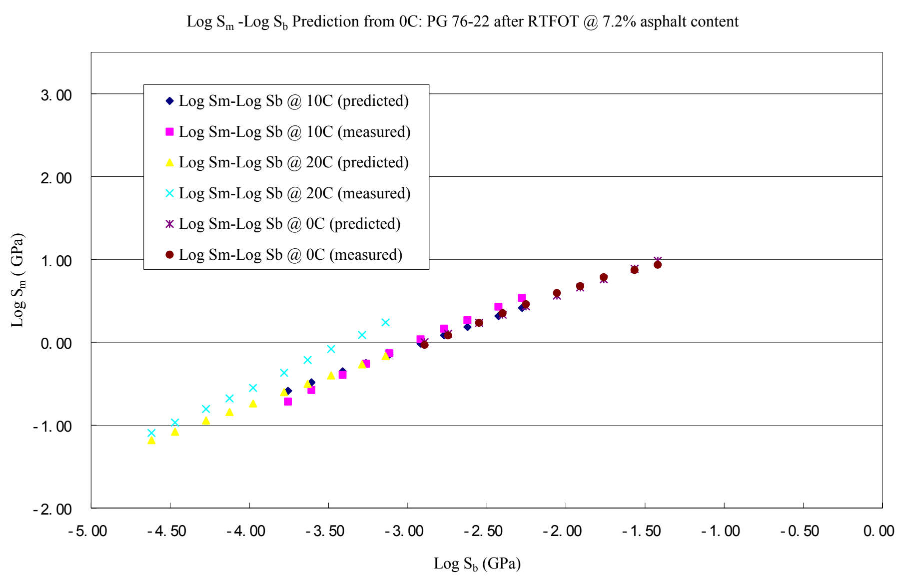

Figure 4.53 Stiffness prediction from PG 76-22, RTFOT aged @ 7.2% AC @ 0°.

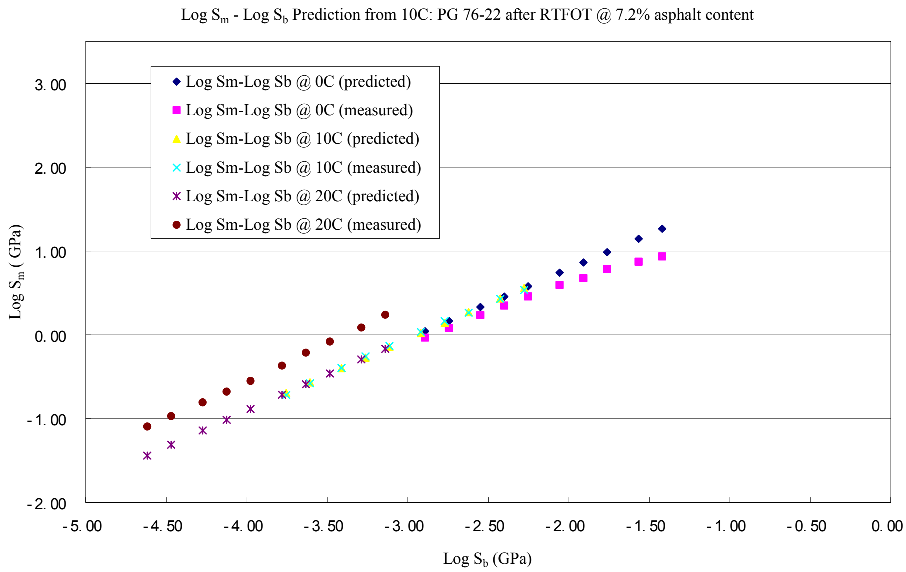

Figure 4.54 Stiffness prediction from PG 76-22, RTFOT aged @ 7.2% AC @ 10°.

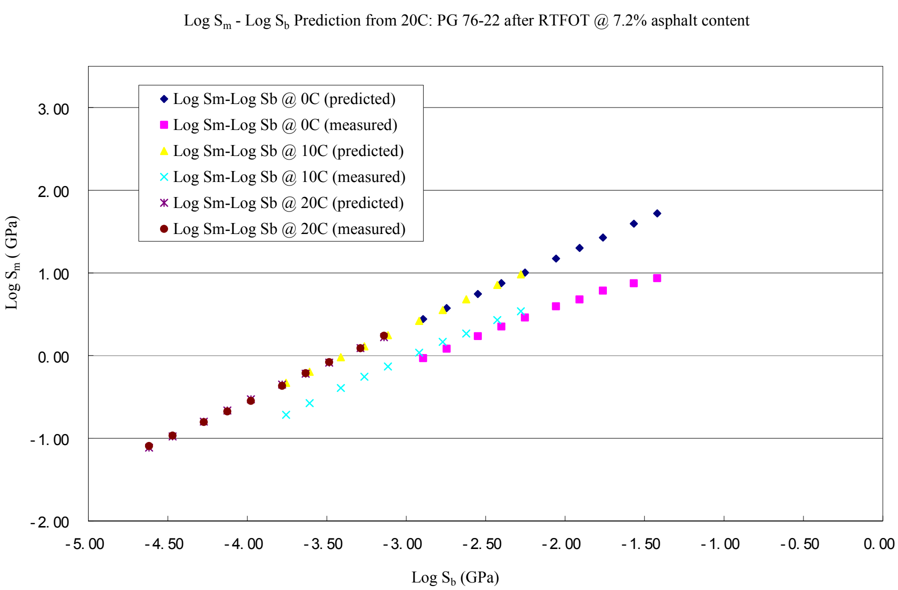

Figure 4.55 Stiffness prediction from PG 76-22, RTFOT aged @ 7.2% AC @ 20°.

4.5.2 Prediction of Mixture Stiffness for SBS Modified Mixture

One of the goals of this research is to find if the properties of the SBS modified mixtures could be predicted by using the binder-to-mixture stiffness relationship of unmodified mixture and the SBS modified binder properties. The stiffness prediction was made by taking the unmodified binder-to-mixture stiffness relationships and the SBS modified binder properties at the same temperature. The resulting predictions were plotted in Figure 4.56 through Figure 4.59.

Theses figures showed that the stiffness prediction by taking the unmodified binder-to-mixture stiffness and SBS modified binder properties is not bad for the SBS modified mixtures, especially at low temperatures, the predicted values are very close to the measure stiffness.

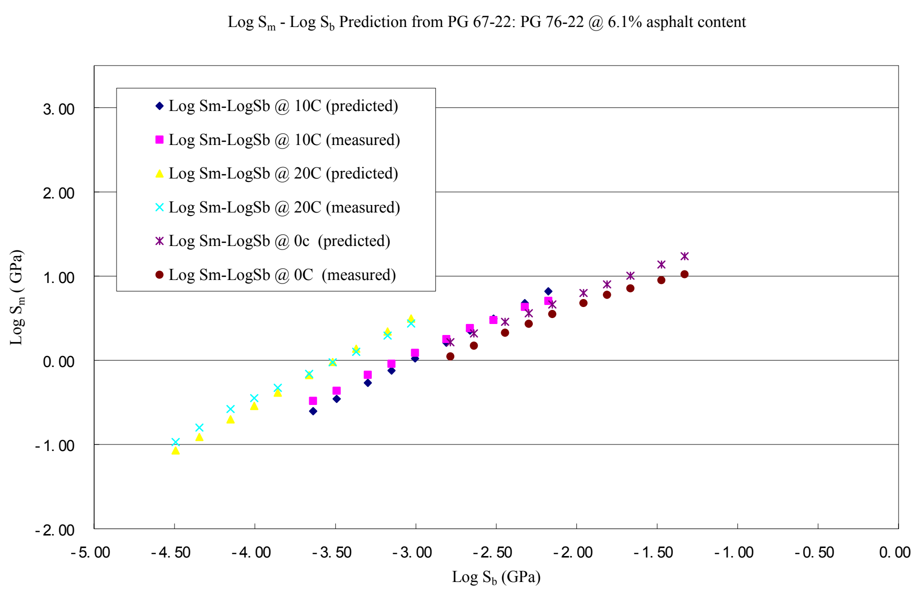

Figure 4.56 Stiffness prediction from PG 67-22, extracted binder @ 6.1% AC.

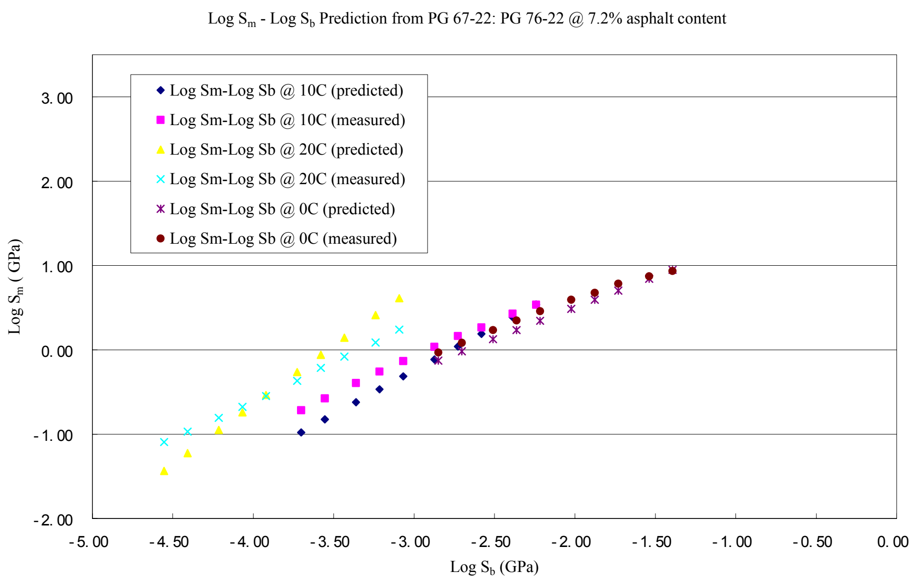

Figure 4.57 Stiffness prediction from PG 67-22, extracted binder @ 7.2% AC.

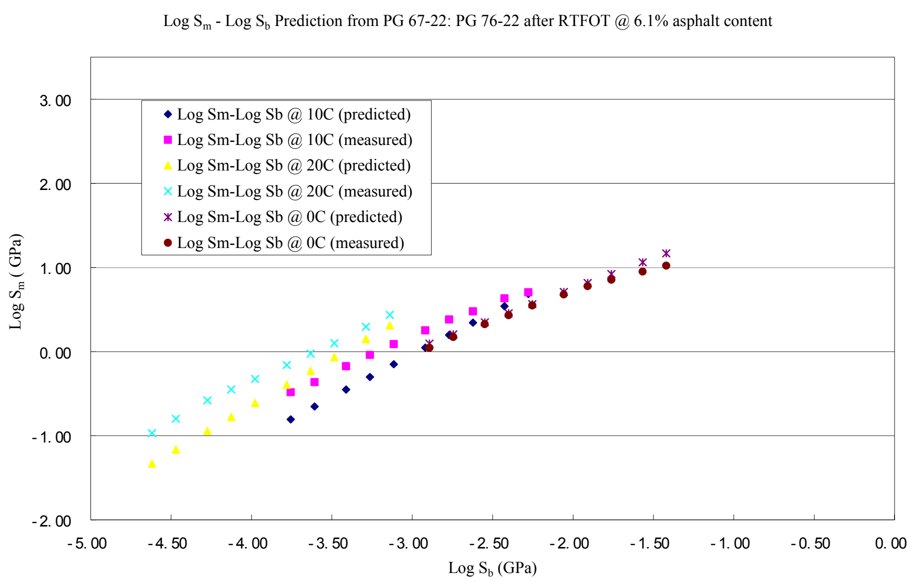

Figure 4.58 Stiffness prediction from PG 67-22, RTFOT aged @ 6.1% AC.

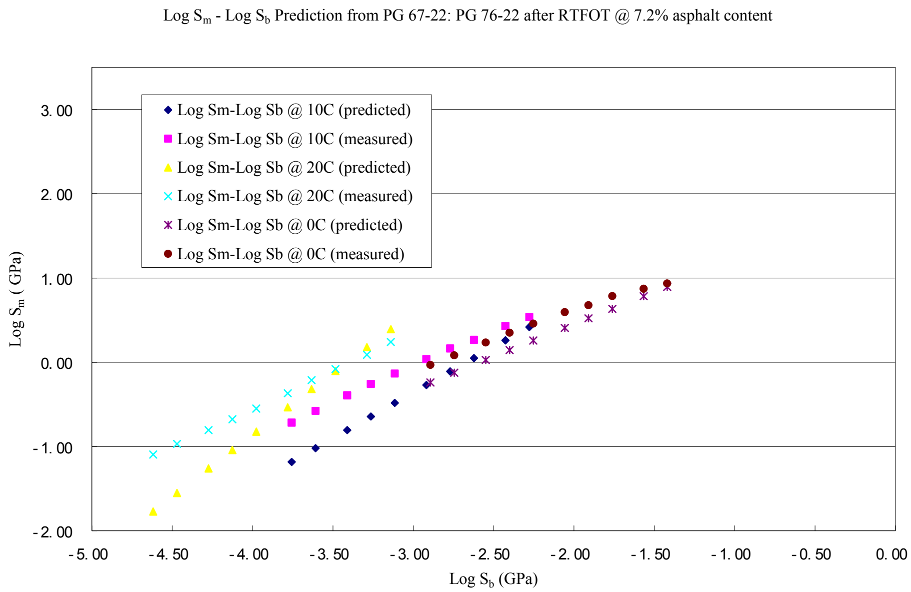

Figure 4.59 Stiffness prediction from PG 67-22, RTFOT aged @ 7.2% AC.

4.5.3 Use Energy Ratio for Comparison

As mentioned in Chapter 2, the energy ratio (ER) was developed at the University of Florida as a method to compare the cracking performances of different asphalt mixtures. This method was also used here to compare the difference in predicted performance observed by using the different way to generate the mixture properties needed for evaluation. ER was defined as follows: the energy ratio of the dissipated creep strain energy of the mixture to the minimum DCSE required for the mixture to perform satisfactorily. The resulting equation for energy ratio is:

$$ER = \frac{a \times DCSE_f}{m^{2.98} \times D_1} \qquad (2.36)$$

where $a = 0.0299\,\sigma^{-3.1}(6.36 - S_t) + 2.46 \times 10^{-8}$

σ = tensile stress of asphalt layer, psi

S_t = tensile strength, MPa

$DCSE_f$ = dissipated creep strain energy, KJ/m^3

D_1 = creep parameter, 1/psi

m = creep parameter.

To facilitate the computation, a tensile stress, σ was assumed as 230 psi, S_t and $DCSE_f$ were the measured for different mixtures using the Superpave IDT. Different data interpretation methods were used to obtain D_1 and m at each temperature. Each method is described in more detail in Table 4.7.

Table 4.7 Summary of Data Interpretation Methods

Method	Description
1	Mixture test data at one temperature combined with the binder shift factor to predict D_1 and m at multiple temperatures.
2	Mixture test data at one temperature combined with the master curve and shift factor to predict S_m at multiple temperatures assuming m from mix test at one temperature
3	Unmodified binder-to-mixture stiffness relationship at one temperature combined with the modified binder properties at the same temperature to predict the modified mixture properties.

Each method is described in more detail in the following paragraph.

Method 1:

1. Lock-in D_0 = 0.048 (1/GPa)
2. Determine D_1 and m at 20° from regression
3. Fix m = m at 20° (assuming m is a constant at three temperatures for the same mixture)
4. Calculate D_1 at 0° and 10° using the following relationship:

$$D_{1(0)} = D_{1(20)} \times \frac{1}{(a_{T(0)})^m} \tag{4.4}$$

$$D_{1(10)} = D_{1(20)} \times \frac{1}{(a_{T(10)})^m} \tag{4.5}$$

5. Repeat Steps 1-4 based on D_1 and m obtained at 0° and 10°, respectively.

By following the procedures above, the potential use of mixture tests at a single temperature to predict response and/or performance at multiple temperatures was evaluated from the measured data.

Method 2:

1. Predict the mixture stiffness at 20° using the binder-to-mixture stiffness at 20°
2. Lock-in D_0 = 0.048 (1/GPa)
3. Determine the D_1 and m at 20° from regression
4. Use the binder-to-mixture stiffness relationship at 20° to predict the mixture stiffness at 0° and 10° for different times
5. Calculate D_1 at 0° and 10° using the predicted mixture stiffness from step 4 and assuming:

   m = m at 20°

   D_0 = 0.048 (1/GPa)
6. Repeat Steps 1-5 starting 0° and 10°, respectively.

By the procedure above, the energy ratio was obtained from the predicted mixture data by using the binder-to-mixture stiffness relationship.

Method 3:

1. Develop the binder-to-mixture stiffness relationship for the unmodified mixture at each of the three temperatures
2. Predict the stiffness of modified mixture using the unmodified binder-to-mixture stiffness relationship at the same temperature
3. Lock-in D_0 = 0.048 (1/GPa)

4. Determine D_1 and m for the modified mixture.

Following the three procedures above, the resulting energy ratio (ER) was used to evaluate how well the binder-to-mixture stiffness relationship predicted the mixture properties. The comparisons were presented in Figures 4.60 through 4.85.

The comparison indicates that the using the binder-to-stiffness relationship gave a good prediction for energy ratio at 0° and 10° in most cases, but the results at 20° and the prediction from unmodified mixtures to SBS modified mixtures are not as good as at 0° and 10°.

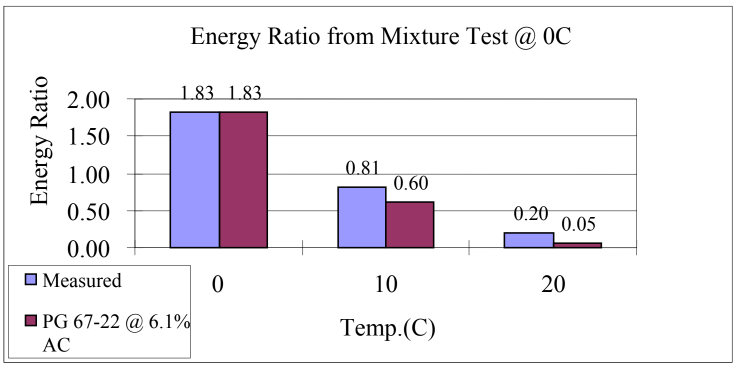

Figure 4.60 Energy ratio prediction: PG 67-22, 6.1% AC @ 0°.

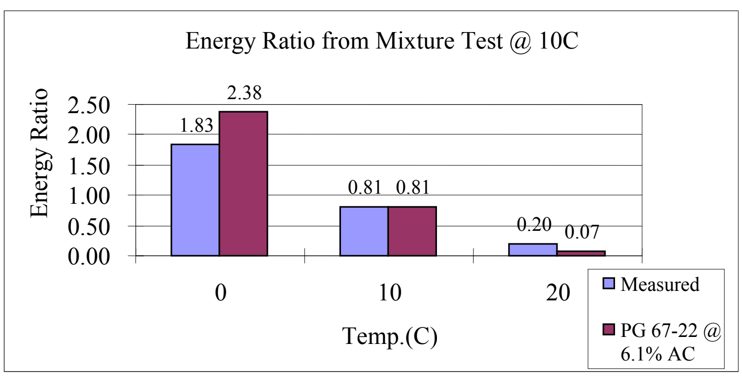

Figure 4.61 Energy ratio prediction: PG 67-22, 6.1% AC @ 10°.

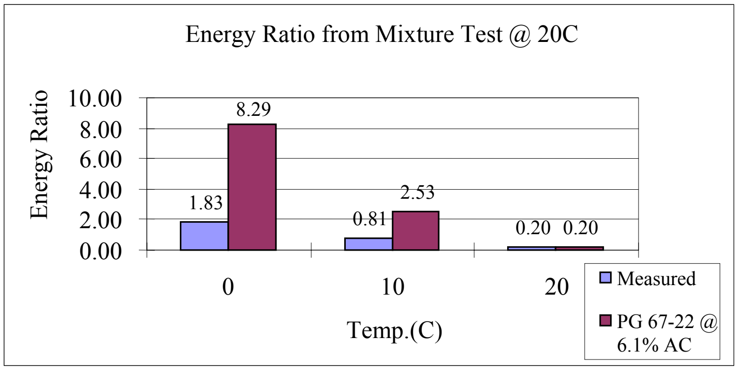

Figure 4.62 Energy ratio prediction: PG 67-22, 6.1% AC @ 20°.

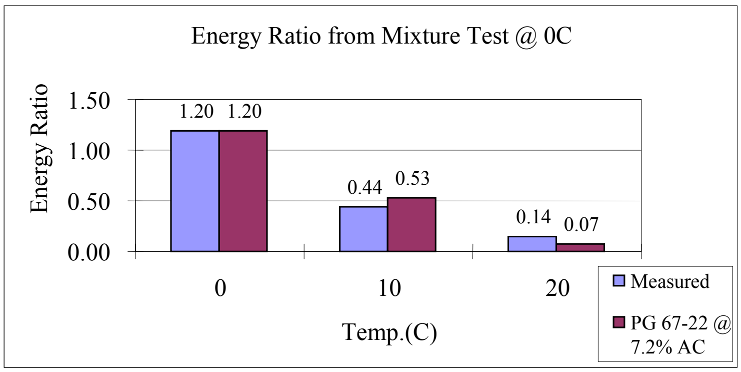

Figure 4.63 Energy ratio prediction: PG 67-22, 7.2% AC @ 0°.

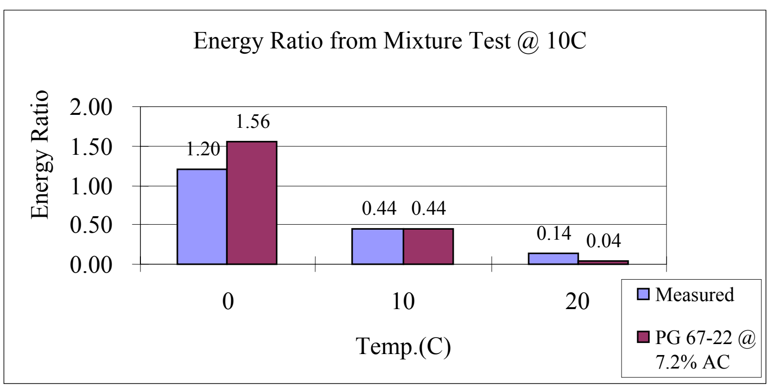

Figure 4.64 Energy ratio prediction: PG 67-22, 7.2% AC @ 10°.

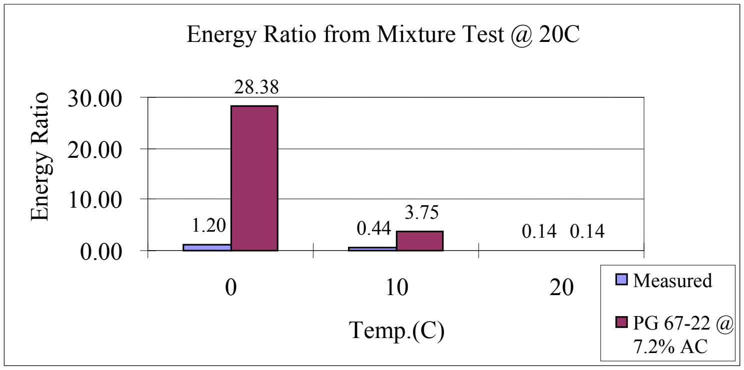

Figure 4.65 Energy ratio prediction: PG 67-22, 7.2% AC @ 20°.

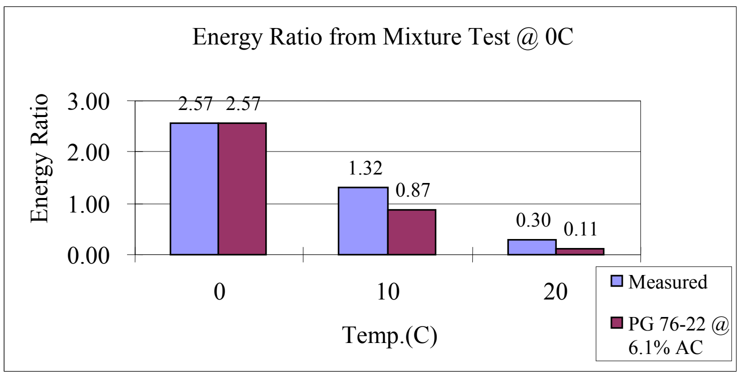

Figure 4.66 Energy ratio prediction: PG 76-22, 6.1% AC @ 0°.

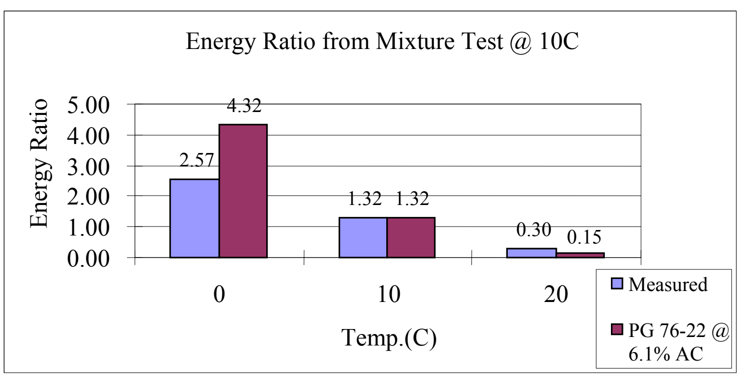

Figure 4.67 Energy ratio prediction: PG 76-22, 6.1% AC @ 10°.

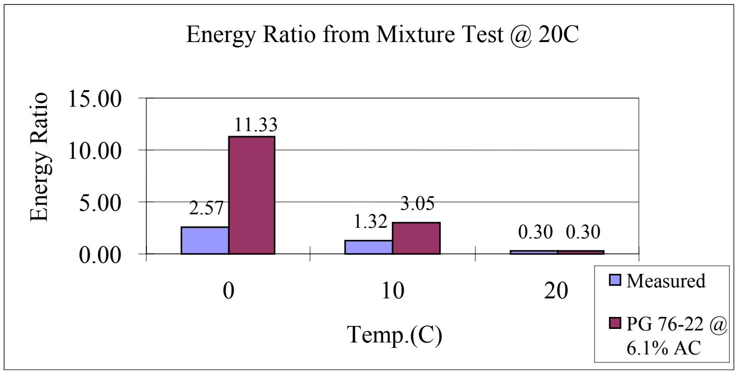

Figure 4.68 Energy ratio prediction: PG 76-22, 6.1% AC @ 20°.

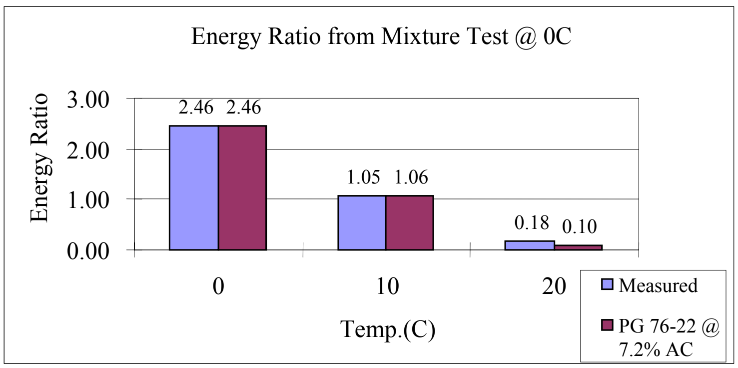

Figure 4.69 Energy ratio prediction: PG 76-22, 7.2% AC @ 0°.

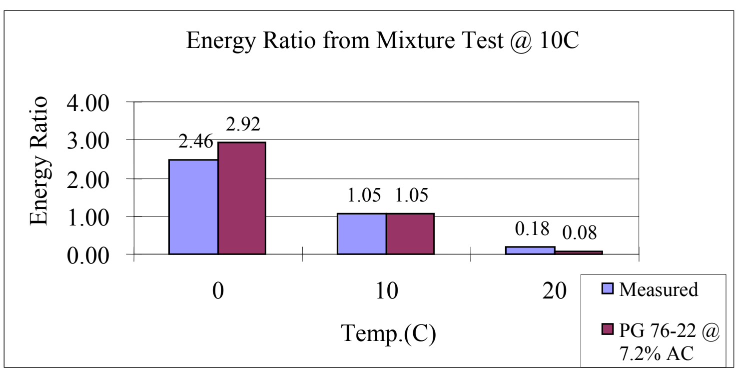

Figure 4.70 Energy ratio prediction: PG 76-22, 7.2% AC @ 10°.

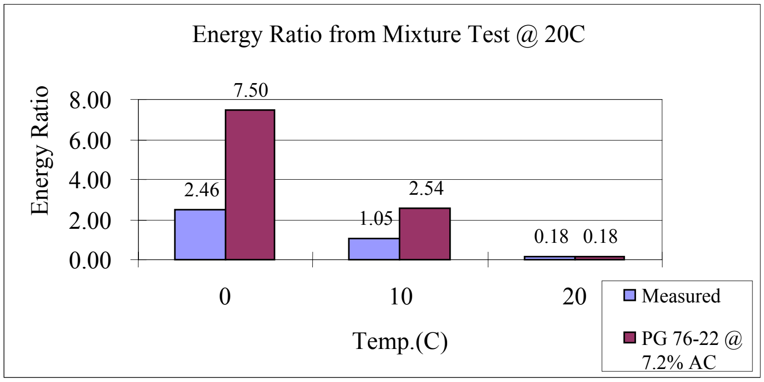

Figure 4.71 Energy ratio prediction: PG 76-22, 7.2% AC @ 20°.

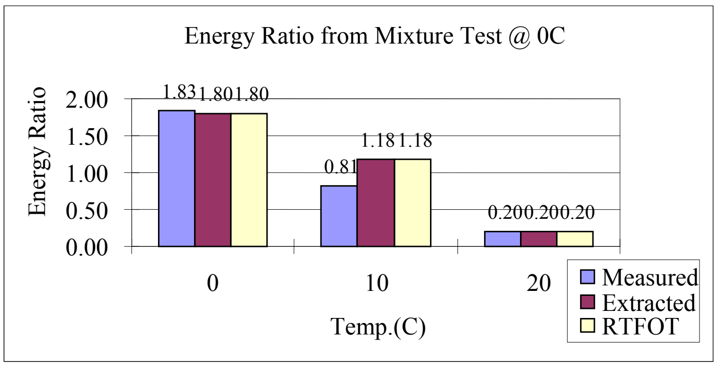

Figure 4.72 Energy ratio prediction: PG 67-22, 6.1% asphalt content @ 0°.

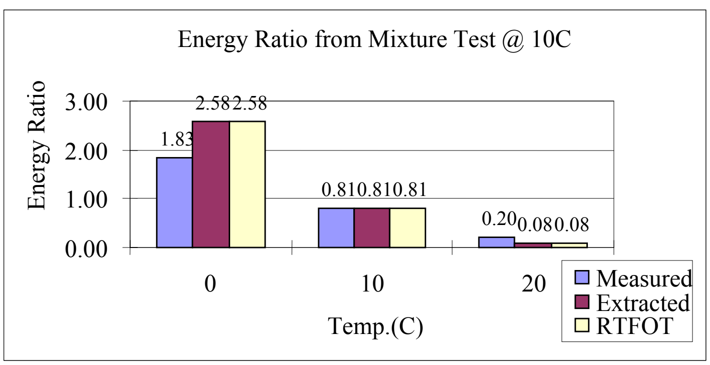

Figure 4.73 Energy ratio prediction: PG 67-22, 6.1% asphalt content @ 10°.

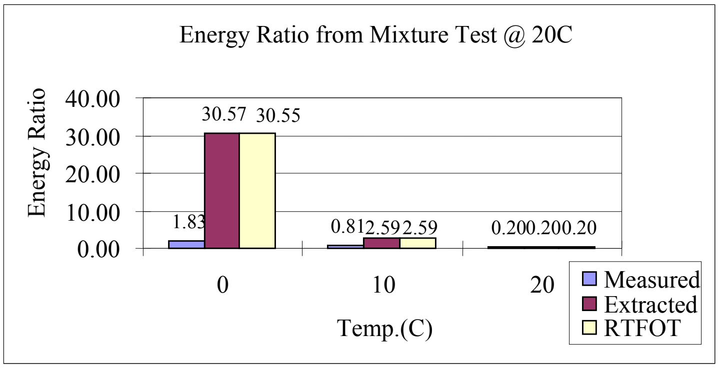

Figure 4.74 Energy ratio prediction: PG 67-22, 6.1% asphalt content @ 20°.

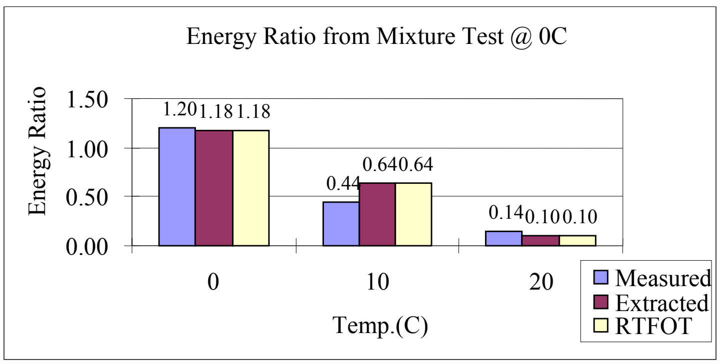

Figure 4.75 Energy ratio prediction: PG 67-22, 7.2% asphalt content @ 0°.

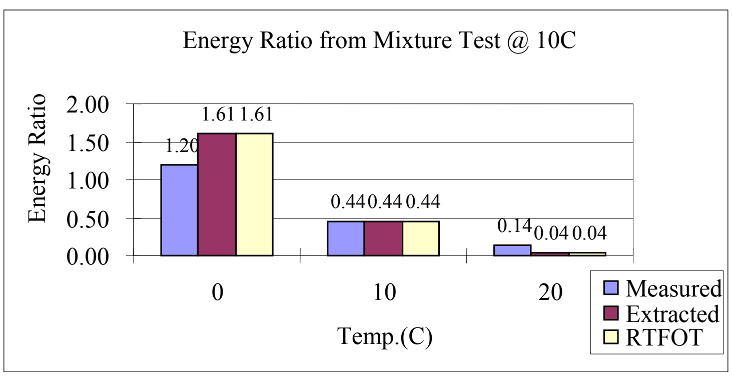

Figure 4.76 Energy ratio prediction: PG 67-22, 7.2% asphalt content @ 10°.

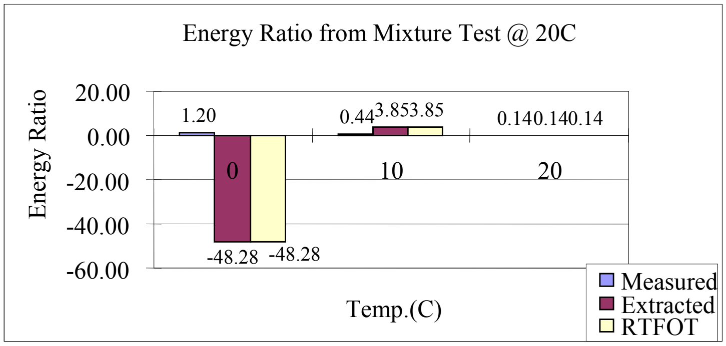

Figure 4.77 Energy ratio prediction: PG 67-22, 7.2% asphalt content @ 20°.

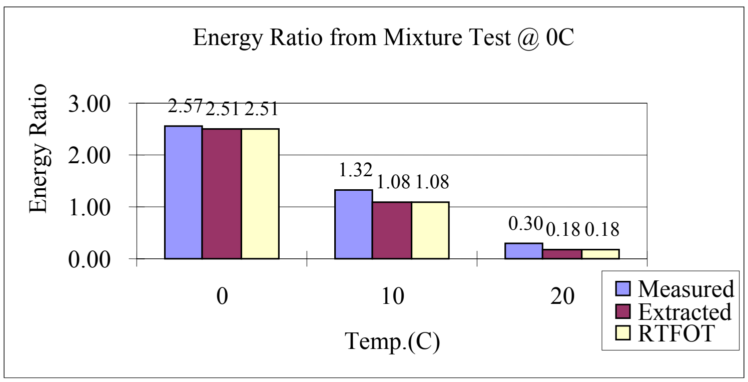

Figure 4.78 Energy ratio prediction: PG 76-22, 6.1% asphalt content @ 0°.

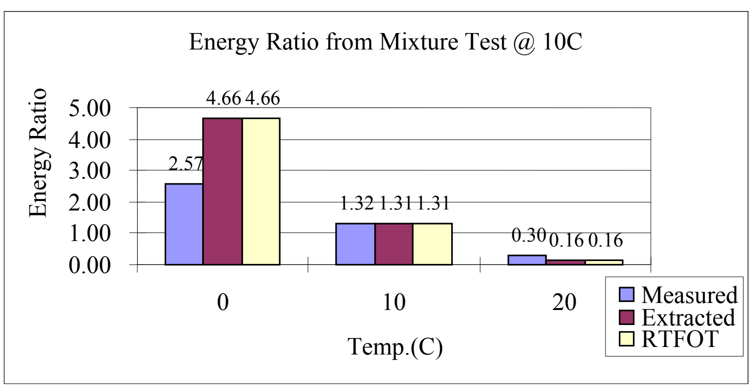

Figure 4.79 Energy ratio prediction: PG 76-22, 6.1% asphalt content @ 10°.

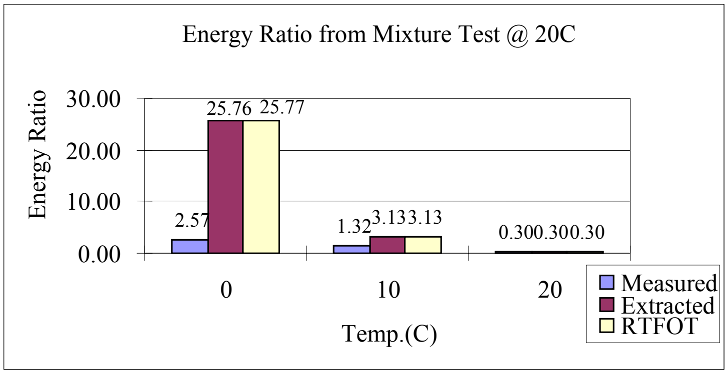

Figure 4.80 Energy ratio prediction: PG 76-22, 6.1% asphalt content @ 20°.

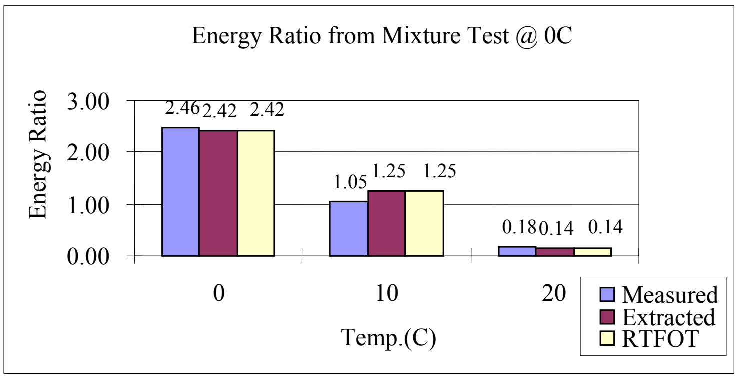

Figure 4.81 Energy ratio prediction: PG 76-22, 7.2% asphalt content @ 0°.

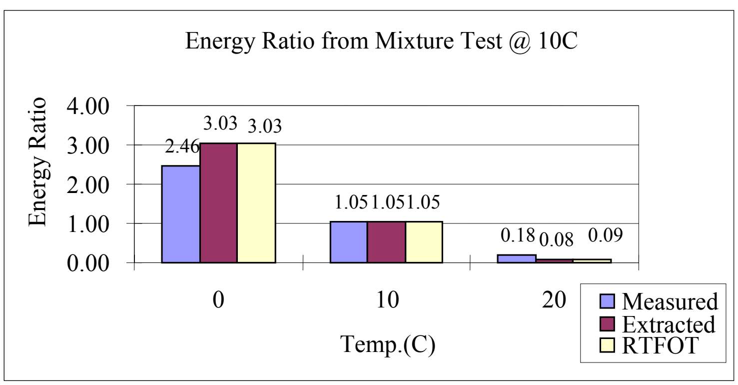

Figure 4.82 Energy ratio prediction: PG 76-22, 7.2% asphalt content @ 10°.

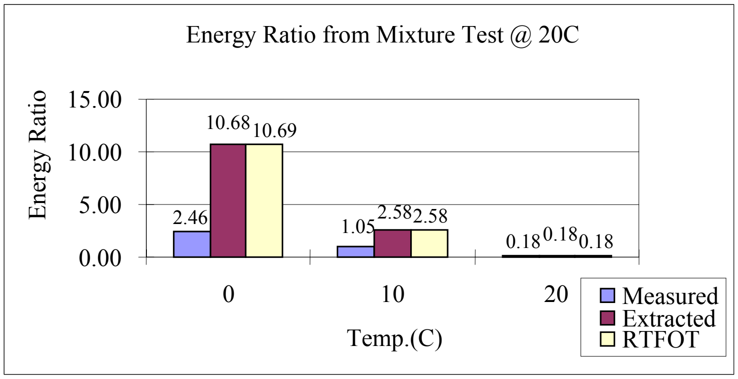

Figure 4.83 Energy ratio prediction: PG 76-22, 7.2% asphalt content @ 20°.

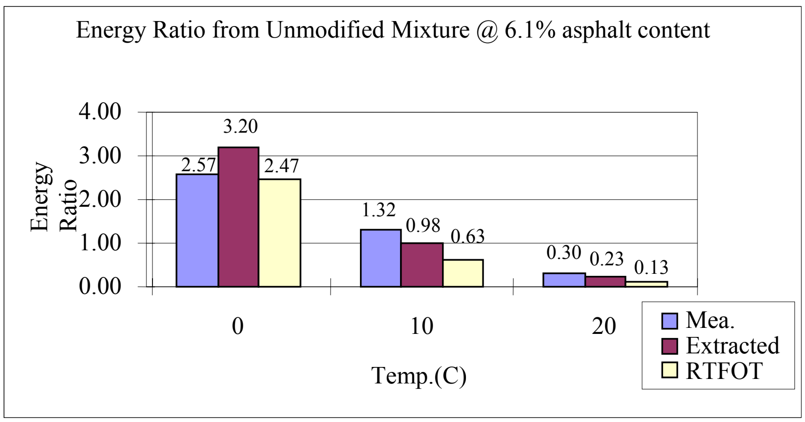

Figure 4.84 Energy ratio prediction from unmodified mixture @ 6.1% asphalt content.

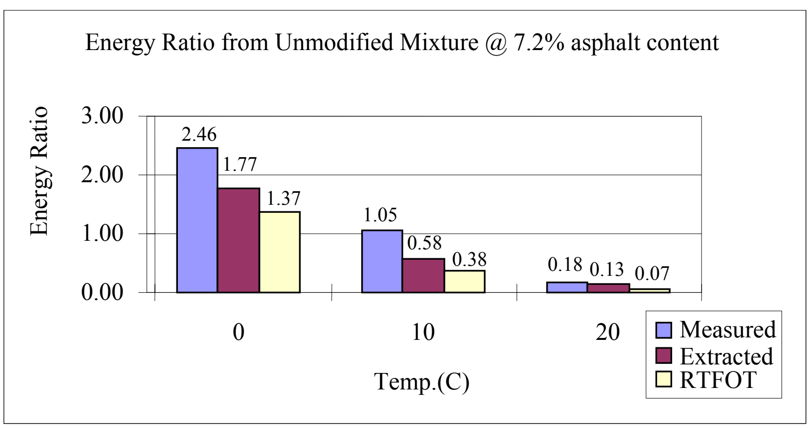

Figure 4.85 Energy ratio prediction from unmodified mixture @ 7.2% asphalt content.

CHAPTER 5
CLOSURE

5.1 Summary of Findings

Both the unmodified and SBS modified binders were obtained from the binder extraction process of the short-term oven aged (STOA) mixture and from the rolling thin film oven test aged virgin binder. The bending beam rheometer test and dynamic shear rheometer test were conducted on both binders at -10°, 10°, 20°, respectively. The binder test results were used to construct the binder creep compliance master curve. The binder-to-mixture stiffness relationship was developed using the binder creep compliance master curve and the mixture IDT test results at 0°, 10°, 20°. The binder-to-mixture stiffness relationship was then used to predict the mixture performance in different ways.

The findings of this study can be generalized as follows:

1. There is one binder-to-mixture stiffness relationship at each of the three temperatures. There is no single binder-to-mixture stiffness relationship for all temperatures in this study. Microdamage appears to develop at 0° and 10° and possibly at 20°.
2. The shift factors are different for the binders than for the mixtures.
3. To accurately generate the mixture master curve, the shift factors and the mixture data must be obtained from mixture tests at multiple temperatures
4. m-value of the binder is a constant independent of temperature
5. The use of the relationship at the lowest temperature does not give a conservative results for the crack prediction using HMA fracture mechanics.
6. The use of the binder-to-mixture stiffness relationship of unmodified binder to predict the performance of modified mixture does not give an accurate prediction.

7. The development and use of one single binder-to-mixture stiffness relationship for the mixtures with the same asphalt content ignoring the difference between different temperatures gives a good estimation of the mixture stiffness.
8. The use of the binder-to-mixture stiffness relationship at 0° and 10° to predict the mixture performance at 0° and 10° in most cases gives a accurate prediction.

5.2 Conclusion

Based on the above findings of this research the following conclusions were made about the development and use of the binder-to-mixture stiffness relationship.

1. There is no single binder-to-mixture stiffness relationship at all temperatures and the shift factors are different for the binders than for the mixtures.
2. Accurate determination of the mixture creep compliance master curve require mixture data at multiple temperatures
3. It seems that the prediction for the mixture performance at 0° and 10° is mostly accurate using the binder-to-mixture stiffness relationship at 0° and 10°.

5.3 Recommendation

It seems that microdamage is a possible factor affecting the binder-to-mixture stiffness relationship. Thus, for further studies it is recommended that the effect of the microdamage be characterized in the development of the binder-to-mixture stiffness relationship.

APPENDIX A
BENDING BEAM RHEOMETER TEST RESULTS

Table A.1 Bending Beam Rheometer Test Results: PG 67-22, 6.1% Asphalt Content

Time (sec.)	Replicate	Measured Stiffness (MPa)	Average	m-value	Average
8	1	119	122	0.395	0.389
	2	126		0.392	
	3	121		0.381	
15	1	91.7	94.60	0.423	0.416
	2	97.8		0.417	
	3	94.3		0.409	
30	1	67.8	70.23	0.454	0.446
	2	72.6		0.445	
	3	70.3		0.439	
60	1	49.0	51.07	0.484	0.475
	2	52.8		0.472	
	3	51.4		0.469	
120	1	34.7	36.43	0.515	0.505
	2	37.8		0.500	
	3	36.8		0.500	
240	1	24.0	25.37	0.546	0.535
	2	26.4		0.528	
	3	25.7		0.535	

Table A.2 Bending Beam Rheometer Test Results: PG 76-22, 6.1% Asphalt Content

Time (sec.)	Replicate	Measured Stiffness (MPa)	Average	m-value	Average
8	1	106	109.33	0.379	0.385
	2	111		0.388	
	3	111		0.387	
15	1	82.7	84.93	0.401	0.408
	2	86.0		0.414	
	3	86.1		0.410	
30	1	62.0	63.40	0.425	0.434
	2	63.9		0.442	
	3	64.3		0.436	
60	1	45.9	46.57	0.450	0.460
	2	46.7		0.470	
	3	47.1		0.461	
120	1	33.3	33.53	0.474	0.487
	2	33.4		0.499	
	3	33.9		0.487	
240	1	23.8	23.73	0.498	0.513
	2	23.4		0.527	
	3	24.0		0.513	

Table A.3 Bending Beam Rheometer Test Results: PG 67-22, 7.2% Asphalt Content

Time (sec.)	Replicate	Measured Stiffness (MPa)	Average	m-value	Average
8	1	114	113.33	0.403	0.398
	2	112		0.398	
	3	114		0.394	
15	1	87.4	87.43	0.428	0.423
	2	86.7		0.423	
	3	88.2		0.419	
30	1	64.3	64.57	0.455	0.451
	2	64.0		0.451	
	3	65.3		0.447	
60	1	46.6	46.83	0.483	0.479
	2	46.4		0.479	
	3	47.5		0.475	
120	1	33.1	33.33	0.510	0.507
	2	33.0		0.507	
	3	33.9		0.503	
240	1	22.9	23.17	0.538	0.535
	2	23.0		0.535	
	3	23.6		0.531	

Table A.4 Bending Beam Rheometer Test Results: PG 76-22, 7.2% Asphalt Content

Time (sec.)	Replicate	Measured Stiffness (MPa)	Average	m-value	Average
8	1	94.5	95.80	0.396	0.395
	2	95.5		0.395	
	3	97.4		0.394	
15	1	72.9	74.00	0.423	0.421
	2	73.8		0.421	
	3	75.3		0.418	
30	1	53.8	54.77	0.453	0.448
	2	54.6		0.449	
	3	55.9		0.443	
60	1	39.0	39.80	0.483	0.477
	2	39.6		0.478	
	3	40.8		0.469	
120	1	27.6	28.33	0.513	0.505
	2	28.2		0.507	
	3	29.2		0.495	
240	1	19.1	19.73	0.543	0.533
	2	19.6		0.536	
	3	20.5		0.521	

Table A.5 Bending Beam Rheometer Test Results: PG 67-22, RTFOT Aged

Time (sec.)	Replicate	Measured Stiffness (MPa)	Average	m-value	Average
8	1	117	123.67	0.392	0.391
	2	124		0.389	
	3	130		0.391	
15	1	90.5	95.47	0.421	0.418
	2	95.9		0.416	
	3	100.0		0.418	
30	1	66.8	70.90	0.453	0.449
	2	71.2		0.446	
	3	74.7		0.447	
60	1	48.3	51.40	0.485	0.479
	2	51.7		0.476	
	3	54.2		0.476	
120	1	34.2	36.53	0.517	0.509
	2	36.8		0.506	
	3	38.6		0.505	
240	1	23.6	25.37	0.548	0.540
	2	25.6		0.536	
	3	26.9		0.535	

Table A.6 Bending Beam Rheometer Test Results: PG 76-22, RTFOT Aged

Time (sec.)	Replicate	Measured Stiffness (MPa)	Average	m-value	Average
80	1	92.9	92.0	0.400	0.402
	2	93.6		0.409	
	3	89.5		0.398	
15	1	71.3	70.70	0.430	0.430
	2	71.8		0.435	
	3	69.0		0.426	
30	1	52.4	51.93	0.463	0.461
	2	52.6		0.463	
	3	50.8		0.457	
60	1	37.7	37.40	0.496	0.492
	2	37.8		0.491	
	3	36.7		0.488	
120	1	26.4	26.30	0.528	0.522
	2	26.6		0.519	
	3	25.9		0.519	
240	1	18.1	18.10	0.561	0.553
	2	18.4		0.547	
	3	17.8		0.550	

APPENDIX B
DYNAMIC SHEAR RHEOMETER TEST RESULTS

Table B.1 Dynamic Shear Rheometer Test Results at 10°: PG 67-22, 6.1% Asphalt Conter

G* Result					δ Result			
Freq.(Hz)	Samples			Average	Samples			
	Sample 1	Sample 2	Sample 3		Sample 1	Sample 2	Samp	
0.5	8.07E+06	8.24E+06	7.86E+06	8.06E+06	47.10	47.63	47.4	
1	1.14E+07	1.17E+07	1.11E+07	1.14E+07	45.09	45.51	45.4	
2	1.60E+07	1.65E+07	1.56E+07	1.60E+07	42.88	42.98	42.7	
4	2.21E+07	2.27E+07	2.15E+07	2.21E+07	40.87	40.73	40.9	
8	2.99E+07	3.10E+07	2.93E+07	3.00E+07	38.61	38.55	38.8	
15	3.90E+07	4.03E+07	3.80E+07	3.91E+07	36.72	36.86	36.8	

Table B.2 Dynamic Shear Rheometer Test Results at 10°: PG 76-22, 6.1% Asphalt Conter

G* Result					δ Result			
Freq.(Hz)	Samples			Average	Samples			
	Sample 1	Sample 2	Sample 3		Sample 1	Sample 2	Samp	
0.5	1.10E+07	1.01E+07	9.39E+06	1.02E+07	45.73	45.54	45.2	
1	1.55E+07	1.42E+07	1.33E+07	1.44E+07	44.23	43.88	43.5	
2	2.17E+07	1.97E+07	1.84E+07	1.99E+07	41.44	41.45	41.8	
4	2.94E+07	2.68E+07	2.50E+07	2.71E+07	39.23	39.32	39.4	
8	3.94E+07	3.58E+07	3.36E+07	3.63E+07	37.32	37.44	37.3	
15	5.08E+07	4.62E+07	4.33E+07	4.68E+07	35.37	35.35	35.4	

Table B.3 Dynamic Shear Rheometer Test Results at 10°: PG 67-22, 7.2% Asphalt Conter

G* Result / δ Result

Freq.(Hz)	Samples			Average	Samples			
	Sample 1	Sample 2	Sample 3		Sample 1	Sample 2	Samp	
0.5	8.46E+06	7.67E+06	7.37E+06	7.84E+06	47.59	47.80	47.6	
1	1.18E+07	1.09E+07	1.06E+07	1.11E+07	45.35	46.39	45.8	
2	1.67E+07	1.54E+07	1.49E+07	1.56E+07	43.44	44.07	43.7	
4	2.31E+07	2.14E+07	2.06E+07	2.17E+07	41.21	41.86	41.5	
8	3.12E+07	2.92E+07	2.80E+07	2.95E+07	38.93	39.47	39.2	
15	4.06E+07	3.80E+07	3.66E+07	3.84E+07	36.93	37.52	37.4	

Table B.4 Dynamic Shear Rheometer Test Results at 10°: PG 76-22, 7.2% Asphalt Conter

G* Result / δ Result

Freq.(Hz)	Samples			Average	Samples			
	Sample 1	Sample 2	Sample 3		Sample 1	Sample 2	Samp	
0.5	8.00E+06	8.01E+06	7.62E+06	7.88E+06	47.01	46.14	45.9	
1	1.13E+07	1.13E+07	1.08E+07	1.12E+07	44.66	44.72	44.7	
2	1.58E+07	1.59E+07	1.51E+07	1.56E+07	42.92	42.60	42.1	
4	2.18E+07	2.18E+07	2.07E+07	2.14E+07	40.50	40.40	40.5	
8	2.95E+07	2.95E+07	2.81E+07	2.90E+07	38.56	38.49	38.5	
15	3.83E+07	3.83E+07	3.64E+07	3.77E+07	36.71	36.82	36.7	

Table B.5 Dynamic Shear Rheometer Test Results at 10°: PG 67-22, RTFOT Aged

G* Result					δ Result			
Freq.(Hz)	Samples			Average	Samples			
	Sample 1	Sample 2	Sample 3		Sample 1	Sample 2	Samp	
0.5	9.69E+06	1.15E+07	9.41E+06	1.02E+07	46.30	46.23	46.6	
1	1.39E+07	1.65E+07	1.36E+07	1.47E+07	44.44	45.88	45.8	
2	1.96E+07	2.26E+07	1.89E+07	2.03E+07	42.64	42.25	42.5	
4	2.70E+07	3.12E+07	2.60E+07	2.80E+07	40.08	40.06	39.7	
8	3.62E+07	4.18E+07	3.51E+07	3.77E+07	37.77	37.61	37.7	
15	4.67E+07	5.40E+07	4.51E+07	4.86E+07	35.90	35.49	35.6	

Table B.6 Dynamic Shear Rheometer Test Results at 10°: PG 76-22, RTFOT Aged

G* Result					δ Result			
Freq.(Hz)	Samples			Average	Samples			
	Sample 1	Sample 2	Sample 3		Sample 1	Sample 2	Samp	
0.5	8.28E+06	7.31E+06	7.75E+06	7.78E+06	46.66	46.24	47.2	
1	1.15E+07	1.04E+07	1.11E+07	1.10E+07	44.91	44.75	44.5	
2	1.62E+07	1.45E+07	1.54E+07	1.53E+07	42.56	42.47	42.2	
4	2.22E+07	2.00E+07	2.12E+07	2.11E+07	40.40	40.60	40.2	
8	3.02E+07	2.69E+07	2.86E+07	2.86E+07	38.26	38.41	38.2	
15	3.90E+07	3.50E+07	3.72E+07	3.70E+07	36.59	36.48	36.4	

Table B.7 Dynamic Shear Rheometer Test Results at 20°: PG 67-22, 6.1% Asphalt Conter

G* Result — δ Result

Freq.(Hz)	Samples			Average	Samples			
	Sample 1	Sample 2	Sample 3		Sample 1	Sample 2	Sampl	
0.5	1.33E+06	1.45E+06	1.41E+06	1.39E+06	57.69	57.24	57.3	
1	2.02E+06	2.24E+06	2.15E+06	2.14E+06	56.22	55.91	56.0	
2	3.09E+06	3.41E+06	3.29E+06	3.26E+06	54.44	54.22	54.3	
4	4.66E+06	5.13E+06	4.92E+06	4.90E+06	52.59	52.51	52.3	
8	6.89E+06	7.59E+06	7.28E+06	7.25E+06	50.61	50.48	50.5	
15	9.75E+06	1.07E+07	1.03E+07	1.02E+07	48.55	48.58	48.4	

Table B.8 Dynamic Shear Rheometer Test Results at 20°: PG 76-22, 6.1% Asphalt Conter

G* Result — δ Result

Freq.(Hz)	Samples			Average	Samples			
	Sample 1	Sample 2	Sample 3		Sample 1	Sample 2	Samp	
0.5	1.73E+06	1.76E+06	1.79E+06	1.76E+06	54.16	53.92	54.0	
1	2.57E+06	2.62E+06	2.71E+06	2.63E+06	53.29	53.16	53.1	
2	3.84E+06	3.91E+06	4.06E+06	3.94E+06	51.75	51.63	51.6	
4	5.64E+06	5.75E+06	5.97E+06	5.79E+06	50.14	50.04	50.1	
8	8.24E+06	8.35E+06	8.67E+06	8.42E+06	48.38	48.11	48.3	
15	1.14E+07	1.16E+07	1.20E+07	1.17E+07	46.47	46.22	46.6	

Table B.9 Dynamic Shear Rheometer Test Results at 20°: PG 67-22, 7.2% Asphalt Conter

G* Result | δ Result

Freq.(Hz)	Samples			Average	Samples			
	Sample 1	Sample 2	Sample 3		Sample 1	Sample 2	Samp	
0.5	1.27E+06	1.27E+06	1.27E+06	1.27E+06	57.64	58.00	57.4	
1	1.98E+06	1.95E+06	1.96E+06	1.96E+06	56.61	56.39	56.5	
2	3.02E+06	2.99E+06	3.00E+06	3.00E+06	54.73	54.90	54.6	
4	4.57E+06	4.49E+06	4.53E+06	4.53E+06	52.76	53.08	52.8	
8	6.79E+06	6.66E+06	6.71E+06	6.72E+06	51.00	51.07	50.9	
15	9.61E+06	9.42E+06	9.48E+06	9.50E+06	48.99	49.12	48.9	

Table B.10 Dynamic Shear Rheometer Test Results at 20°: PG 76-22, 7.2% Asphalt Conte

G* Result | δ Result

Freq.(Hz)	Samples			Average	Samples			
	Sample 1	Sample 2	Sample 3		Sample 1	Sample 2	Samp	
0.5	1.55E+06	1.54E+06	1.60E+06	1.57E+06	53.17	53.51	53.5	
1	2.32E+06	2.33E+06	2.41E+06	2.35E+06	52.38	53.04	52.7	
2	3.45E+06	3.49E+06	3.59E+06	3.51E+06	51.00	51.64	51.5	
4	5.06E+06	5.14E+06	5.27E+06	5.16E+06	49.65	50.35	50.2	
8	7.36E+06	7.49E+06	7.67E+06	7.50E+06	48.09	48.75	48.5	
15	1.02E+07	1.04E+07	1.07E+07	1.04E+07	46.33	47.04	46.9	

Table B.11 Dynamic Shear Rheometer Test Results at 20°: PG 67-22, RTFOT Aged

G* Result | δ Result

Freq.(Hz)	Samples			Average	Samples			
	Sample 1	Sample 2	Sample 3		Sample 1	Sample 2	Samp	
0.5	1.56E+06	1.58E+06	1.67E+06	1.60E+06	56.54	56.86	56.6	
1	2.39E+06	2.40E+06	2.54E+06	2.44E+06	55.25	55.60	55.2	
2	3.62E+06	3.65E+06	3.86E+06	3.71E+06	53.52	53.61	53.5	
4	5.42E+06	5.46E+06	5.73E+06	5.54E+06	51.54	51.84	51.6	
8	7.95E+06	8.06E+06	8.45E+06	8.15E+06	49.55	49.58	49.5	
15	1.11E+07	1.13E+07	1.18E+07	1.14E+07	47.48	47.52	47.4	

Table B.12 Dynamic Shear Rheometer Test Results at 20°: PG 76-22, RTFOT Aged

G* Result | δ Result

Freq.(Hz)	Samples			Average	Samples			
	Sample 1	Sample 2	Sample 3		Sample 1	Sample 2	Samp	
0.5	1.41E+06	1.39E+06	1.45E+06	1.42E+06	54.14	54.06	54.2	
1	2.12E+06	2.12E+06	2.18E+06	2.14E+06	53.47	53.45	53.5	
2	3.18E+06	3.18E+06	3.28E+06	3.22E+06	52.14	51.97	52.1	
4	4.70E+06	4.72E+06	4.86E+06	4.76E+06	50.79	50.76	50.6	
8	6.89E+06	6.91E+06	7.10E+06	6.97E+06	49.18	49.11	49.0	
15	9.65E+06	9.66E+06	9.91E+06	9.74E+06	47.33	47.51	47.2	

APPENDIX C
BINDER CREEP COMPLIANCE MASTER CURVE DATA

The following equations are used to calculate the shift factor, a_T, reduced time, ξ.

$$\log a_T = -0.175(T - T_{ref}) \tag{4.3}$$

where a_T = shift factor

T = temperature the data shift from

T_{ref} = temperature the data shift to

$$\xi = \frac{t}{a_{Tt}} \tag{2.29}$$

where ξ = reduced time

t = real time

a_T = temperature shift factor.

In this study, the bending beam rheometer (BBR) test results at -10° was shifted to 20° and combined with the dynamic shear rheometer (DSR) test results to develop the binder creep compliance master curve. The dynamic shear test results at 10° were also presented.

The power model parameters, D_1 and m were obtained by locking-in D_0 and running the regression.

Table C.1 Binder Master Curve Data: PG 67-22, Extracted Binder, 6.1% Asphalt Content

	t (sec.)	log (*t*)	ξ	log ξ	*D*(*t*)(1/Pa)	log *D*(*t*)
BBR @ -10°C	8	0.90	4.499E-05	-4.347	8.20E-09	-8.09
	15	1.18	8.435E-05	-4.074	1.06E-08	-7.97
	30	1.48	1.687E-04	-3.773	1.42E-08	-7.85
	60	1.78	3.374E-04	-3.472	1.96E-08	-7.71
	120	2.08	6.748E-04	-3.171	2.74E-08	-7.56
	240	2.38	1.350E-03	-2.870	3.94E-08	-7.40
DSR @ 10°	0.067	-1.17	1.191E-03	-2.924	6.29E-08	-7.20
	0.125	-0.90	2.223E-03	-2.653	8.29E-08	-7.08
	0.25	-0.60	4.446E-03	-2.352	1.13E-07	-6.95
	0.5	-0.30	8.891E-03	-2.051	1.56E-07	-6.81
	1	0.00	1.778E-02	-1.750	2.15E-07	-6.67
	2	0.30	3.557E-02	-1.449	2.97E-07	-6.53
DSR @ 20°	0.067	-1.17	6.700E-02	-1.174	2.93E-07	-6.53
	0.125	-0.90	1.250E-01	-0.903	4.17E-07	-6.38
	0.25	-0.60	2.500E-01	-0.602	6.22E-07	-6.21
	0.5	-0.30	5.000E-01	-0.301	9.32E-07	-6.03
	1	0.00	1.000E+00	0.000	1.40E-06	-5.85
	2	0.30	2.000E+00	0.301	2.11E-06	-5.68

$D(t) = 4.834 \times 10^{-9} + t^{0.476} \times 2.101 \times 10^{-7}$ (10°)
$D(t) = 1.65 \times 10^{-8} + t^{0.596} \times 1.384 \times 10^{-6}$ (20°)

Table C.2 Power Model Parameter: PG 67-22, Extracted Binder, 6.1% Asphalt Content

	log ξ	*D*(*t*)	*D*0'	*D*'(ξ)	log *D*'(ξ)
BBR @ -10°C	-4.347	8.200E-09	3.33E-10	7.867E-09	-8.104
	-4.074	1.060E-08	3.33E-10	1.027E-08	-7.989
	-3.773	1.420E-08	3.33E-10	1.387E-08	-7.858
	-3.472	1.960E-08	3.33E-10	1.927E-08	-7.715
	-3.171	2.740E-08	3.33E-10	2.707E-08	-7.568
	-2.870	3.940E-08	3.33E-10	3.907E-08	-7.408
DSR @ 20°	-1.174	2.929E-07	3.33E-10	2.925E-07	-6.534
	-0.903	4.173E-07	3.33E-10	4.169E-07	-6.380
	-0.602	6.223E-07	3.33E-10	6.219E-07	-6.206
	-0.301	9.321E-07	3.33E-10	9.318E-07	-6.031
	0.000	1.401E-06	3.33E-10	1.400E-06	-5.854
	0.301	2.108E-06	3.33E-10	2.108E-06	-5.676
	log D_1 =	-5.879212	*m* =	0.524	
	D_1 =	1.321E-06			

Table C.3 Binder Master Curve Data: PG 67-22, Extracted Binder, 7.2% Asphalt Content

	t (sec.)	log (*t*)	ξ	log ξ	*D*(*t*)(1/Pa)	log *D*(*t*)
BBR @ -10°C	8	0.90	4.499E-05	-4.347	8.82E-09	-8.05
	15	1.18	8.435E-05	-4.074	1.14E-08	-7.94
	30	1.48	1.687E-04	-3.773	1.55E-08	-7.81
	60	1.78	3.374E-04	-3.472	2.14E-08	-7.67
	120	2.08	6.748E-04	-3.171	3.00E-08	-7.52
	240	2.38	1.350E-03	-2.870	4.32E-08	-7.36
DSR @ 10°	0.067	-1.17	1.191E-03	-2.924	6.43E-08	-7.19
	0.125	-0.90	2.223E-03	-2.653	8.54E-08	-7.07
	0.25	-0.60	4.446E-03	-2.352	1.18E-07	-6.93
	0.5	-0.30	8.891E-03	-2.051	1.63E-07	-6.79
	1	0.00	1.778E-02	-1.750	2.27E-07	-6.64
	2	0.30	3.557E-02	-1.449	3.16E-07	-6.50
DSR @ 20°	0.067	-1.17	6.700E-02	-1.174	3.20E-07	-6.49
	0.125	-0.90	1.250E-01	-0.903	4.59E-07	-6.34
	0.25	-0.60	2.500E-01	-0.602	6.88E-07	-6.16
	0.5	-0.30	5.000E-01	-0.301	1.04E-06	-5.98
	1	0.00	1.000E+00	0.000	1.57E-06	-5.80
	2	0.30	2.000E+00	0.301	2.38E-06	-5.62

$D(t) = 5.55 \times 10^{-9} + t^{0.490} \times 2.211 \times 10^{-7}$ (10°)
$D(t) = 1.854 \times 10^{-8} + t^{0.606} \times 1.552 \times 10^{-6}$ (20°)

Table C.4 Power Model Parameter: PG 67-22, Extracted Binder, 7.2% Asphalt Content

	log ξ	*D*(*t*)	*D*0'	*D*'(ξ)	log *D*'(ξ)
BBR @ -10°C	-4.347	8.820E-09	3.33E-10	8.487E-09	-8.071
	-4.074	1.140E-08	3.33E-10	1.107E-08	-7.956
	-3.773	1.550E-08	3.33E-10	1.517E-08	-7.819
	-3.472	2.140E-08	3.33E-10	2.107E-08	-7.676
	-3.171	3.000E-08	3.33E-10	2.967E-08	-7.528
	-2.870	4.320E-08	3.33E-10	4.287E-08	-7.368
DSR @ 20°	-1.174	3.202E-07	3.33E-10	3.198E-07	-6.495
	-0.903	4.587E-07	3.33E-10	4.584E-07	-6.339
	-0.602	6.885E-07	3.33E-10	6.882E-07	-6.162
	-0.301	1.038E-06	3.33E-10	1.038E-06	-5.984
	0.000	1.571E-06	3.33E-10	1.570E-06	-5.804
	0.301	2.381E-06	3.33E-10	2.380E-06	-5.623
	log D_1 =	-5.831571	*m* = 0.527		
	D_1 =	1.474E-06			

Table C.5 Binder Master Curve Data: PG 76-22, Extracted Binder, 6.1% Asphalt Content

	t (sec.)	log (t)	ξ	log ξ	$D(t)$(1/Pa)	log $D(t)$
BBR @ -10°C	8	0.90	4.499E-05	-4.347	9.17E-09	-8.04
	15	1.18	8.435E-05	-4.074	1.18E-08	-7.93
	30	1.48	1.687E-04	-3.773	1.58E-08	-7.80
	60	1.78	3.374E-04	-3.472	2.15E-08	-7.67
	120	2.08	6.748E-04	-3.171	2.98E-08	-7.53
	240	2.38	1.350E-03	-2.870	4.21E-08	-7.38
DSR @ 10°	0.067	-1.17	1.191E-03	-2.924	5.18E-08	-7.29
	0.125	-0.90	2.223E-03	-2.653	6.83E-08	-7.17
	0.25	-0.60	4.446E-03	-2.352	9.38E-08	-7.03
	0.5	-0.30	8.891E-03	-2.051	1.30E-07	-6.89
	1	0.00	1.778E-02	-1.750	1.80E-07	-6.74
	2	0.30	3.557E-02	-1.449	2.52E-07	-6.60
DSR @ 20°	0.067	-1.17	6.700E-02	-1.174	2.51E-07	-6.60
	0.125	-0.90	1.250E-01	-0.903	3.54E-07	-6.45
	0.25	-0.60	2.500E-01	-0.602	5.22E-07	-6.28
	0.5	-0.30	5.000E-01	-0.301	7.73E-07	-6.11
	1	0.00	1.000E+00	0.000	1.15E-06	-5.94
	2	0.30	2.000E+00	0.301	1.71E-06	-5.77

$D(t) = 5.899 \times 10^{-9} + t^{0.494} \times 1.744 \times 10^{-7}(10°)$

$D(t) = 1.513 \times 10^{-8} + t^{0.581} \times 1.134 \times 10^{-6}(20°)$

Table C.6 Power Model Parameter: PG 76-22, Extracted Binder, 6.1% Asphalt Content

	log ξ	$D(t)$	$D0'$	$D'(ξ)$	log $D'(ξ)$
BBR @ -10°C	-4.347	9.170E-09	3.33E-10	8.837E-09	-8.054
	-4.074	1.180E-08	3.33E-10	1.147E-08	-7.941
	-3.773	1.580E-08	3.33E-10	1.547E-08	-7.811
	-3.472	2.150E-08	3.33E-10	2.117E-08	-7.674
	-3.171	2.980E-08	3.33E-10	2.947E-08	-7.531
	-2.870	4.210E-08	3.33E-10	4.177E-08	-7.379
DSR @ 20°	-1.174	2.509E-07	3.33E-10	2.506E-07	-6.601
	-0.903	3.539E-07	3.33E-10	3.536E-07	-6.452
	-0.602	5.219E-07	3.33E-10	5.216E-07	-6.283
	-0.301	7.732E-07	3.33E-10	7.729E-07	-6.112
	0.000	1.149E-06	3.33E-10	1.149E-06	-5.940
	0.301	1.711E-06	3.33E-10	1.711E-06	-5.767
	log D_1 =	-5.970712	m = 0.488		
	D_1 =	1.070E-06			

Table C.7 Binder Master Curve Data: PG 76-22, Extracted Binder, 7.2% Asphalt Content

	t (sec.)	log (*t*)	ξ	log ξ	*D*(*t*)(1/Pa)	log *D*(*t*)
BBR @ -10°C	8	0.90	4.499E-05	-4.347	1.04E-08	-7.98
	15	1.18	8.435E-05	-4.074	1.35E-08	-7.87
	30	1.48	1.687E-04	-3.773	1.83E-08	-7.74
	60	1.78	3.374E-04	-3.472	2.51E-08	-7.60
	120	2.08	6.748E-04	-3.171	3.53E-08	-7.45
	240	2.38	1.350E-03	-2.870	5.07E-08	-7.29
DSR @ 10°	0.067	-1.17	1.191E-03	-2.924	6.58E-08	-7.18
	0.125	-0.90	2.223E-03	-2.653	8.73E-08	-7.06
	0.25	-0.60	4.446E-03	-2.352	1.21E-07	-6.92
	0.5	-0.30	8.891E-03	-2.051	1.68E-07	-6.78
	1	0.00	1.778E-02	-1.750	2.34E-07	-6.63
	2	0.30	3.557E-02	-1.449	3.28E-07	-6.48
DSR @ 20°	0.067	-1.17	6.700E-02	-1.174	2.86E-07	-6.54
	0.125	-0.90	1.250E-01	-0.903	4.05E-07	-6.39
	0.25	-0.60	2.500E-01	-0.602	6.00E-07	-6.22
	0.5	-0.30	5.000E-01	-0.301	8.93E-07	-6.05
	1	0.00	1.000E+00	0.000	1.33E-06	-5.88
	2	0.30	2.000E+00	0.301	1.99E-06	-5.70

$D(t) = 6.575 \times 10^{-9} + t^{0.498} \times 2.275 \times 10^{-7} (10°)$

$D(t) = 1.702 \times 10^{-8} + t^{0.587} \times 1.316 \times 10^{-6} (20°)$

Table C.8 Power Model Parameter: PG 76-22, Extracted Binder, 7.2% Asphalt Content

	log ξ	*D*(*t*)	*D*0'	*D*'(ξ)	log *D*'(ξ)
BBR @ -10°C	-4.347	1.040E-08	3.33E-10	1.007E-08	-7.997
	-4.074	1.350E-08	3.33E-10	1.317E-08	-7.881
	-3.773	1.830E-08	3.33E-10	1.797E-08	-7.746
	-3.472	2.510E-08	3.33E-10	2.477E-08	-7.606
	-3.171	3.530E-08	3.33E-10	3.497E-08	-7.456
	-2.870	5.070E-08	3.33E-10	5.037E-08	-7.298
DSR @ 20°	-1.174	2.863E-07	3.33E-10	2.859E-07	-6.544
	-0.903	4.053E-07	3.33E-10	4.050E-07	-6.393
	-0.602	6.003E-07	3.33E-10	5.999E-07	-6.222
	-0.301	8.931E-07	3.33E-10	8.928E-07	-6.049
	0.000	1.333E-06	3.33E-10	1.333E-06	-5.875
	0.301	1.994E-06	3.33E-10	1.993E-06	-5.700
	log D_1 =	-5.907328	*m* =	0.487	
	D_1 =	1.238E-06			

Table C.9 Binder Master Curve Data: PG 67-22, RTFOT Aged

	t (sec.)	log (*t*)	ξ	log ξ	*D*(*t*)(1/Pa)	log *D*(*t*)
BBR @ -10°C	8	0.90	4.499E-05	-4.347	8.09E-09	-8.09
	15	1.18	8.435E-05	-4.074	1.05E-08	-7.98
	30	1.48	1.687E-04	-3.773	1.41E-08	-7.85
	60	1.78	3.374E-04	-3.472	1.95E-08	-7.71
	120	2.08	6.748E-04	-3.171	2.74E-08	-7.56
	240	2.38	1.350E-03	-2.870	3.94E-08	-7.40
DSR @ 10°	0.067	-1.17	1.191E-03	-2.924	5.24E-08	-7.28
	0.125	-0.90	2.223E-03	-2.653	7.03E-08	-7.15
	0.25	-0.60	4.446E-03	-2.352	9.87E-08	-7.01
	0.5	-0.30	8.891E-03	-2.051	1.40E-07	-6.85
	1	0.00	1.778E-02	-1.750	2.00E-07	-6.70
	2	0.30	3.557E-02	-1.449	2.87E-07	-6.54
DSR @ 20°	0.067	-1.17	6.700E-02	-1.174	2.59E-07	-6.59
	0.125	-0.90	1.250E-01	-0.903	3.67E-07	-6.43
	0.25	-0.60	2.500E-01	-0.602	5.45E-07	-6.26
	0.5	-0.30	5.000E-01	-0.301	8.12E-07	-6.09
	1	0.00	1.000E+00	0.000	1.21E-06	-5.92
	2	0.30	2.000E+00	0.301	1.82E-06	-5.74

$D(t) = 7.419 \times 10^{-9} + t^{0.538} \times 1.879 \times 10^{-7} (10°)$

$D(t) = 1.532 \times 10^{-8} + t^{0.589} \times 1.198 \times 10^{-6} (20°)$

Table C.10 Power Model Parameter: PG 67-22, RTFOT Aged

	log ξ	*D*(*t*)	*D*0'	*D*'(ξ)	log *D*'(ξ)
BBR @ -10°C	-4.347	8.090E-09	3.33E-10	7.757E-09	-8.110
	-4.074	1.050E-08	3.33E-10	1.017E-08	-7.993
	-3.773	1.410E-08	3.33E-10	1.377E-08	-7.861
	-3.472	1.950E-08	3.33E-10	1.917E-08	-7.717
	-3.171	2.740E-08	3.33E-10	2.707E-08	-7.568
	-2.870	3.940E-08	3.33E-10	3.907E-08	-7.408
DSR @ 20°	-1.174	2.591E-07	3.33E-10	2.588E-07	-6.587
	-0.903	3.673E-07	3.33E-10	3.670E-07	-6.435
	-0.602	5.448E-07	3.33E-10	5.445E-07	-6.264
	-0.301	8.118E-07	3.33E-10	8.114E-07	-6.091
	0.000	1.213E-06	3.33E-10	1.213E-06	-5.916
	0.301	1.817E-06	3.33E-10	1.817E-06	-5.741
	log D_1=	-5.943006	*m* = 0.507		
	D_1=	1.140E-06			

Table C.11 Binder Master Curve Data: PG 76-22, RTFOT Aged

	t (sec.)	log (*t*)	ξ	log ξ	*D*(*t*)(1/Pa)	log *D*(*t*)
BBR @ -10°C	8	0.90	4.499E-05	-4.347	1.09E-08	-7.96
	15	1.18	8.435E-05	-4.074	1.41E-08	-7.85
	30	1.48	1.687E-04	-3.773	1.93E-08	-7.71
	60	1.78	3.374E-04	-3.472	2.67E-08	-7.57
	120	2.08	6.748E-04	-3.171	3.80E-08	-7.42
	240	2.38	1.350E-03	-2.870	5.52E-08	-7.26
DSR @ 10°	0.067	-1.17	1.191E-03	-2.924	6.60E-08	-7.18
	0.125	-0.90	2.223E-03	-2.653	8.70E-08	-7.06
	0.25	-0.60	4.446E-03	-2.352	1.19E-07	-6.92
	0.5	-0.30	8.891E-03	-2.051	1.64E-07	-6.79
	1	0.00	1.778E-02	-1.750	2.26E-07	-6.65
	2	0.30	3.557E-02	-1.449	3.12E-07	-6.51
DSR @ 20°	0.067	-1.17	6.700E-02	-1.174	3.12E-07	-6.51
	0.125	-0.90	1.250E-01	-0.903	4.44E-07	-6.35
	0.25	-0.60	2.500E-01	-0.602	6.62E-07	-6.18
	0.5	-0.30	5.000E-01	-0.301	9.91E-07	-6.00
	1	0.00	1.000E+00	0.000	1.49E-06	-5.83
	2	0.30	2.000E+00	0.301	2.24E-06	-5.65

$D(t) = 5.491 \times 10^{-9} + t^{0.478} \times 2.202 \times 10^{-7}(10°)$

$D(t) = 1.808 \times 10^{-8} + t^{0.595} \times 1.469 \times 10^{-6}(20°)$

Table C.12 Power Model Parameter: PG 76-22, RTFOT Aged

	log ξ	*D*(*t*)	*D*0'	*D*'(ξ)	log *D*'(ξ)
BBR @ -10°C	-4.347	1.090E-08	3.33E-10	1.057E-08	-7.976
	-4.074	1.410E-08	3.33E-10	1.377E-08	-7.861
	-3.773	1.930E-08	3.33E-10	1.897E-08	-7.722
	-3.472	2.670E-08	3.33E-10	2.637E-08	-7.579
	-3.171	3.800E-08	3.33E-10	3.767E-08	-7.424
	-2.870	5.520E-08	3.33E-10	5.487E-08	-7.261
DSR @ 20°	-1.174	3.122E-07	3.33E-10	3.119E-07	-6.506
	-0.903	4.443E-07	3.33E-10	4.440E-07	-6.353
	-0.602	6.619E-07	3.33E-10	6.616E-07	-6.179
	-0.301	9.906E-07	3.33E-10	9.903E-07	-6.004
	0.000	1.487E-06	3.33E-10	1.487E-06	-5.828
	0.301	2.237E-06	3.33E-10	2.237E-06	-5.650
	log D_1=	-5.860253	*m* = 0.493		
	D_1=	1.380E-06			

APPENDIX D
MIX DESIGN AND VOLUMETRIC PROPERTIES OF MIXTURES

WHITE ROCK COARSE

Nominal maximum aggregate size = 12.5mm

AGGREGATE			S1A	S1B	SCREEN	FILLER
	Individual % by mass		10.200	63.267	25.511	1.022
	Individual specific gravity		2.425	2.451	2.527	2.690
	Gsb		2.469	2.469	2.469	2.469
SPECIFIC GRAVITY	%AC		6.0	6.5	7.0	
	Gb		1.035	1.035	1.035	
	Gmm(measured)		2.347	2.329	2.311	
	Gse(calculated)		2.553	2.550	2.547	
	Gmb	Ni=7	1.942	1.946	1.942	
		Ni=8	1.956	1.959	1.955	
		Ni=9	1.968	1.971	1.968	
	Gmb	Nd=75	2.198	2.199	2.203	
		Nd=100	2.228	2.231	2.231	
		Nd=125	2.250	2.253	2.253	
	Gmb	Nmax=115	2.241	2.244	2.245	
		Nmax=160	2.270	2.275	2.275	
		Nmax=205	2.291	2.296	2.296	
VOLUMETRIC PROPERTY	VMA	Nd=75	16.322	16.721	17.052	
		Nd=100	15.176	15.515	15.983	
		Nd=125	14.349	14.692	15.163	
	Va	Nd=75	6.316	5.540	4.672	
		Nd=100	5.034	4.172	3.444	
		Nd=125	4.107	3.238	2.502	
	VFA	Nd=75	61.302	66.866	72.598	
		Nd=100	66.831	73.107	78.450	
		Nd=125	71.375	77.958	83.497	
% of Gmm	N_i	7	82.8	83.6	84.0	
		8	83.4	84.1	84.6	
		9	83.9	84.7	85.2	
	N_{des}	75	93.7	94.5	95.3	
		100	95.0	95.8	96.6	
		125	95.9	96.8	97.5	
	N_{max}	115	95.5	96.4	97.2	
		160	96.8	97.7	98.5	
		205	97.6	98.6	99.4	
MIXTURE PROPERTY AT 4% AIR VOID	N_d	75	100	125	Requirement	
	%AC	7.2	6.6	6.1		
	Va	4.0	4.0	4.0		
	VMA	17.2	15.6	14.5	>14	
	VFA	75.0	74.0	73.0	65-78	
% of Gmm	N_i	84.2	84.3	84.1	=< 89	
	N_{max}	97.4	97.9	97.8	=< 98	

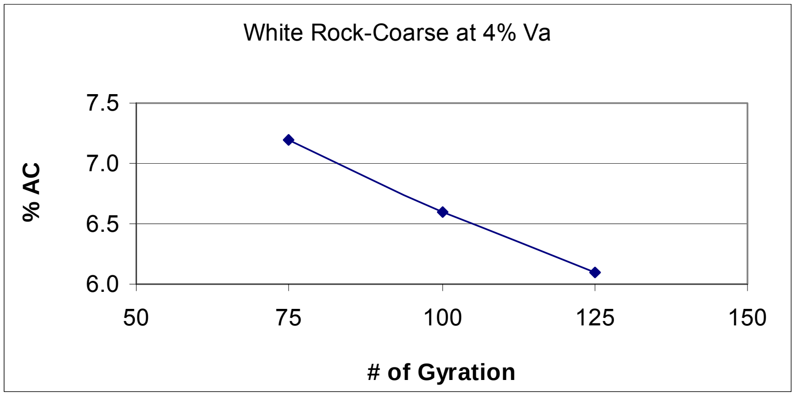
White Rock-Coarse at 4% Va
% AC
7.5
7.0
6.5
6.0
50
75
100
125
150
# of Gyration

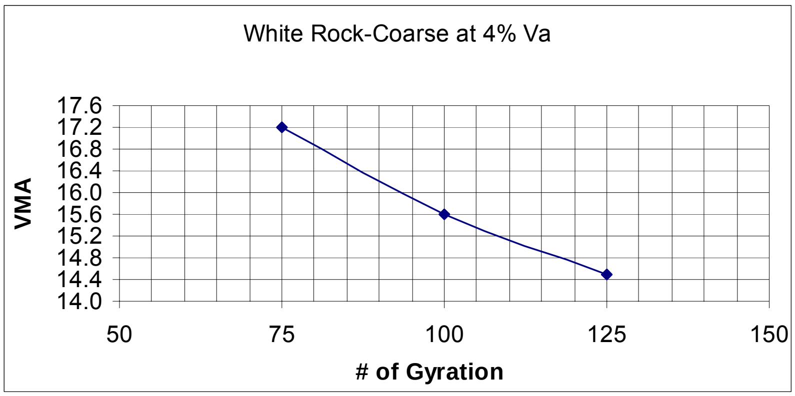
White Rock-Coarse at 4% Va
VMA
17.6
17.2
16.8
16.4
16.0
15.6
15.2
14.8
14.4
14.0
50
75
100
125
150
# of Gyration

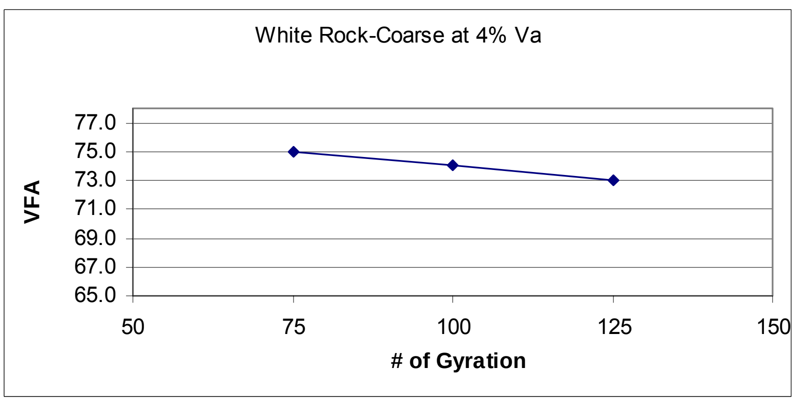
White Rock-Coarse at 4% Va
VFA
77.0
75.0
73.0
71.0
69.0
67.0
65.0
50
75
100
125
150
# of Gyration

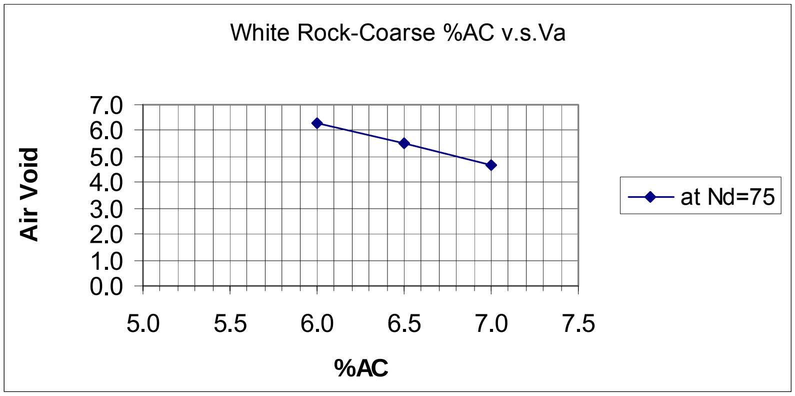
White Rock-Coarse %AC v.s.Va
Air Void
7.0
6.0
5.0
4.0
3.0
2.0
1.0
0.0
5.0
5.5
6.0
6.5
7.0
7.5
%AC
at Nd=75

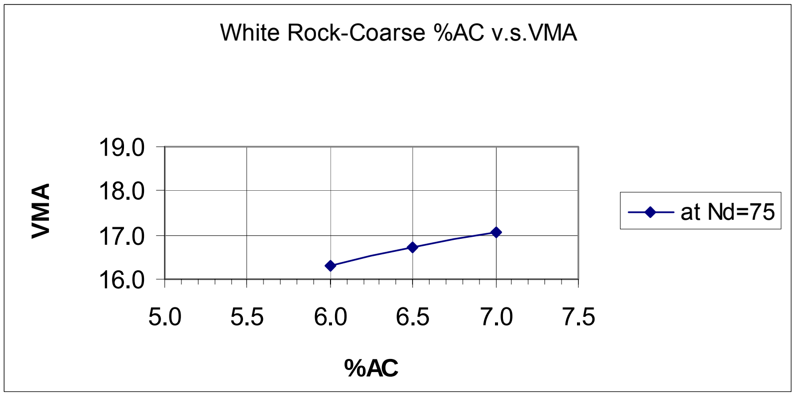
White Rock-Coarse %AC v.s.VMA
VMA
19.0
18.0
17.0
16.0
5.0
5.5
6.0
6.5
7.0
7.5
%AC
at Nd=75

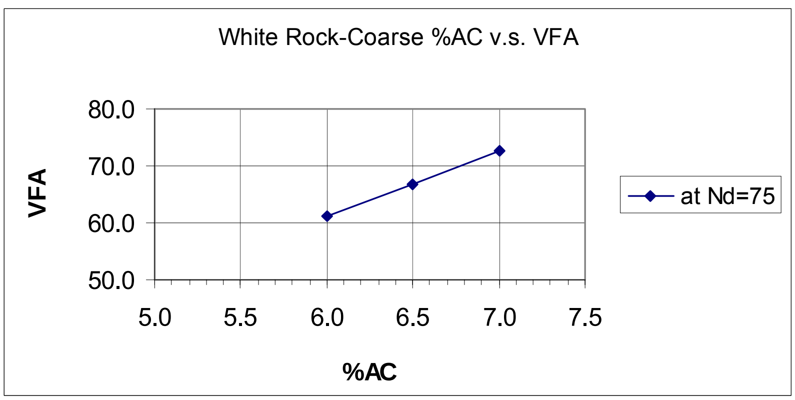
White Rock-Coarse %AC v.s. VFA
VFA
80.0
70.0
60.0
50.0
5.0
5.5
6.0
6.5
7.0
7.5
%AC
at Nd=75

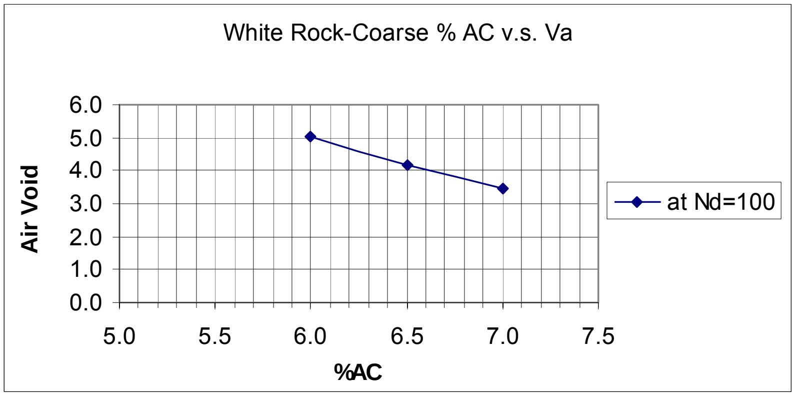
White Rock-Coarse % AC v.s. Va
Air Void
6.0
5.0
4.0
3.0
2.0
1.0
0.0
5.0
5.5
6.0
6.5
7.0
7.5
%AC
at Nd=100

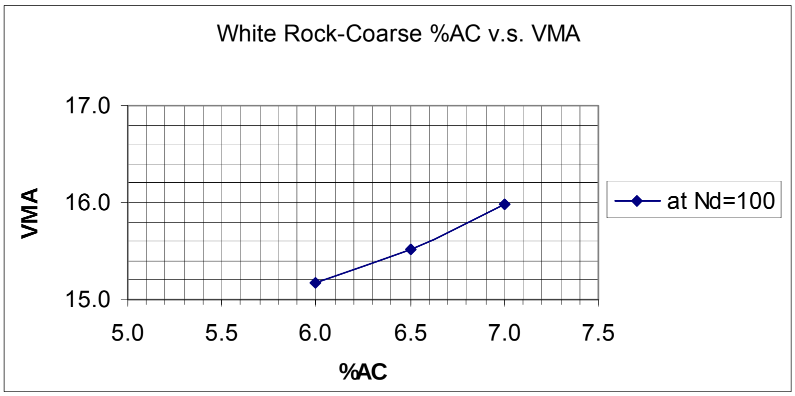
White Rock-Coarse %AC v.s. VMA
VMA
17.0
16.0
15.0
5.0
5.5
6.0
6.5
7.0
7.5
%AC
at Nd=100

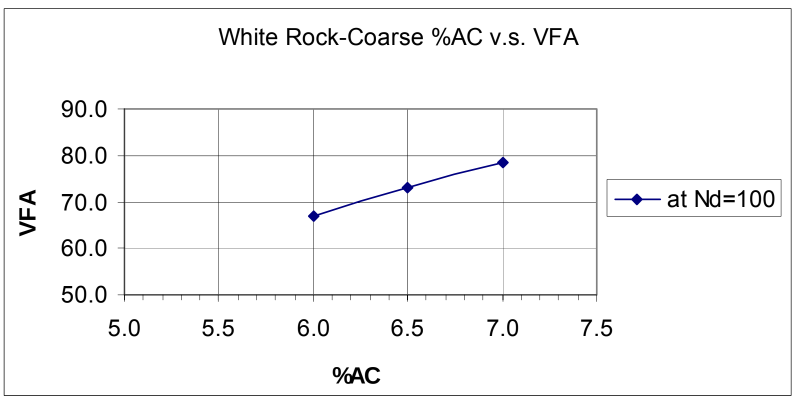
White Rock-Coarse %AC v.s. VFA
VFA
90.0
80.0
70.0
60.0
50.0
5.0
5.5
6.0
6.5
7.0
7.5
%AC
at Nd=100

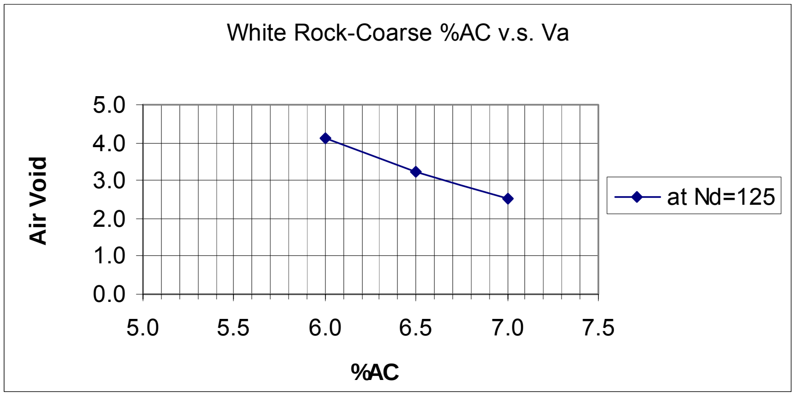
White Rock-Coarse %AC v.s. Va
Air Void
5.0
4.0
3.0
2.0
1.0
0.0
5.0
5.5
6.0
6.5
7.0
7.5
%AC
at Nd=125

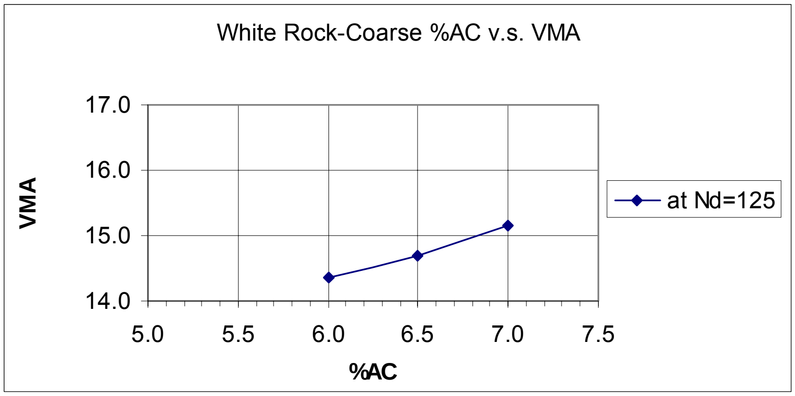
White Rock-Coarse %AC v.s. VMA
VMA
17.0
16.0
15.0
14.0
5.0
5.5
6.0
6.5
7.0
7.5
%AC
at Nd=125

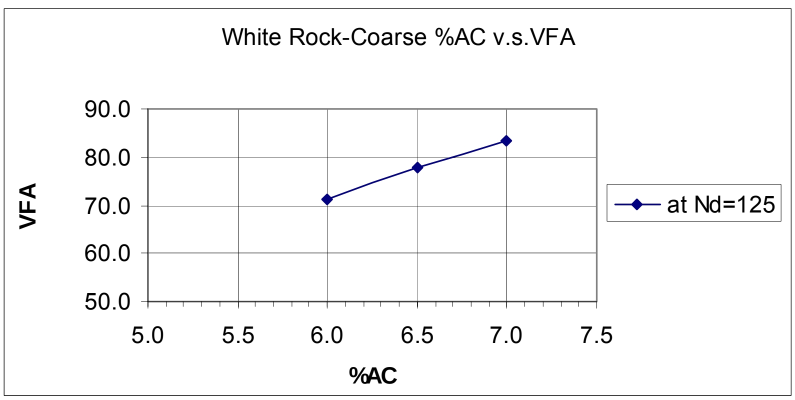
White Rock-Coarse %AC v.s.VFA
VFA
90.0
80.0
70.0
60.0
50.0
5.0
5.5
6.0
6.5
7.0
7.5
%AC
at Nd=125

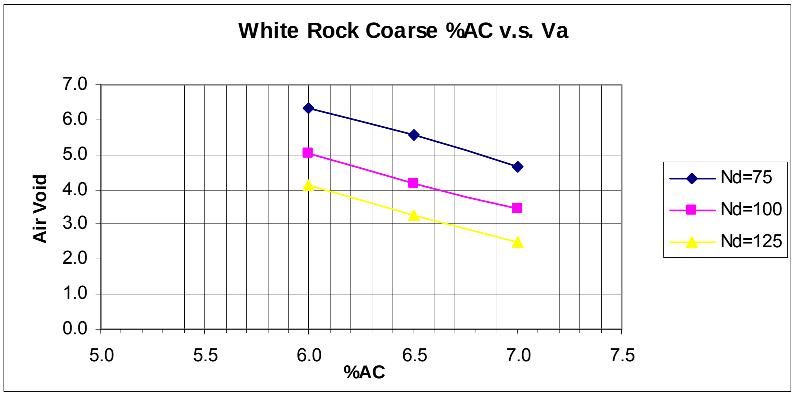
White Rock Coarse %AC v.s. Va
Air Void
7.0
6.0
5.0
4.0
3.0
2.0
1.0
0.0
5.0
5.5
6.0
6.5
7.0
7.5
%AC
Nd=75
Nd=100
Nd=125

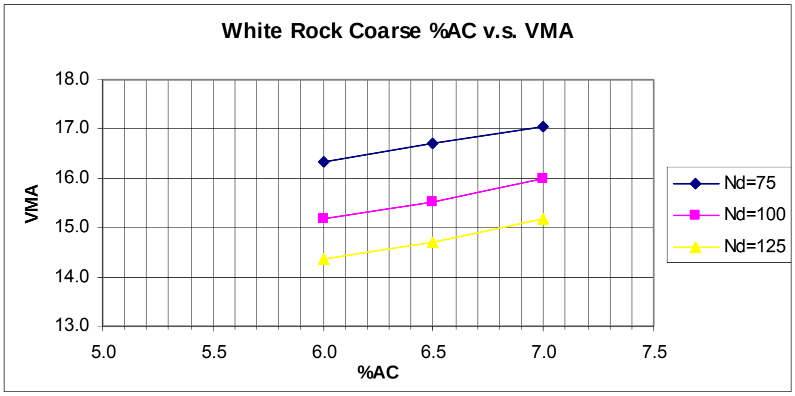
White Rock Coarse %AC v.s. VMA
VMA
18.0
17.0
16.0
15.0
14.0
13.0
5.0
5.5
6.0
6.5
7.0
7.5
%AC
Nd=75
Nd=100
Nd=125

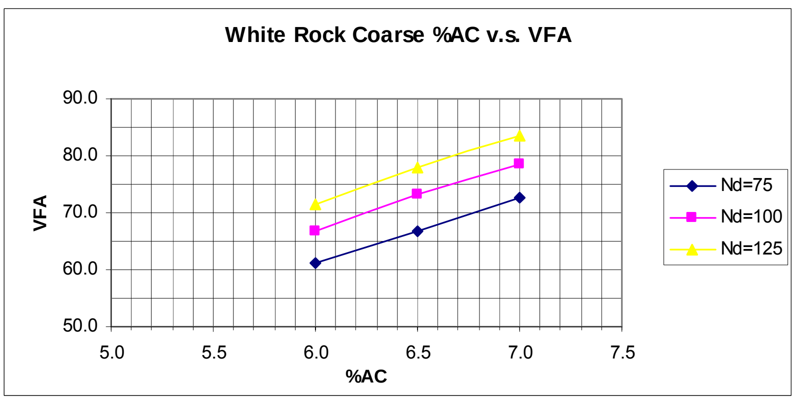
White Rock Coarse %AC v.s. VFA
VFA
90.0
80.0
70.0
60.0
50.0
5.0
5.5
6.0
6.5
7.0
7.5
%AC
Nd=75
Nd=100
Nd=125

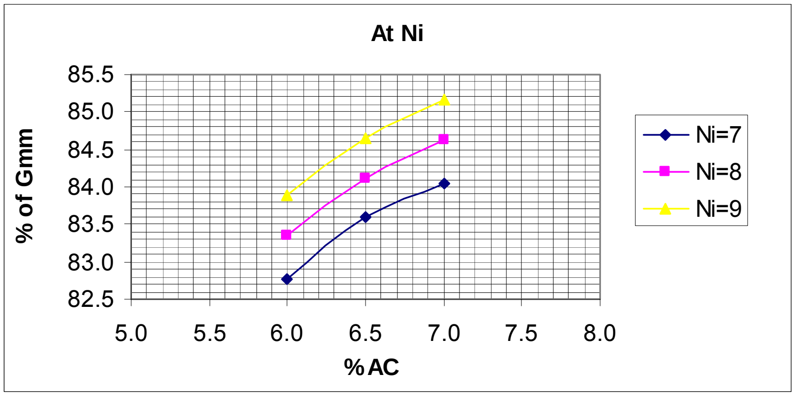
At Ni
% of Gmm
85.5
85.0
84.5
84.0
83.5
83.0
82.5
5.0
5.5
6.0
6.5
7.0
7.5
8.0
% AC
Ni=7
Ni=8
Ni=9

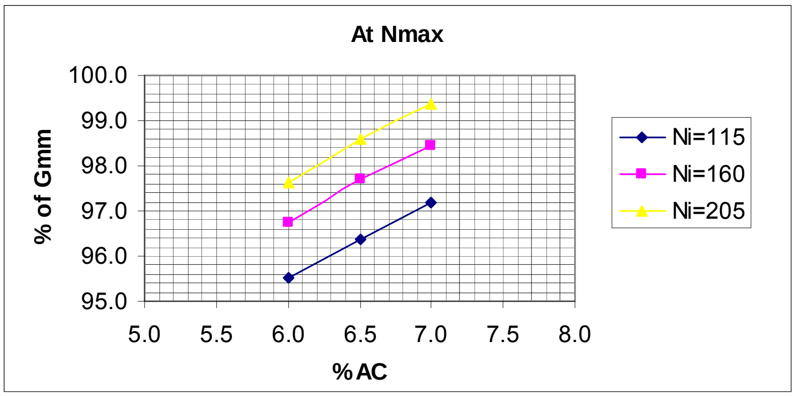
At Nmax
% of Gmm
100.0
99.0
98.0
97.0
96.0
95.0
5.0
5.5
6.0
6.5
7.0
7.5
8.0
% AC
Ni=115
Ni=160
Ni=205

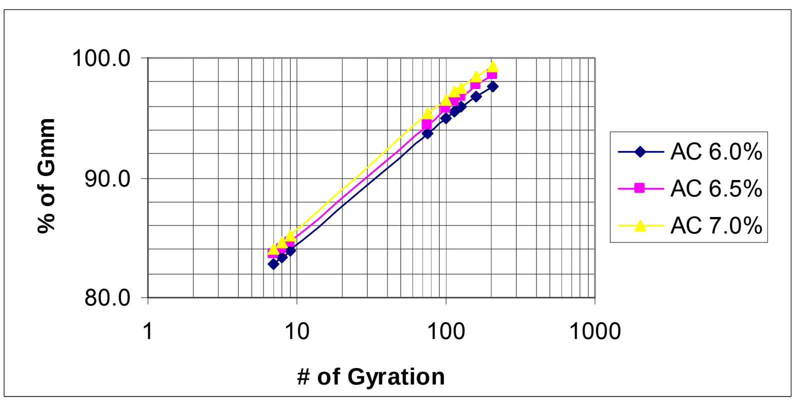
% of Gmm
100.0
90.0
80.0
1
10
100
1000
# of Gyration
AC 6.0%
AC 6.5%
AC 7.0%

APPENDIX E
BINDER-TO-MIXTURE STIFFNESS RELATIONSHIP DATA

Table E.1 *a*,*b* Regression: PG 67-22, Extracted Binder, 6.1% Asphalt Content

0°			10°			20°		
log S_b	log S'_b	*a*,*b*	log S_b	log S'_b	*a*,*b*	log S_b	log S'_b	
-1.295	-2.955		-2.205	-3.568		-3.121	-4.005	
-1.450	-3.072		-2.363	-3.710		-3.279	-4.188	
-1.657	-3.216	*a* =	-2.571	-3.920	*a* =	-3.487	-4.495	
-1.814	-3.325	1.747E-02	-2.728	-4.100	1.426E-01	-3.645	-4.685	
-1.971	-3.465		-2.886	-4.272		-3.802	-4.882	
-2.178	-3.677		-3.094	-4.542		-4.011	-5.148	
-2.336	-3.789	*b* =	-3.252	-4.747	*b* =	-4.168	-5.350	
-2.493	-3.952	0.886	-3.409	-4.956	1.205	-4.326	-5.561	
-2.702	-4.171		-3.618	-5.228		-4.534	-5.852	
-2.859	-4.347		-3.776	-5.432		-4.692	-6.080	

Table E.2 Predicted Stiffness Using *a*,*b*: PG 67-22, Extracted Binder, 6.1% Asphalt Conte

0°			10°			20°		
log S'_m	log S_b	log S_m	log S'_m	log S_b	log S_m	log S'_m	log S_b	log S
1.261	-1.295	1.222	0.791	-2.205	0.740	0.400	-3.121	0.391
1.153	-1.450	1.131	0.641	-2.363	0.627	0.234	-3.279	0.24
1.010	-1.657	1.018	0.441	-2.571	0.460	0.013	-3.487	-0.00
0.901	-1.814	0.932	0.288	-2.728	0.315	-0.155	-3.645	-0.15
0.791	-1.971	0.821	0.135	-2.886	0.177	-0.324	-3.802	-0.31
0.645	-2.178	0.654	-0.068	-3.094	-0.041	-0.548	-4.011	-0.53
0.534	-2.336	0.564	-0.223	-3.252	-0.209	-0.718	-4.168	-0.70
0.422	-2.493	0.434	-0.378	-3.409	-0.379	-0.889	-4.326	-0.87
0.274	-2.702	0.258	-0.584	-3.618	-0.603	-1.117	-4.534	-1.11
0.162	-2.859	0.116	-0.741	-3.776	-0.771	-1.289	-4.692	-1.30

Table E.3 *a*,*b* Regression: PG 67-22, Extracted Binder, 7.2% Asphalt Content

0°			10°			20°		
log S_b	log S'_b	*a*,*b*	log S_b	log S'_b	*a*,*b*	log S_b	log S'_b	
-1.331	-2.668		-2.247	-3.160		-3.169	-3.243	
-1.488	-2.748		-2.406	-3.364		-3.327	-3.469	
-1.696	-2.896	*a* =	-2.615	-3.606	*a* =	-3.537	-3.683	
-1.853	-3.028	3.92E-02	-2.774	-3.787	4.12E-01	-3.695	-4.025	1.
-2.011	-3.153		-2.932	-3.998		-3.854	-4.319	
-2.220	-3.347		-3.142	-4.254		-4.064	-4.687	
-2.379	-3.489	*b* =	-3.300	-4.443	*b* =	-4.222	-4.950	
-2.537	-3.655	0.89	-3.459	-4.636	1.23	-4.381	-5.189	
-2.747	-3.883		-3.668	-4.906		-4.590	-5.546	
-2.905	-4.055		-3.827	-5.121		-4.749	-5.790	

Table E.4 Predicted Stiffness Using *a*,*b*: PG 67-22, Extracted Binder, 7.2% Asphalt Conte

0°			10°			20°		
log S'_m	log S_b	log S_m	log S'_m	log S_b	log S_m	log S'_m	log S_b	
0.994	-1.331	0.932	0.536	-2.247	0.527	0.522	-3.169	
0.880	-1.488	0.866	0.375	-2.406	0.359	0.304	-3.327	
0.728	-1.696	0.745	0.160	-2.615	0.156	0.015	-3.537	
0.613	-1.853	0.636	-0.003	-2.774	0.005	-0.205	-3.695	
0.497	-2.011	0.533	-0.167	-2.932	-0.172	-0.426	-3.854	
0.342	-2.220	0.373	-0.385	-3.142	-0.389	-0.720	-4.064	
0.225	-2.379	0.254	-0.550	-3.300	-0.549	-0.944	-4.222	
0.107	-2.537	0.116	-0.716	-3.459	-0.714	-1.168	-4.381	
-0.049	-2.747	-0.076	-0.937	-3.668	-0.944	-1.467	-4.590	
-0.168	-2.905	-0.221	-1.104	-3.827	-1.128	-1.694	-4.749	

Table E.5 *a,b* Regression: PG 76-22, Extracted Binder, 6.1% Asphalt Content

0°			10°			20°		
log S_b	log S'_b	*a,b*	log S_b	log S'_b	*a,b*	log S_b	log S'_b	
-1.329	-3.210		-2.177	-3.611		-3.029	-3.947	
-1.474	-3.301		-2.323	-3.701		-3.176	-4.126	
-1.666	-3.424	*a* =	-2.517	-3.896	*a* =	-3.370	-4.367	
-1.812	-3.521	9.34E-03	-2.664	-4.017	4.89E-02	-3.517	-4.519	
-1.958	-3.644		-2.811	-4.178		-3.664	-4.689	
-2.152	-3.807		-3.005	-4.382		-3.858	-4.891	
-2.298	-3.953	*b* =	-3.151	-4.541	*b* =	-4.005	-5.042	
-2.445	-4.086	0.84	-3.298	-4.704	1.03	-4.152	-5.200	
-2.639	-4.277		-3.492	-4.936		-4.346	-5.466	
-2.786	-4.436		-3.639	-5.082		-4.493	-5.673	

Table E.6 Predicted Stiffness Using *a,b*: PG 76-22, Extracted Binder, 6.1% Asphalt Conte

0°			10°			20°		
log S'_m	log S_b	log S_m	log S'_m	log S_b	log S_m	log S'_m	log S_b	
1.073	-1.329	1.022	0.752	-2.177	0.706	0.423	-3.029	
0.977	-1.474	0.951	0.632	-2.323	0.635	0.287	-3.176	
0.850	-1.666	0.854	0.473	-2.517	0.479	0.107	-3.370	
0.753	-1.812	0.777	0.352	-2.664	0.382	-0.029	-3.517	
0.655	-1.958	0.680	0.231	-2.811	0.253	-0.166	-3.664	
0.526	-2.152	0.550	0.069	-3.005	0.088	-0.349	-3.858	
0.427	-2.298	0.433	-0.053	-3.151	-0.041	-0.487	-4.005	
0.329	-2.445	0.326	-0.176	-3.298	-0.173	-0.626	-4.152	
0.197	-2.639	0.173	-0.339	-3.492	-0.363	-0.810	-4.346	
0.098	-2.786	0.044	-0.463	-3.639	-0.483	-0.950	-4.493	

Table E.7 *a*,*b* Regression: PG 76-22, Extracted Binder, 7.2% Asphalt Content

0°			10°			20°		
log S_b	log S_b'	*a*,*b*	log S_b	log S_b'	*a*,*b*	log S_b	log S_b'	
-1.394	-2.664		-2.241	-3.149		-3.093	-3.506	
-1.539	-2.740		-2.387	-3.278		-3.239	-3.688	
-1.731	-2.847	*a* =	-2.581	-3.475	*a* =	-3.433	-3.888	
-1.877	-2.978	3.42E-02	-2.728	-3.597	1.46E-01	-3.580	-4.046	(
-2.023	-3.078		-2.874	-3.751		-3.726	-4.229	
-2.216	-3.243		-3.068	-3.951		-3.920	-4.443	
-2.363	-3.374	*b* =	-3.215	-4.099	*b* =	-4.067	-4.593	
-2.509	-3.512	0.82	-3.361	-4.259	1.02	-4.214	-4.744	
-2.703	-3.694		-3.555	-4.474		-4.407	-4.935	
-2.849	-3.831		-3.702	-4.639		-4.554	-5.080	

Table E.8 Predicted Stiffness Using *a*,*b*: PG 76-22, Extracted Binder, 7.2% Asphalt Conte

0°			10°			20°		
log S_m'	log S_b	log S_m	log S_m'	log S_b	log S_m	log S_m'	log S_b	
0.980	-1.394	0.936	0.559	-2.241	0.536	0.222	-3.093	
0.883	-1.539	0.873	0.435	-2.387	0.429	0.090	-3.239	
0.754	-1.731	0.785	0.271	-2.581	0.266	-0.086	-3.433	
0.655	-1.877	0.678	0.146	-2.728	0.164	-0.219	-3.580	
0.556	-2.023	0.595	0.021	-2.874	0.035	-0.353	-3.726	
0.425	-2.216	0.458	-0.145	-3.068	-0.133	-0.531	-3.920	
0.325	-2.363	0.350	-0.271	-3.215	-0.258	-0.665	-4.067	
0.225	-2.509	0.235	-0.398	-3.361	-0.393	-0.800	-4.214	
0.092	-2.703	0.082	-0.566	-3.555	-0.576	-0.980	-4.407	
-0.008	-2.849	-0.032	-0.693	-3.702	-0.716	-1.116	-4.554	

Table E.9 *a,b* Regression: PG 67-22, RTFOT Aged, 6.1% Asphalt Content

0°			10°			20°		
log S_b	log S'_b	*a,b*	log S_b	log S'_b	*a,b*	log S_b	log S'_b	
-1.288	-2.955		-2.170	-3.568		-3.057	-4.005	
-1.439	-3.072		-2.322	-3.710		-3.210	-4.188	
-1.639	-3.216	*a* =	-2.524	-3.920	*a* =	-3.412	-4.495	
-1.791	-3.325	1.88E-02	-2.677	-4.100	1.57E-01	-3.565	-4.685	1.
-1.943	-3.465		-2.829	-4.272		-3.717	-4.882	
-2.144	-3.677		-3.031	-4.542		-3.919	-5.148	
-2.296	-3.789	*b* =	-3.184	-4.747	*b* =	-4.072	-5.350	
-2.449	-3.952	0.91	-3.337	-4.956	1.24	-4.225	-5.561	
-2.651	-4.171		-3.539	-5.228		-4.427	-5.852	
-2.803	-4.347		-3.691	-5.432		-4.579	-6.080	

Table E.10 Predicted Stiffness Using *a,b*: PG 67-22, RTFOT Aged, 6.1% Asphalt Conten

0°			10°			20°		
log S'_m	log S_b	log S_m	log S'_m	log S_b	log S_m	log S'_m	log S_b	
1.266	-1.288	1.222	0.797	-2.170	0.740	0.410	-3.057	
1.159	-1.439	1.131	0.648	-2.322	0.627	0.244	-3.210	
1.016	-1.639	1.018	0.448	-2.524	0.460	0.024	-3.412	
0.908	-1.791	0.932	0.296	-2.677	0.315	-0.143	-3.565	
0.798	-1.943	0.821	0.144	-2.829	0.177	-0.311	-3.717	
0.653	-2.144	0.654	-0.059	-3.031	-0.041	-0.535	-3.919	
0.542	-2.296	0.564	-0.213	-3.184	-0.209	-0.705	-4.072	
0.431	-2.449	0.434	-0.368	-3.337	-0.379	-0.875	-4.225	
0.284	-2.651	0.258	-0.573	-3.539	-0.603	-1.102	-4.427	
0.172	-2.803	0.116	-0.729	-3.691	-0.771	-1.274	-4.579	

Table E.11 *a*,*b* Regression: PG 76-22, RTFOT Aged, 6.1% Asphalt Content

0°			10°			20°		
log S_b	log S'_b	*a*,*b*	log S_b	log S'_b	*a*,*b*	log S_b	log S'_b	(
-1.420	-3.210		-2.278	-3.611		-3.140	-3.947	
-1.567	-3.301		-2.426	-3.701		-3.288	-4.126	
-1.762	-3.424	*a* =	-2.622	-3.896	*a* =	-3.484	-4.368	(
-1.909	-3.521	1.08E-02	-2.770	-4.017	5.87E-02	-3.633	-4.519	4.(
-2.057	-3.644		-2.919	-4.178		-3.781	-4.689	
-2.253	-3.807		-3.115	-4.382		-3.977	-4.891	
-2.401	-3.953	*b* =	-3.263	-4.541	*b* =	-4.126	-5.042	*l*
-2.549	-4.087	0.83	-3.411	-4.704	1.02	-4.274	-5.200	1
-2.745	-4.277		-3.608	-4.936		-4.470	-5.466	
-2.893	-4.436		-3.756	-5.082		-4.619	-5.672	

Table E.12 Predicted Stiffness Using *a*,*b*: PG 76-22, RTFOT Aged, 6.1% Asphalt Conten

0°			10°			20°		
log S'_m	log S_b	log S_m	log S'_m	log S_b	log S_m	log S'_m	log S_b	
1.073	-1.420	1.022	0.751	-2.278	0.706	0.442	-3.140	
0.978	-1.567	0.951	0.631	-2.426	0.635	0.308	-3.288	
0.850	-1.762	0.854	0.471	-2.622	0.479	0.129	-3.484	
0.753	-1.909	0.777	0.350	-2.770	0.382	-0.006	-3.633	
0.656	-2.057	0.680	0.228	-2.919	0.253	-0.143	-3.781	
0.527	-2.253	0.550	0.067	-3.115	0.088	-0.323	-3.977	
0.428	-2.401	0.433	-0.056	-3.263	-0.041	-0.461	-4.126	
0.330	-2.549	0.326	-0.179	-3.411	-0.173	-0.598	-4.274	
0.199	-2.745	0.173	-0.342	-3.608	-0.363	-0.781	-4.470	
0.099	-2.893	0.044	-0.466	-3.756	-0.483	-0.920	-4.619	

Table E.13 *a*,*b* Regression: PG 67-22, RTFOT Aged, 7.2% Asphalt Content

0°			10°			20°		
log S_b	log S'_b	*a*,*b*	log S_b	log S'_b	*a*,*b*	log S_b	log S'_b	
-1.288	-2.668		-2.170	-3.160		-3.057	-3.243	
-1.439	-2.748		-2.322	-3.364		-3.210	-3.469	
-1.639	-2.896	*a* =	-2.524	-3.606	*a* =	-3.412	-3.683	
-1.791	-3.028	3.97E-02	-2.677	-3.787	4.19E-01	-3.565	-4.025	1.1
-1.943	-3.153		-2.829	-3.998		-3.717	-4.319	
-2.144	-3.347		-3.031	-4.254		-3.919	-4.687	
-2.296	-3.489	*b* =	-3.184	-4.443	*b* =	-4.072	-4.950	
-2.449	-3.655	0.93	-3.337	-4.636	1.28	-4.225	-5.189	1
-2.651	-3.883		-3.539	-4.906		-4.427	-5.546	
-2.803	-4.055		-3.691	-5.121		-4.579	-5.790	

Table E.14 Predicted Stiffness Using *a*,*b*: PG 67-22, RTFOT Aged, 7.2% Asphalt Conten

0°			10°			20°		
log S'_m	log S_b	log S_m	log S'_m	log S_b	log S_m	log S'_m	log S_b	
0.988	-1.288	0.932	0.531	-2.170	0.527	0.504	-3.057	
0.874	-1.439	0.866	0.369	-2.322	0.359	0.286	-3.210	
0.721	-1.639	0.745	0.154	-2.524	0.156	-0.005	-3.412	
0.605	-1.791	0.636	-0.010	-2.677	0.005	-0.226	-3.565	
0.488	-1.943	0.533	-0.174	-2.829	-0.172	-0.448	-3.717	
0.332	-2.144	0.373	-0.392	-3.031	-0.389	-0.744	-3.919	
0.214	-2.296	0.254	-0.558	-3.184	-0.549	-0.968	-4.072	
0.096	-2.449	0.116	-0.725	-3.337	-0.714	-1.194	-4.225	
-0.062	-2.651	-0.076	-0.946	-3.539	-0.944	-1.494	-4.427	
-0.181	-2.803	-0.221	-1.114	-3.691	-1.128	-1.722	-4.579	

Table E.15 *a*,*b* Regression: PG 76-22, RTFOT Aged, 7.2% Asphalt Content

0°			10°			20°		
log S_b	log S'_b	*a*,*b*	log S_b	log S'_b	*a*,*b*	log S_b	log S'_b	
-1.420	-2.664		-2.278	-3.149		-3.140	-3.506	
-1.567	-2.740		-2.426	-3.278		-3.288	-3.688	
-1.762	-2.847	*a* =	-2.622	-3.475	*a* =	-3.484	-3.888	
-1.909	-2.978	3.48E-02	-2.770	-3.597	1.49E-01	-3.633	-4.046	6.
-2.057	-3.078		-2.919	-3.751		-3.781	-4.229	
-2.253	-3.243		-3.115	-3.951		-3.977	-4.443	
-2.401	-3.374	*b* =	-3.263	-4.099	*b* =	-4.126	-4.593	
-2.549	-3.512	0.81	-3.411	-4.259	1.01	-4.274	-4.744	1
-2.745	-3.694		-3.608	-4.474		-4.470	-4.935	
-2.893	-3.831		-3.756	-4.639		-4.619	-5.080	

Table E.16 Predicted Stiffness Using *a*,*b*: PG 76-22, RTFOT Aged, 7.2% Asphalt Conten

0°			10°			20°		
log S'_m	log S_b	log S_m	log S'_m	log S_b	log S_m	log S'_m	log S_b	
0.980	-1.420	0.936	0.555	-2.278	0.536	0.215	-3.140	
0.883	-1.567	0.873	0.431	-2.426	0.429	0.082	-3.288	
0.754	-1.762	0.785	0.266	-2.622	0.266	-0.094	-3.484	
0.655	-1.909	0.678	0.141	-2.770	0.164	-0.228	-3.633	
0.556	-2.057	0.595	0.016	-2.919	0.035	-0.362	-3.781	
0.425	-2.253	0.458	-0.151	-3.115	-0.133	-0.540	-3.977	
0.325	-2.401	0.350	-0.277	-3.263	-0.258	-0.675	-4.126	
0.225	-2.549	0.235	-0.404	-3.411	-0.393	-0.810	-4.274	
0.093	-2.745	0.082	-0.572	-3.608	-0.576	-0.990	-4.470	
-0.008	-2.893	-0.032	-0.700	-3.756	-0.716	-1.126	-4.619	

APPENDIX F
ENERGY RATIO USING MIXTURE TEST AT ONE TEMPERATURE

The following equation was used to calculate the energy ratio (ER):

$$ER = \frac{a \times DCSE_f}{m^{2.98} \times D_1} \quad (2.36)$$

where:

$a = 0.0299\sigma^{-3.1}(6.36 - S_t) + 2.46 \times 10^{-8}$

σ = tensile stress of asphalt layer, assumed 230 psi

S_t = tensile strength, MPa

$DCSE_f$ = dissipated creep strain energy, KJ/m^3

D_1 = creep parameter, 1/psi

m = creep parameter

S_t and $DCSE_f$ were obtained from IDT test. D_1 and m were obtained from the following procedure:

1. Lock-in D_0 = 0.048 (1/GPa)
2. Determine D_1 and m at 20° from regression
3. Fix m = m at 20° (assuming m is a constant at three temperatures for the same mixture)
4. Calculate D_1 at 0° and 10° using the following relationship:

$$D_{1(0)} = D_{1(20)} \times \frac{1}{(a_{T(0)})^m} \quad (4.4)$$

$$D_{1(10)} = D_{1(20)} \times \frac{1}{(a_{T(10)})^m} \quad (4.5)$$

5. Repeat Step 1-4 for D_1 and m at 0° and 10°.

Table F.1 IDT Test Result: PG 67-22, 6.1% Asphalt Content

Temp.	Tensile Strength (PMa)	DCSE (KJ/m^3)	*m*	D_1 (1/psi)
0°	2.67	1.27	0.51	1.93E-07
10°	1.87	3.85	0.61	6.04E-07
20°	1.02	3.01	0.61	1.61E-06

Table F.2 IDT Test Result: PG 67-22, 7.2% Asphalt Content

Temp.	Tensile Strength (PMa)	DCSE (KJ/m^3)	*m*	D_1 (1/psi)
0°	2.54	1.73	0.52	2.99E-07
10°	1.69	4.70	0.62	1.21E-06
20°	0.73	3.64	0.63	3.68E-06

Table F.3 IDT Test Result: PG 76-22, 6.1% Asphalt Content

Temp.	Tensile Strength (PMa)	DCSE (KJ/m^3)	*m*	D_1 (1/psi)
0°	3.00	2.08	0.45	2.63E-07
10°	1.95	3.59	0.45	7.69E-07
20°	1.19	2.28	0.52	1.55E-06

Table F.4 IDT Test Result: PG 76-22, 7.2% Asphalt Content

Temp.	Tensile Strength (PMa)	DCSE (KJ/m^3)	*m*	D_1 (1/psi)
0°	2.89	2.38	0.44	3.48E-07
10°	1.93	4.85	0.47	1.33E-06
20°	0.94	2.11	0.48	4.10E-06

Table F.5 Energy Ratio from Mixture Test: PG 67-22, 6.1% Asphalt Content

Fix *m* @		D_1 (1/psi)	*m*	Energy Ratio (ER)
0°	0°	1.17E-07	0.560	1.83
	10°	1.11E-06		0.60
	20°	1.06E-05		0.05
10°	0°	9.43E-08	0.551	2.38
	10°	8.68E-07		0.81
	20°	7.99E-06		0.07
20°	0°	2.33E-08	0.579	8.29
	10°	2.40E-07		2.53
	20°	2.48E-06		0.20

Table F.6 Energy Ratio from Mixture Test: PG 67-22, 7.2% Asphalt Content

Fix *m* @		D_1 (1/psi)	*m*	Energy Ratio (ER)
0°	0°	4.43E-07	0.459	1.20
	10°	2.81E-06		0.53
	20°	1.79E-05		0.07
10°	0°	1.78E-07	0.570	1.56
	10°	1.77E-06		0.44
	20°	1.76E-05		0.04
20°	0°	4.15E-09	0.760	28.38
	10°	8.87E-08		3.75
	20°	1.90E-06		0.14

Table F.7 Energy Ratio from Mixture Test: PG 76-22, 6.1% Asphalt Content

Fix *m* @		D_1 (1/psi)	*m*	Energy Ratio (ER)
0°	0°	3.22E-07	0.417	2.57
	10°	1.73E-06		0.87
	20°	9.30E-06		0.11
10°	0°	1.61E-07	0.443	4.32
	10°	9.56E-07		1.32
	20°	5.69E-06		0.15
20°	0°	5.01E-08	0.473	11.33
	10°	3.38E-07		3.05
	20°	2.27E-06		0.30

Table F.8 Energy Ratio from Mixture Test: PG 76-22, 7.2% Asphalt Content

Fix *m* @		D_1 (1/psi)	*m*	Energy Ratio (ER)
0°	0°	4.45E-07	0.398	2.46
	10°	2.21E-06		1.06
	20°	1.10E-05		0.10
10°	0°	2.77E-07	0.441	2.92
	10°	1.64E-06		1.05
	20°	9.67E-06		0.08
20°	0°	9.71E-08	0.456	7.50
	10°	6.11E-07		2.54
	20°	3.84E-06		0.18

APPENDIX G
ENERGY RATIO PREDICTION USING BINDER-TO-MIXTURE STIFFNESS RELATIONSHIP

To calculate D_1 and m, the following procedure was followed:

1. Predict the mixture stiffness at 20° using the binder-to-mixture stiffness at 20°;
2. Lock-in D_0 = 0.048 (1/GPa);
3. Determine the D_1 and m at 20° from regression;
4. Use the binder-to-mixture stiffness relationship at 20° to predict the mixture stiffness at 0° and 10° for different times;
5. Calculate D_1 at 0° and 10° using the predicted mixture stiffness on step 4 and assuming:

$$m = m \text{ at } 20°$$

$$D_0 = 0.048\ (1/GPa);$$

6. Repeat Step 1-5 for 0° and 10°.

Table G.1 Energy Ratio from Binder-to-mixture Stiffness Relationship: PG 67-22, Extracted Binder, 6.1% Asphalt Content

Fix *m* @		D_1 (1/Psi)	*m*	Energy Ratio (ER)
0°	0°	9.84E-08	0.596	1.80
	10°	4.73E-07		1.18
	20°	2.27E-06		0.20
10°	0°	8.57E-08	0.554	2.58
	10°	8.56E-07		0.81
	20°	7.09E-06		0.08
20°	0°	6.32E-09	0.579	30.57
	10°	2.35E-07		2.59
	20°	2.47E-06		0.20

Table G.2 Energy Ratio from Binder-to-mixture Stiffness Relationship: PG 67-22, Extracted Binder, 7.2% Asphalt Content

Fix *m* @		D_1 (1/psi)	*m*	Energy Ratio (ER)
0°	0°	4.29E-07	0.466	1.18
	10°	2.23E-06		0.64
	20°	1.14E-05		0.10
10°	0°	1.72E-07	0.570	1.61
	10°	1.77E-06		0.44
	20°	1.69E-05		0.04
20°	0°	-2.43E-09	0.761	-48.28
	10°	8.62E-08		3.85
	20°	1.89E-06		0.14

Table G.3 Energy Ratio from Binder-to-mixture Stiffness Relationship: PG 76-22, Extracted Binder, 6.1% Asphalt Content

Fix *m* @		D_1 (1/psi)	*m*	Energy Ratio (ER)
0°	0°	3.10E-07	0.426	2.51
	10°	1.30E-06		1.08
	20°	5.23E-06		0.18
10°	0°	1.47E-07	0.445	4.66
	10°	9.48E-07		1.31
	20°	5.13E-06		0.16
20°	0°	2.20E-08	0.473	25.76
	10°	3.29E-07		3.13
	20°	2.27E-06		0.30

Table G.4 Energy Ratio from Binder-to-mixture Stiffness Relationship: PG 76-22, Extracted Binder, 7.2% Asphalt Content

Fix *m* @		D_1 (1/psi)	*m*	Energy Ratio (ER)
0°	0°	4.34E-07	0.404	2.42
	10°	1.79E-06		1.25
	20°	7.17E-06		0.14
10°	0°	2.66E-07	0.441	3.03
	10°	1.63E-06		1.05
	20°	9.19E-06		0.08
20°	0°	6.82E-08	0.456	10.68
	10°	6.03E-07		2.58
	20°	3.84E-06		0.18

Table G.5 Energy Ratio from Binder-to-mixture Stiffness Relationship: PG 67-22, RTFOT Aged, 6.1% Asphalt Content

Fix *m* @		D_1 (1/psi)	*m*	Energy Ratio (ER)
0°	0°	9.83E-08	0.596	1.80
	10°	4.73E-07		1.18
	20°	2.27E-06		0.20
10°	0°	8.57E-08	0.554	2.58
	10°	8.56E-07		0.81
	20°	7.09E-06		0.08
20°	0°	6.33E-09	0.579	30.55
	10°	2.35E-07		2.59
	20°	2.47E-06		0.20

Table G.6 Energy Ratio from Binder-to-mixture Stiffness Relationship: PG 76-22, RTFOT Aged, 6.1% Asphalt Content

Fix *m* @		D_1 (1/psi)	*m*	Energy Ratio (ER)
0°	0°	3.10E-07	0.426	2.51
	10°	5.22E-06		1.08
	20°	1.30E-06		0.18
10°	0°	1.47E-07	0.445	4.66
	10°	9.48E-07		1.31
	20°	5.13E-06		0.16
20°	0°	2.20E-08	0.473	25.77
	10°	3.29E-07		3.13
	20°	2.27E-06		0.30

Table G.7 Energy Ratio from Binder-to-mixture Stiffness Relationship: PG 67-22, RTFOT Aged, 7.2% Asphalt Content

Fix *m* @		D_1 (1/Psi)	*m*	Energy Ratio (ER)
0°	0°	4.29E-07	0.466	1.18
	10°	2.23E-06		0.64
	20°	1.14E-05		0.10
10°	0°	1.72E-07	0.570	1.61
	10°	1.77E-06		0.44
	20°	1.69E-05		0.04
20°	0°	-2.43E-09	0.761	-48.28
	10°	8.62E-08		3.85
	20°	1.89E-06		0.14

Table G.8 Energy Ratio from Binder-to-mixture Stiffness Relationship: PG 76-22, RTFOT Aged, 7.2% Asphalt Content

Fix *m* @		D_1 (1/psi)	*m*	Energy Ratio (ER)
0°	0°	4.34E-07	0.404	2.42
	10°	1.79E-06		1.25
	20°	7.16E-06		0.14
10°	0°	2.66E-07	0.441	3.03
	10°	1.63E-06		1.05
	20°	9.19E-06		0.09
20°	0°	6.82E-08	0.456	10.69
	10°	6.03E-07		2.58
	20°	3.84E-06		0.18

APPENDIX H
ENERGY RATIO PREDICTION USING UNMODIFIED BINDER-TO-MIXTURE STIFFNESS RELATIONSHIP FOR MODIFIED MIXTURE

To predict the energy ratio from unmodified binder-to-mixture stiffness relationship to modified mixture, the following procedure was followed:

1. Develop the binder-to-mixture stiffness relationship for the unmodified mixture at each of the three temperatures;
2. Predict the stiffness of modified mixture using the unmodified binder-to-mixture stiffness relationship at the same temperature ;
3. Lock-in D_0 = 0.048 (1/GPa); and
4. Determine D_1 and m for the modified mixture.

Table H.1 Energy Ratio from Unmodified Binder-to-mixture Stiffness Relationship: PG 76-22, Extracted Binder, 6.1% Asphalt Content

	D_1 (1/psi)	*m*	Energy Ratio (ER)
0°	1.19E-07	0.542	3.20
10°	7.85E-07	0.521	0.98
20°	1.93E-06	0.543	0.23

Table H.2 Energy Ratio from Unmodified Binder-to-mixture Stiffness Relationship: PG 76-22, Extracted Binder, 7.2% Asphalt Content

	D_1 (1/psi)	*m*	Energy Ratio (ER)
0°	5.01E-07	0.427	1.77
10°	1.73E-06	0.528	0.58
20°	1.44E-06	0.708	0.13

Table H.3 Energy Ratio from Unmodified Binder-to-mixture Stiffness Relationship: PG 76-22, RTFOT Aged, 6.1% Asphalt Content

	D_1 (1/Psi)	*m*	Energy Ratio (ER)
0°	1.94E-07	0.501	2.47
10°	1.16E-06	0.530	0.63
20°	3.10E-06	0.561	0.13

Table H.4 Energy Ratio from Unmodified Binder-to-mixture Stiffness Relationship: PG 76-22, RTFOT Aged, 7.2% Asphalt Content

	D_1 (1/Psi)	*m*	Energy Ratio (ER)
0°	6.07E-07	0.436	1.37
10°	2.37E-06	0.550	0.38
20°	2.54E-06	0.736	0.07

REFERENCES

Bonnaure, F., G. Gest, A. Gravois, and P. Uge. 1977. "A New Method of Predicting the Stiffness of Asphalt Paving Mixtures." *Proceedings, Association of Asphalt Paving Technologists*, Vol. 46, 1977, p. 64-100.

Buttlar, W. G. 1996. "Relationship Between Asphalt Binder and Mixture Stiffness at Low Temperatures for the Control of Thermal Cracking Performance Predictions." *Ph.D. Dissertation*, Pennsylvania State University, University Park, PA.

Christensen, D. W., and D. A. Anderson. 1992. "Interpretation of Dynamic Mechanical Test Data for Paving Grade Asphalt Cements." *Journal of the Association of Asphalt Paving Technologists*, Vol. 61, p. 67-98.

Christensen, R. M., and K. H. Lo. 1979. "Solutions for Effective Shear Properties in Three Phase Sphere and Cylinder Models." *Journal of the Mechanics and Physics of Solids*, Pergamon Press, New York, Vol. 27, p. 315-330.

Christensen, R.M., and K. H. Lo. 1986. *Erratum*: "Solutions for Effective Shear Properties in Three Phase Sphere and Cylinder Models." *Journal of the Mechanics and Physics of Solids*, Pergamon Press, New York, Vol. 34, No. 6, 1986, p. 639.

Ferry, J. D. 1961. *Viscoelastic Properties of Polymers*. New York: John Wiley & Sons, Chapter 11.

Hashin, Z. 1965. "Viscoelastic Behavior of Heterogeneous Media." *Journal of Applied Mechanics*, Transactions of the ASME, New York, No. 9, p. 630-636.

Hashin, Z., and S. Shtrikman. 1963. "A Variational Approach to the Theory of the Elastic Behavior of Multiphase Materials." *Journal of Mechanics and Physics of Solids*, Pergamon Press, New York, Vol.11, p. 137.

Heukelom, W., and A. J. G. Klomp. 1964. "Road Design and Dynamic Loading." *Proceedings, Association of Asphalt Paving Technologists*, Ann Arbor, Michigan, Vol. 33.

Hunter, Robert N. 2000. *Asphalts in Road Construction*. London: Thomas Telford.

Jajliardo, Adam P. 2003. "Development of Specification Criteria to Mitigate Top-down Cracking." *Master's Thesis*, University of Florida.

Kim, Booil. 2003. "Evaluation of the Effects of SBS Polymer Modifier on Cracking Resistance of Superpave Mixture." *Ph.D. Dissertation*, University of Florida, Gainesville, FL.

Nicholls, J. C. 1998. *Asphalt Surfacings.* London; New York, E & FN Spon.

Paul, B. 1960. "Prediction of Elastic Constants of Multiphase Materials." *Journal of Applied Mechanics*, Transactions of the ASME, New York, Vol. 36, p. 218.

Roberts, Freddy L., Prithvi S. Kandhal, E. Ray Brown, Dah-Yinn Lee, and Thomas W. Kennedy. 1996. *Hot Mix Asphalt Materials, Mixture Design, and Construction.* Second Edition, NAPA Education Foundation.

Roque, R., W. G. Buttlar, B. E. Ruth, M. Tia, S. W. Dickison, and B. Reid. 1997. "Evaluation of SHRP Indirect Tension Tester to Mitigate Cracking in Asphalt Concrete Pavements and Overlays." *Final Report* to Florida Department of Transportation, University of Florida, FL, June.

Roque, R., D. R. Hiltunen, W. G. Buttlar, and T. Farwanna. 1994a. "Development of the SHRP SUPERPAVE^{TM} Mixture Specification Test Method to Control Thermal Cracking Performance of Pavements." Symposium on Engineering Properties of Asphalt Mixture and Relation to Performance, *ASTM STP 1265*, G. A. Huber and D. S. Decker, Eds., American Society for Testing and Materials, Philadelphia, PA.

Roque, R., D. R. Hiltunen, P. Romero, and W. G. Buttlar. 1994b. "Canadian SHRP Investigation to Evaluate Asphalt Mixture and Binder Criteria to Predict and Control Thermal Cracking." *Report* to C-SHRP, The Pennsylvania Transportation Institute, University Park, PA, June.

Shin, E. Eugene, Alekh Bhurke, Edward Scott, Steve Rozeveld, and Lawrence T. Draza. 1996. "Microstructure, Morphology, and Failure Modes of Polymer-Modified Asphalts." *Transportation Research Record No. 1535*.

Tia, Mang. 2001. "Lecture Notes: Bituminous Materials." Department of Civil and Coastal Engineering, University of Florida, Gainesville, Florida, Fall.

Twumasi, Franklin K. 2001. "Laboratory Evaluation of the Effects of Ground Tire Rubber (GTR) on the Rutting and Cracking Performance of Superpave Mixes." *Master's Thesis*, University of Florida, Gainesville, FL.

Usmani, Arthur M. 1997. *Asphalt Science and Technology*. New York: Marcel Dekker.

Van Draat, W.E. Fijn, and P. Sommer. 1965. "Ein Great Zur Bestimmung der Dynamichen Elastizitasmoduln von Asphalt." *Strasse und Autobahn*, Vol. 6.

Zhang, Zhiwang. 2000. "Identification and Crack Growth Law for Asphalt Mixtures Using the Superpave Indirect Tensile Test (IDT)." *Ph.D. Dissertation*, University of Florida.